THESIS FOR THE DEGREE OF DOCTOR OF PHILOSOPHY

Development and Stabilization of Hybrid Structure of Asphaltene and Graphene

Govindan Induchoodan

Examiner: Eva Olsson
Supervisor: Prof. Jan Swenson
Co-supervisor: Prof. Helén Jansson

Department of Architecture and Civil Engineering / Department of Physics

CHALMERS UNIVERSITY OF TECHNOLOGY

Gothenburg, Sweden 2023

Abstract

Petroleum and its derivatives, such as bitumen, are complex colloidal system. Their chemical behavior is influenced by various internal and external factors. Adding graphene derivatives to this system will only increase its complexity, thus it must be carefully considered to ensure successful integration. In this thesis, we examine the challenges of introducing graphene derivatives into bitumen and focus on three key questions: a) phase stability of graphene derivatives in bitumen, b) interaction between graphene and asphaltene aggregates, and c) an environmentally friendly and optimal method to modify graphene derivatives for improved bitumen properties. We use various characterization techniques to answer these questions and find that the best strategy for introducing graphene derivatives into bitumen is non-covalently functionalized graphene using the Molecular Wedging method (MW-graphene). The MW-graphene is compatible with asphaltene aggregates and stabilizes in bitumen through mutual interaction. The use of MW-graphene improves the mechanical stability of asphaltene aggregates in bitumen.

Appended Papers

1. Influence of graphene oxide on asphaltene nanoaggregates, **G. Induchoodan**, H. Jansson, J. Swenson, Colloids and Surfaces A: Physicochemical and Engineering Aspects, 630 (2021) 127614.

2. The Critical Role of Asphaltene Nanoaggregates in Stabilizing Functionalized Graphene in Crude Oil Derivatives, 2022, **G. Induchoodan**, H. Jansson, A.S. Mohammadi, J. Swenson, Colloids and Surfaces A: Physicochemical and Engineering Aspects, 660 (2023) 130865.

3. Augmenting the Stability of Asphaltene Aggregates with Sustainable Functionalized Graphene, **G. Induchoodan**, H. Jansson, J. Swenson, (in manuscript).

4. A 'Roadmap' to Utilizing the Potential of Graphene Derivatives in Bitumen, 2022, **G. Induchoodan**, H. Jansson, J. Swenson, Journal of Physical Chemistry B, (in manuscript).

Contribution Report

1. My contribution to the study includes conceptualization, methodology, validation, writing - original draft. The paper is written by Prof. Jan Swenson, Prof. Helén Jansson, and me. I performed all the experiments except TLC-FID and XPS. The samples for this paper were prepared in-house by me. We performed a total of 6 experiments: SEM-EDX, XRD, XPS, Transmission light microscopy, TLC-FID, and FTIR. The experimental data were analyzed and interpreted by me with help from Jan Swenson and Helén Jansson,

2. My contribution to the study includes conceptualization, methodology, validation, writing - original draft. The paper is written by Prof. Jan Swenson, Prof. Helén Jansson, and me. I performed all the experiments except XPS. The samples for this paper were prepared in-house by me. We performed a total of 7 experiments: SAXS, DSC, DLS, rotational rheometer, XPS, transmission light microscopy, and Raman microscopy. Dr. Amir Mohammadi helped me in setting up the DLS and interpreting the DLS data. The remaining experimental data were analyzed and interpreted by me with help from Jan Swenson and Helén Jansson,

3. My contribution to the study includes conceptualization, methodology, validation, writing - original draft. The paper is written by Prof. Jan Swenson, Prof. Helén Jansson, and me. The samples for this paper were prepared in-house by me. We performed a total of 5 experiments: DSC, UV-Vis, XPS, transmission light microscopy, and FTIR. Dr. Amir helped me in setting up the UV-Vis for measurements. The experimental data were analyzed and interpreted by me with help from Jan Swenson and Helén Jansson,

4. My contribution to the study includes conceptualization and writing - original draft. The paper is written by Prof. Jan Swenson, Prof. Helén Jansson, and me. The paper is based on the studies presented in Papers 1-3, with the contributions given above for those papers.

Publications not included

1. Tailoring polymer nanocomposite microstructure by controlling orientation, dispersion and exfoliation of GnP in LDPE via extrusion flow, 2016, **G. Induchoodan**, R. Kadar. Annual Transactions of the Nordic Rheology Society -16. (Published in journal proceeding)

2. Graphene embedded bituminous roads: a new look into the design of complex nanocomposites, 2019, **G. Induchoodan**, B.Adl-Zarrabi, J.Swenson, L.Tang. 10th anniversary international conference on nanomaterials - research & application p. 107-112. (Published in special journal proceeding)

3. Particle Emission and Dispersion Test for the Early Planning Stage: New and Advanced Wear Measurement Technique for Characterization of Environmental Impacts of Roads, (2019), **G. Induchoodan**, B.Ebharimi, B.Adl-Zarrabi. Euro Asphalt Euro Bitumen 2020. (Published in journal proceeding)

Patents not included

1. Functionalized graphene structure, PCT Application No. PCT/SE2022/051168, Inventor **G. Induchoodan**, 12 December 2022.

2. Functionalized graphene nanocomposite, Inventor **G. Induchoodan**, In draft

Content

List of Abbreviation

- ASTM - American society for testing and materials
- ATR - Attenuated total reflectance
- CCC – Critical clustering concentration
- CII – Critical Instability Index
- CMC – Critical micellization concentration
- CNAC – Critical nano-agglomeration concentration
- CPC – Complex polymeric colloid
- CXO - Cyclohexanone
- DBSA – Dodecyl benzenesulfonic acid
- DMF - Dimethylformamide
- DLS – Dynamic light scattering
- DRIFT – Diffuse reflectance infrared Fourier transform spectroscopy
- DSC – Differential scanning calorimetry
- DSR - Dynamic shear rheometer
- EDX - Energy-dispersive X-ray spectroscopy
- fGO - Functionalised graphene oxide
- FTICRMS - Fourier-transform ion cyclotron resonance mass spectrometry
- FTIR - Fourier transform infrared spectroscopy
- GnP – Graphene nanoplatelet
- GO – Graphene oxide
- IMF – Intermolecular force
- NMP - N-Methyl-2-Pyrrolidone
- NMR – Nuclear magnetic resonance spectroscopy
- PAHs - Polycyclic-aromatic core
- PAM – 1-amino pyrene
- PBA – 1-pyrene butyric acid
- PBrA – 1-pyrene boronic acid
- PMB – Polymer modified bitumen
- PSA – 1-pyrene sulfonic acid
- rGO – Reduced graphene oxide
- SARA – Saturates, Aromatics, Resins, Asphaltenes
- SEM - Scanning electron microscopy
- SAXS- Small angle X-ray scattering
- THF – Tetrahydrofuran
- TLC-FID -Thin-layer chromatography flame ionization detection
- XPS- X-ray photoelectron spectroscopy

- XRD - X-ray diffraction
- UV-Vis – Ultraviolet-visible light spectroscopy

List of Figures

List of Tables

Preface

> Look again at that dot. That's here. That's home. That's us. On it everyone you love, everyone you know, everyone you ever heard of, every human being who ever was, lived out their lives. The aggregate of our joy and suffering, thousands of confident religions, ideologies, and economic doctrines, every hunter and forager, every hero and coward, every creator and destroyer of civilization, every king and peasant, every young couple in love, every mother and father, hopeful child, inventor and explorer, every teacher of morals, every corrupt politician, every "superstar," every "supreme leader," every saint and sinner in the history of our species lived there-on a mote of dust suspended in a sunbeam.
>
> \- Carl Sagan

These were the famous words Carl Sagan used to describe the entirety of humanity when looking at the earth from beyond the orbit of Neptune. From the first moment we learned to stand on two legs to our journey beyond the earth's boundaries, humanity has always been driven by two forces, curiosity and desire. These two driving forces have helped us build everything, from our tools, technology, medicine, and modern human society. We stand on the shoulders of giants, driven by the same human curiosity and desire that has propelled our species forward since the dawn of time. It is this drive that led to the discovery of graphene, a wonder material that was once considered impossible. This thesis is a tribute to the human spirit and the unending pursuit of knowledge and innovation.

In this work, we delve into the realm of graphene-incorporated bitumen, seeking to answer the question of how to enhance the properties of this abundant resource. The journey was not without its challenges, both scientific and personal, but through perseverance and determination, we present to you a solution that is both elegant and impactful. This thesis provides a comprehensive exploration of the concept, the challenges faced, and the findings of our research. We also delve into the research planning, outlining the questions asked, the methods employed, and the results obtained. The conclusion of this work is a testament to the boundless potential of graphene to shape the future of our world.

We invite you to join us on this journey, as we explore the possibilities of graphene-incorporated bitumen and celebrate the human spirit that drives us forward.

Acknowledgement

As I conclude this chapter of my life, I am struck by the profound transformation that has taken place within me. I began this journey from India to this unknown foreign land. And yet, through the course of my Ph.D., I have become a citizen of Sweden, with a new home, friends, and family. In many ways, I owe all of this to my Ph.D.

First and foremost, I must thank my supervisors, Prof. Jan Swenson, and Prof. Helén Jansson, for their unwavering guidance and support throughout this journey. We found ourselves on opposite sides of an idea from time to time. But even in those times, I knew you were only trying to push me to be my best, and I am deeply grateful. I must also thank my examiner, Prof. Eva Olsson, who has been a brilliant leader and an inspiring scientist who has motivated me with our conversations. Further, I want to express my gratitude to my funders, NPRA, whose visionary investment in science made this entire journey possible. Without their support, I would not have had the opportunity to pursue my Ph.D.

I want to thank my first teachers, i.e., my parents. You might not have taught me science, but you have taught me an even more valuable lesson, life. You have always believed in me since I was a child, which has motivated me to come so far. Of course, what would I be without my brother who has been my biggest competition, you help me grow. I also want to thank my Anni. You are just super awesome. Further, I want to thank the spirits of my grandparents. I know you are not here to see my progress in life, but I wish to tell you that I can feel your blessings in every step I take. Also, what would this Ph.D. be without my nemesis, "Kitty". You have been my companion since my school days, and you are still a cute, furry monster as the first day I saw you. Now to my fantastic girlfriend, I'm glad I dared to walk up to you and ask you out; you are the best Kajsa. You kept me in one piece when I was working on this thesis.

My friends Ceci, Mohanna, Kengo, Amir, Alle, Pierre, Bobby, Taha, Lorenzo, Vijay, Shaurya...I love you all. We are all idiots traveling in the same boat called insanity. But Lorenzo, my friend, I don't want to travel on the same boat as you and that is for my safety. If I have forgotten to thank anyone here, don’t ever think I forgot to love you. Lastly, Emma, Adrian, Erik, Mattias, Julia, Björn, Inna, and Karin, I'll miss our conversations, but I think the rest of the world will be happy.

Finally, I also want to thank Amir, Marek, Peter, Per, Daniel, Britt-Marie, Angela, Stefan, Tang, everyone at CMAL, and all others who have helped me at various stages in my research. I could not have made it this far without you all. Finally, I wish to thank all my colleagues in Nano & Biophysics and, namely, my group members in Biolab.

1. Introduction

Composites are a combination of two or more materials; these materials include metals, ceramics, or polymers. With the discovery of graphene, researchers have been exploring its potential as a filler in composites (called nanocomposites), including in bitumen.

Bitumen is used in over 70% of global transport infrastructure [1]. The material has limitations such as poor thermal conductivity, low energy absorption, and susceptibility to aging, oxidation, rutting, and fatigue [1]. Graphene, on the other hand, has high thermal conductivity, good energy absorption, excellent oxidation resistance, and high toughness [2]. It is also a highly efficient electrical conductor. Thus, by adding graphene to bitumen, the aspire is to improve its mechanical strength and durability. This combination, graphene and bitumen, could have significant implications for structures that rely on bitumen, such as roads and roofing.

1.1. Aim

This thesis aimed to uncover the potential of incorporating graphene in bitumen. The complexity of bitumen due to its colloidal nature and dynamic chemistry, and the two-dimensional nature of graphene pose an exciting challenge in understanding their interaction.

Our research examined the potential of graphene to enhance the mechanical and physical properties of bitumen through a literature review of previous studies and our own experiments. In addition, we investigated the optimal methods for dispersing graphene in bitumen and the surface characteristics of graphene necessary for effective dispersion.

1.2. Research question

The research was open-ended and exploratory. It aimed at developing new research questions and exploring the potential of graphene in bitumen.

Initially, asked the following questions:

- Is it possible to use graphene in bitumen?
- Which properties of bitumen can be improved by graphene?
- What surface characteristics and physical dimensions of graphene are needed to achieve this?
- Should we work with polymer-modified bitumen (PBM) or bitumen?

To address the abovementioned questions, we began by reviewing the existing scientific literature and recreating the results experimentally. After identifying that some graphene derivatives have the potential to be detrimental, the research questions were modified. Then, the natural question became to identify how to we could overcome this detrimental effect. This was the goal of **paper 2**. Subsequently, we also used the findings from paper 2 to attempt to improve the material properties of bitumen. These findings were reported in **papers 3 and 4**.

1.3. Extended hypothesis/ motivation

Researchers have previously used Nanomaterials to augment the performance of roads [3-11]. Nanomaterials such as nano-silica and carbon nanotubes have been used in road construction to enhance crack resistance, wearability, and reduce tire noise [3-11]. Thus, it is justified that researchers were also motivated to investigate if graphene too can improve bitumen's properties, such as durability, electrical and thermal conductivity, traction [10]. Some examples are shown in figure 1.1. Improving thermal conductivity is of interest in Nordic countries since improved thermal conductivity will help the efficiency of deicing in winter [12]. This could lead to improved road safety and reduced environmental impact, improved durability, better cracking and fatigue resistance. We discuss this in **paper 4**.

However, despite all these potential positive impacts, incorporating graphene into bitumen is more complex than simply blending the two materials. The task involves addressing multiple design challenges that arise due to the nature of graphene, the chemical structure of bitumen, and the ability to study them.

We discuss a few design challenges below:

a). Dispersing graphene: In bitumen, graphene must be evenly dispersed. Bitumen is a highly viscous colloidal system. And graphene is a flexible nanoparticle with a large aspect ratio [1].

b). Stabilizing graphene: Despite the high viscosity, bitumen is a fluid [1]. So, post dispersion, the graphene must also be stabilized in it. However, graphene is not naturally soluble in bitumen [13]. Thus, we have to find other methods [15] to stabilize the dispersed graphene in bitumen over time, and during the processing and laying of roads.

c). Agglomeration of graphene: All nanoparticles agglomerate, and graphene is no exception. *Agglomeration* is a natural phenomenon observed when nanoparticles exceed specific volume fractions in polymers and solvents [16]. In the case of graphene in bitumen, this can have negative impact (**refer to paper 1**).

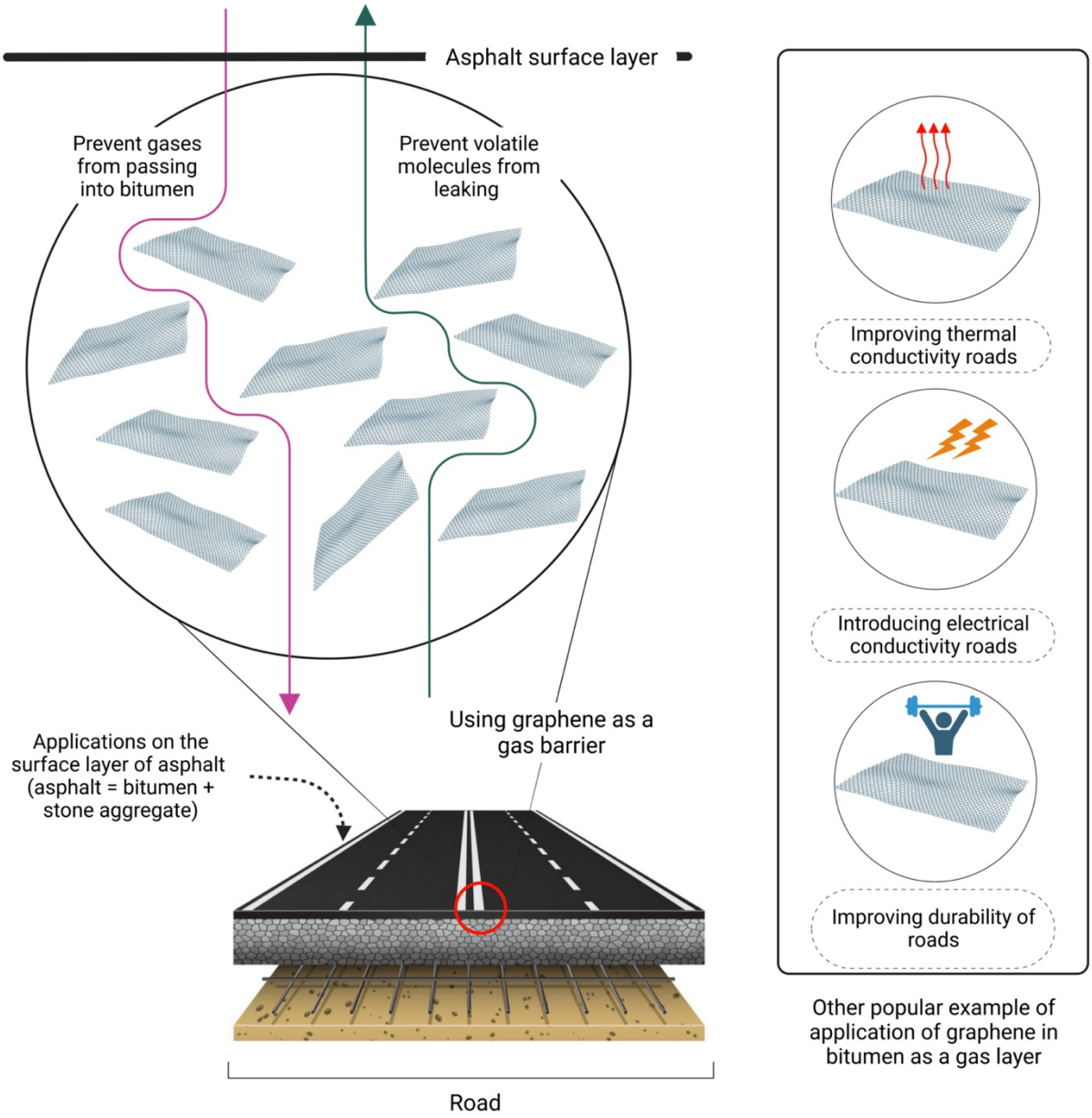

Figure 1.1: Popular theories of applications of graphene incorporated in bitumen [3-11]. Graphene is theorized to introduce a gas barrier that can reduce the oxygen penetration into roads, improve thermal conductivity, introduce electrical conductivity, and improve durability of roads by improving the strength.

Thus, the challenge of directly incorporating graphene in bitumen is complex, but it could be possible to overcome these challenges with the right approach. In theory, by chemically treating graphene, using high-shear mixing at high. temperatures, stabilizing agents, surfactants, and dispersants, it is possible to create a stable graphene dispersion in bitumen.

That said, *we wanted to achieve a good dispersion without shear mixing at high temperatures, stabilize graphene in bitumen without using chemicals, surfactants, or polymers, and account for agglomeration without adding further chemicals. Additionally, we wanted to achieve this in a cost-effective, sustainable, and scalable manner, with minimum disruption to current bitumen production and handling methods.*

1.4. Justification of the research approach

This section discusses the motivations behind the research approach.

1.4.1. Top-down vs bottom-up approach

The study of graphene-incorporated bitumen can be approached from two perspectives: top-down and bottom-up.

The top-down approach involves us researching on improving a desired property. This approach might help determine the optimal method to use graphene in bitumen. However, this approach has several disadvantages. For instance, functionalized graphene is expensive and incorporating it into bitumen be time-consuming. In addition, the challenges of dispersion, stabilization, and agglomeration might still be difficult to overcome.

Further, due to the complex nature of bitumen, such as its high viscosity, opacity, and intricate chemical structure [1], studying graphene-incorporated bitumen using the top-down approach can be challenging in a lab, and provide inconsistent results. This is because, it is difficult to observe the graphene particles in the bitumen, understand and control potential chemical reactions in bitumen that can affect the properties of graphene, and account for changes in the viscosity, volume fractions, chemical species of bitumen. Thus, a top-down approach will have low figures of merit.

On the other hand, the bottom-up approach involves us developing graphene-bitumen nanocomposites from the bottom up, i.e., starting from the individual components. This approach allows for better control of the properties of the graphene and the bitumen and their interactions. Furthermore, this approach also allows for the study of the effects of different parameters, such as temperature, chemical interaction, and time, on the graphene-incorporated bitumen's properties. This approach is ideal for investigating the dispersibility, stabilization, and agglomeration of graphene in bitumen.

1.4.2. Graphene incorporated polymer modified bitumen vs conventional bitumen

There are two main groups of bitumen, PMB and conventional bitumen [1]. Each type of bitumen is used for different applications [1]. When introducing graphene into bitumen, it can be introduced to both PMB and bitumen.

PMBs are found to have improved properties compared to bitumen, such as higher stiffness, higher tensile strength, higher fatigue resistance, and higher temperature resistance [1]. Making it more suitable for use in road construction and other applications where high performance is required. Thus, we can theorize that graphene can further improve the properties of the polymers used to produce PMBs. Thus, graphene-incorporated PMB might be a better choice for proving the applicability of graphene in bitumen.

However, the main disadvantage of incorporating graphene into PMB versus directly incorporating it into bitumen is that it does not directly interact with the bitumen. Instead, it interacts with the polymer, which then improves the properties of the bitumen. Thus, to fully utilize the potential of graphene in bitumen and achieve improved material properties such as thermal conductivity, it is necessary to incorporate graphene into the bitumen directly.

1.4.3. Bitumen vs model bitumen

Bitumen is a complex colloidal system. So, to improve its material properties we have to understanding the structure-function of bitumen in order to predict the changes required in the structure to attain the intended function [17]. Although it is possible to perform such a study, it would be an impractical and inefficient approach on an engineering scale due to the shear molecular complexity of bitumen. Further, bitumen is an umbrella term and not a specific chemical composition. So, the results from studying using bitumen, would have poor figures of merit.

Therefore, we use a model bitumen in this work, with the intent that the results we produce using graphene and our model bitumen can be reproduced by other labs and the results repeated internally by us has to be used. The model bitumen's design and chemical nature are discussed in the next chapters.

1.5. Delimitation of the research

Further research is needed on using functionalized graphene in asphalt. The research was conducted by studying the interaction between graphene and a model bitumen model. These experiments showed that functionalized graphene can improve some properties of bitumen, such as mechanical stability. However, further research is needed to understand how this

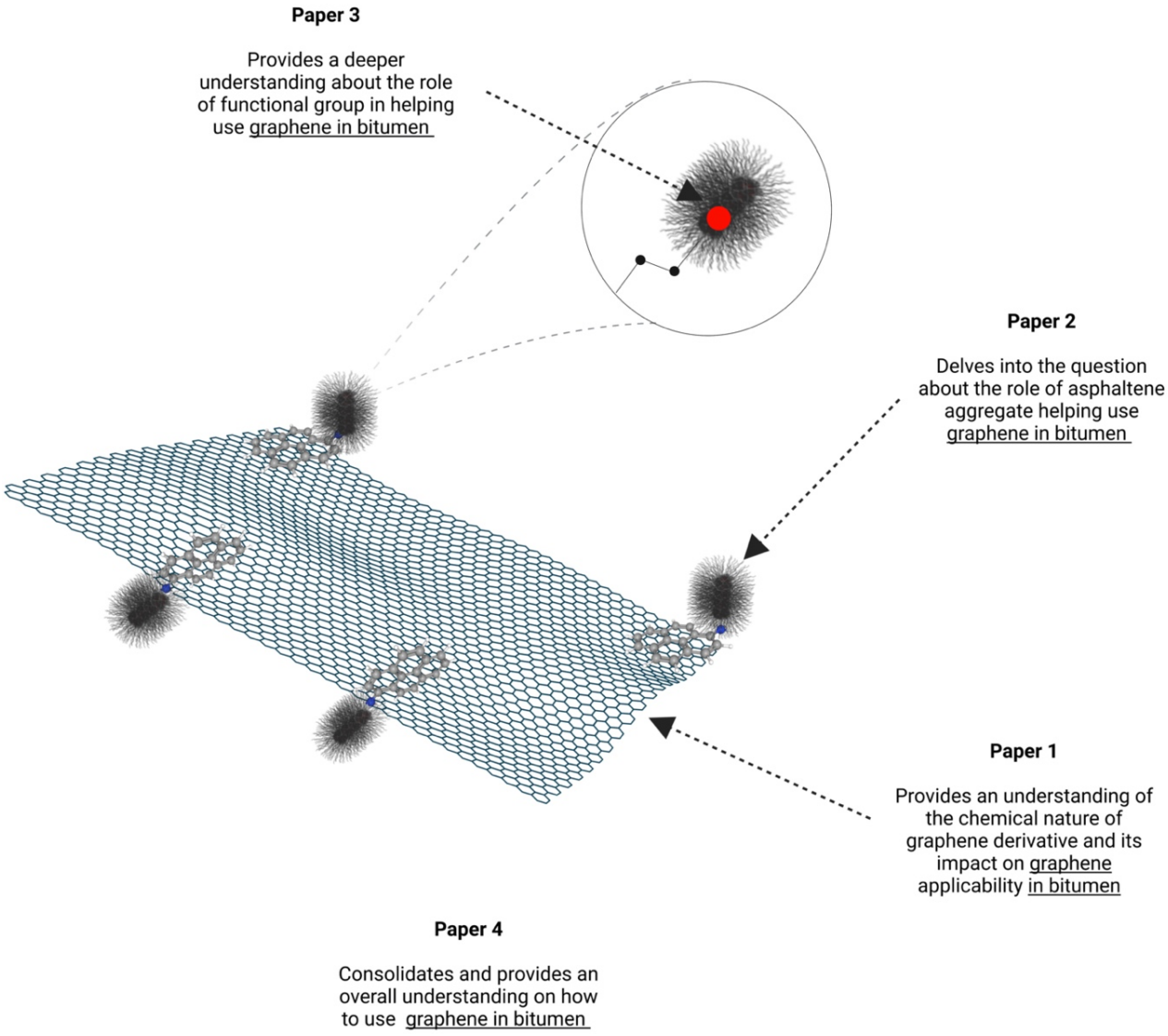

Figure 1.2: Illustration of the 4 papers attached in this thesis, and the scientific contribution of the papers to the research questions addressed in this thesis.

improvement affects bitumen in its full complexity and also in asphalt. Additionally, more work needs to be done in order to develop cost-effective methods for incorporating functionalized graphene into asphalt with minimal negative effects on its properties on a large scale. Finally, the underlying mechanism that of how the asphaltene aggregate assemble around the tethers has to be investigated and understood.

1.6. Thesis structure

The thesis is separated into 10 chapters including the introduction. In this work, **chapter**s **2 and 3** introduce the materials of interest, bitumen and graphene. **Chapter 2** briefly introduces petroleum, bitumen, and its structure. Following it **chapter 3** introduces graphene and brief discussions about graphene functionalization. The research planning is divided into two chapters; **chapter 4** discusses our strategy concerning functionalizing graphene, and **chapter 5** discusses why a model bitumen was used and the characteristics of this model bitumen. **Chapter 6** covers the various characterization techniques used in this work. Finally, **chapters 7, 8, and 9** present the results and conclusion. Lastly, **chapter 10** presents our view on the future outlook of this work.

1.7. Attached papers

The thesis has 4 attached papers. Figure 1.2 illustrates the 4 papers and how the papers discuss and provides a deeper understanding of the design and behavior of the graphitic structure developed in this thesis. **Paper 1** investigates the influence of the chemical structure of graphene on the applicability of graphene derivatives in bitumen. **Paper 2** discusses the behavior and stability of this graphitic structure after interacting with molecules in bitumen. **Paper 3** further develops on the understanding from **paper 2** and presents an understanding of the effect of the functionalization of graphene derivatives and its ability to interact with molecules in bitumen to form a stable structure. Finally, **paper 4** consolidates the understanding developed in this work for other researchers who work with bitumen to develop further possibilities.

2. Petroleum and petroleum derivatives

Petroleum is defined as all the naturally occurring hydrocarbons [18-25]. This includes all states of hydrocarbons, in pure or mixed form, with or without heteroatoms [18-25]. In general, hydrocarbons are molecules with a carbon backbone [18-25]. When petroleum is extracted from the earth, it comes in the form of a complex array of hydrocarbons called *crude /crude oil* [18]. Fractional distillation is the most widely used method to separate the various fractions (petroleum) from crude, see figure 2.1 for an illustration of fractional distillation [21]. During fractional distillation, crude is heated to evaporation, and the vapors of crude are condensed. When the crude vapors condense, they do so at various stages, and the condensed vapors are collected. The condensation point of a hydrocarbon is proportional to its boiling point, and distinct hydrocarbons can have similar boiling points. Thus, during condensation, hydrocarbons with varying carbon numbers, bonds, and heteroatoms can condense at a similar

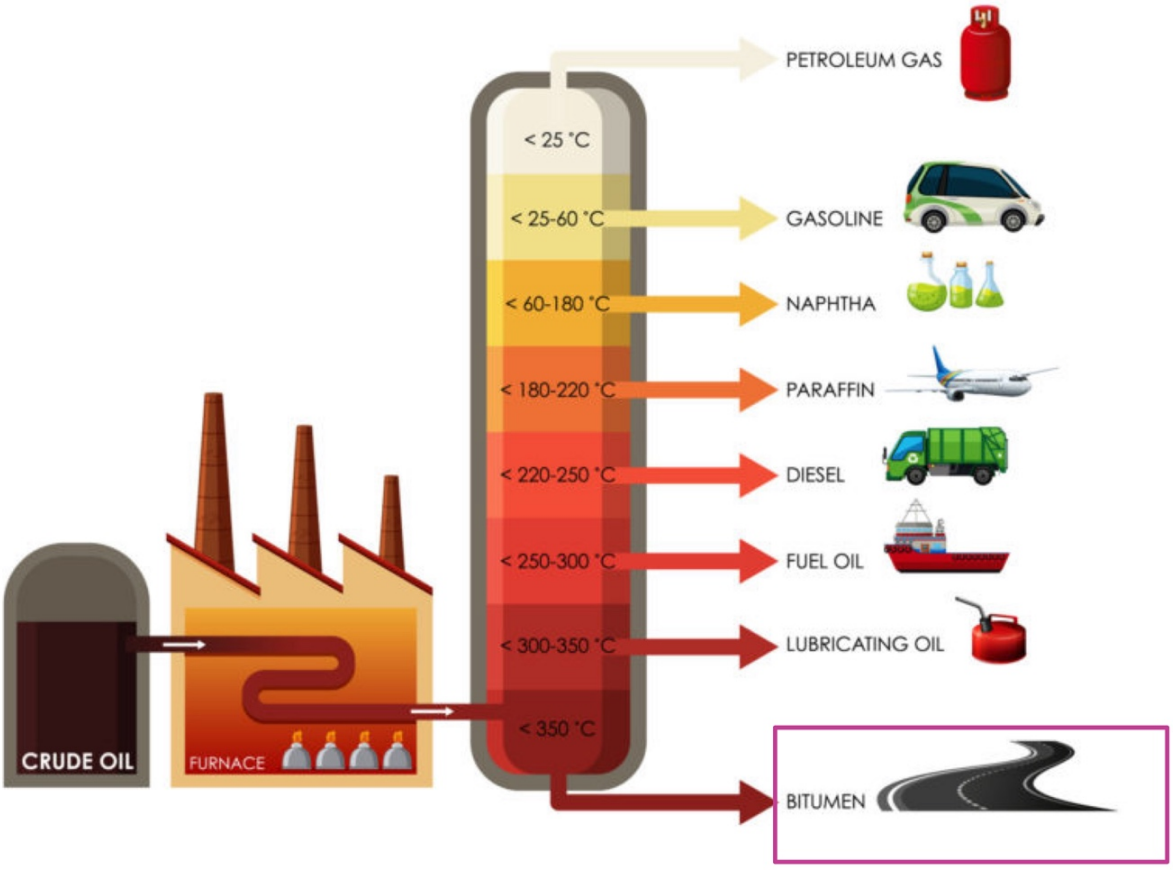

Figure 2.1: - An illustration the fractional distillation of crude. The process helps separate the various petroleum derivatives [1, 18-25].

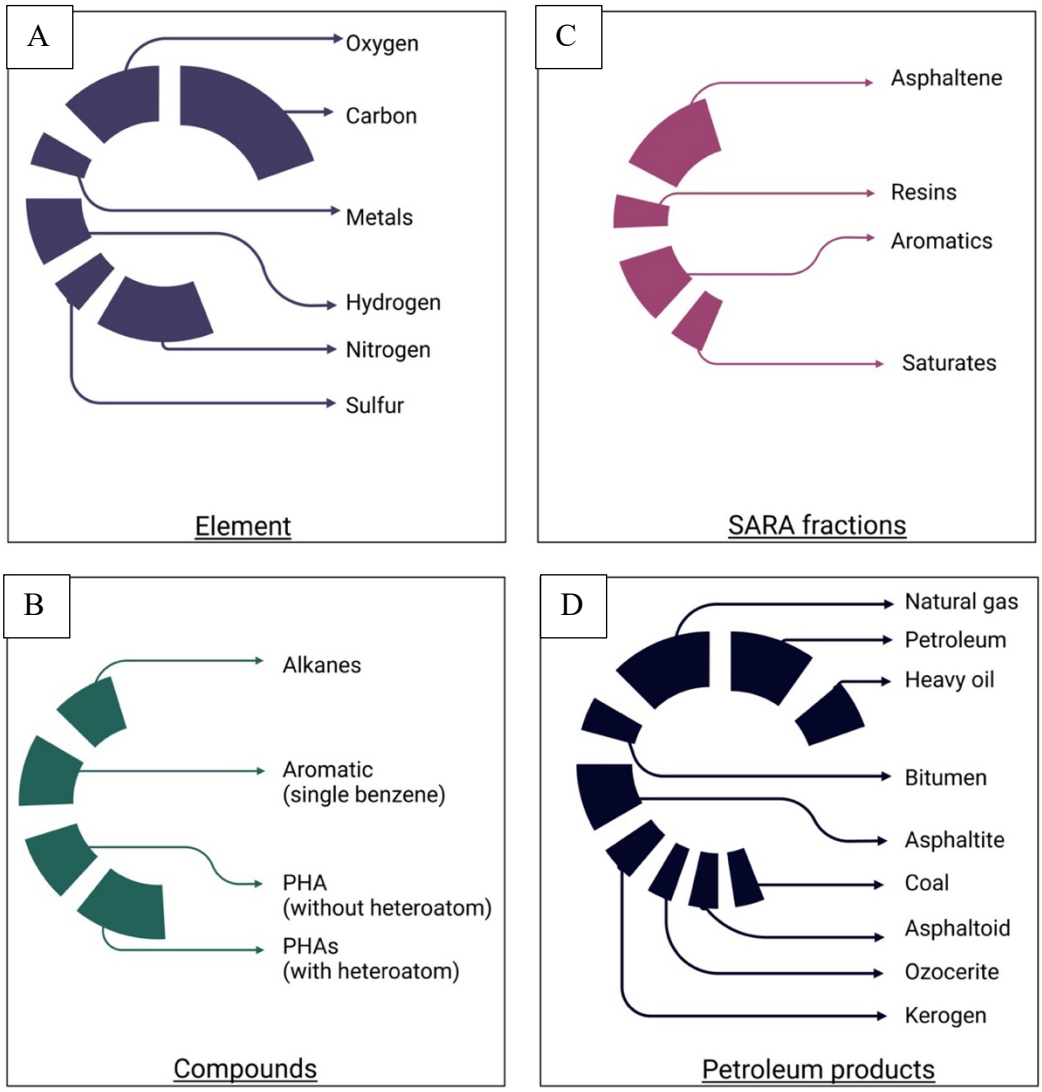

Figure 2.2: Clart of the subdivision of hydrocarbons; A). All hydrocarbons are divided into elemental composition; B). The elements arrange themselves to form alkanes and aromatics of different architecture; C). These organic molecules can be arranged into 4 fractions called SARA. D). All petroleum derivatives can also be arranged based on their commercial use [1, 23, 24].

point [1, 18-25]. The various distilled petroleum fractions can be called *petroleum derivatives.*

2.1. Petroleum derivatives

Petroleum is an elemental composition of carbon, hydrogen, and heteroatoms (such as oxygen, sulfur, and nitrogen), see figure 2.2. These elements arrange themselves to form linear alkanes, branched alkanes, cyclic alkanes, and monoaromatic & polyaromatic analogies [1, 23]. The hydrocarbons mentioned above also bond with the heteroatoms to form compounds such as thiols, pyridines, ketones, and many more. Based on the source and the

probable structure of the condensed hydrocarbons, these hydrocarbons can form constitutional and stereoisomers leading to 10s of thousands (if not 100s of thousands) of structural possibilities for each increase in carbon number. Such structural diversity poses a challenge to determining the properties of individual hydrocarbons [18-23], thus making it nearly impossible to categorize. Thus, petroleum can be more naturally divided into broader fractions based on their chemical compounds, elements, derived products, origin. Refer to figure 2.2 for some examples [24]. Further, a useful method of petroleum categorization is presented below. It is a combination of two categorization methods.

Petroleum can be divided into alkanes, aromatics hydrocarbons without heteroatoms (polarizable aromatics), and aromatic hydrocarbons with heteroatoms (polar compounds) [1]. This can be called the type 1 categorization.

a) If petroleum was to be divided based on the family of hydrocarbons. Petroleum can be divided into alkanes, aromatics hydrocarbons without heteroatoms (polarizable aromatics), and aromatic hydrocarbons with heteroatoms (polar compounds) [9]. This can be called the type 1 categorization.

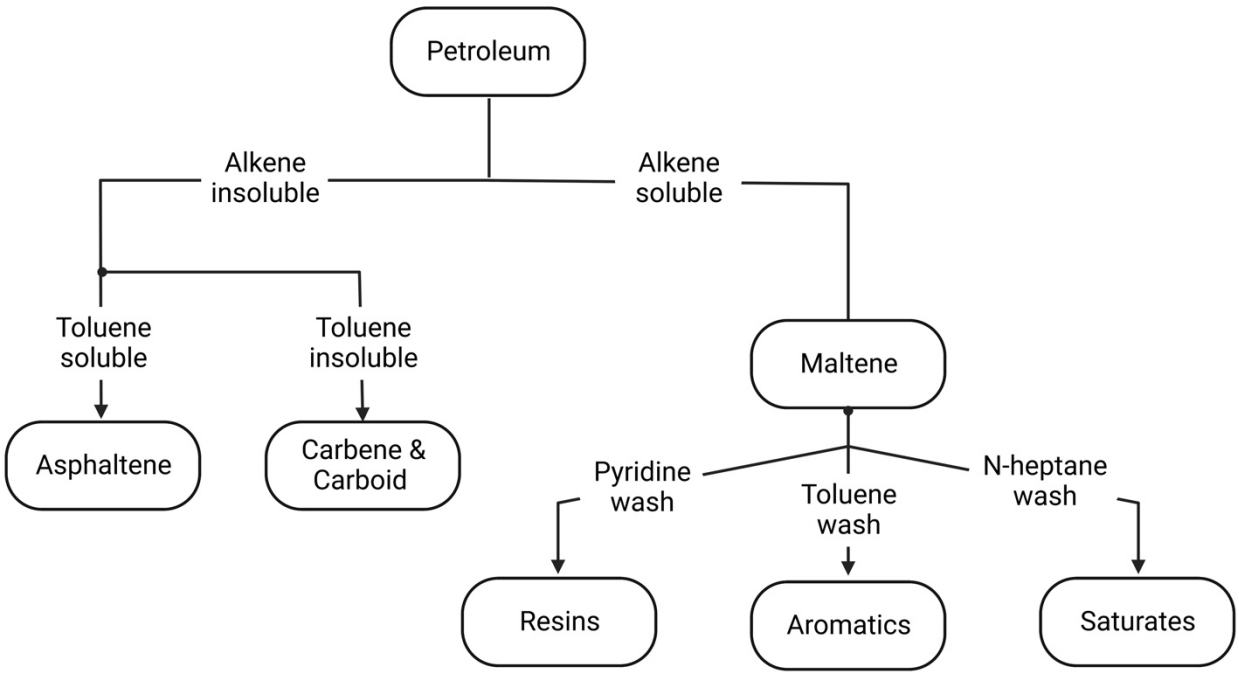

Figure 2.3: ASTM D 4124-01 method of separating SARA fractions from petroleum derivatives. This is done by separated the derivative into alkene soluble and insoluble. The alkene used here is most often n-heptane. The soluble fraction is called maltene. Maltene is separated into its constituent fractions through chromatography into saturates, aromatics and resins.

b) Another method of categorizing petroleum fractions is based on the stability and solubility of various hydrocarbons in liquid hydrocarbons [1]. By this process, petroleum fractions are categorized into alkane insoluble and alkane soluble fraction, see Figure 2.2. This can be called the type 2 categorization.

Both categorizations (type 1 and type 2) can be combined to create a classification called SARA/ SARA fractions [1]. SARA is an acronym for saturates, aromatics, resins, and asphaltenes. Many petroleum derivatives such as heavy oils, bitumen, and petroleum solids can be classified as various ratios of the 4 SARA fractions [1], refer to Figure 2.3.

2.2. SARA fractions

Many petroleum derivatives are known to contains asphaltenes, resins, aromatics, and saturates. The asphaltenes are the toluene soluble alkane-insoluble fraction, while aromatics, resins and saturates together form the alkane-soluble phase called maltene, see Figure 2.2.

2.2.1. Asphaltenes

Asphaltenes are black and exist as nano-solids of approximately 2 nm in size in ambient conditions. Molecular orbital calculations [26] and mass spectroscopy [27] studies indicate that the chemical architecture of asphaltenes is that of a polycyclic-aromatic core (PAHs), with condensed aromatic units making up less than 20% of the structure [28, 29, 30]. The majority of the structure is an alicyclic and open-chain aliphatic, with alkanes existing in the form of end-functionalized structures, which are expected to cover nearly 55% of the structure. The heteroatom count in asphaltenes is displayed to be the highest in any SARA fractions. Hence, the core of asphaltene has a high number of CHO, CHOS, CHNO, and CHNOS molecular series with an average H/C ratio of 1.75 and a O/C ratio of 0.15 [27, 31]. FTICRMS (Fourier-transform ion cyclotron resonance mass spectrometry) indicates that asphaltene has a short range of condensed aromatic units, with most of the aromatic cores having a count of 10 to 20 carbon atoms [27, 31].

2.2.2. Resin

Resins are polar aromatic structures [27, 28] that are black and semi-solid at room temperature. Resins are postulated to have complex aromatic structure with 2-4 fused rings. They may also have a similar composition to asphaltenes, but with fewer heteroatoms. In high viscous petroleum derivatives such as bitumen, a sizable portion of the low-oxygen and hydrogen-deficient molecules are resins and are known to have a peptizing behavior. Studies show that resins have shown to comprise of the largest condensed aromatic structures [27 - 29].

2.2.3. Aromatics

Aromatics, sometimes called naphthene-aromatics, are the polarizable fraction of crude. They are primarily single benzene ring molecules. Further, aromatics are a mixture of the paraffinic-naphthene-aromatic solution with heteroatoms such as sulfur. They ar often found as yellow to red liquid at room temperature [27, 28].

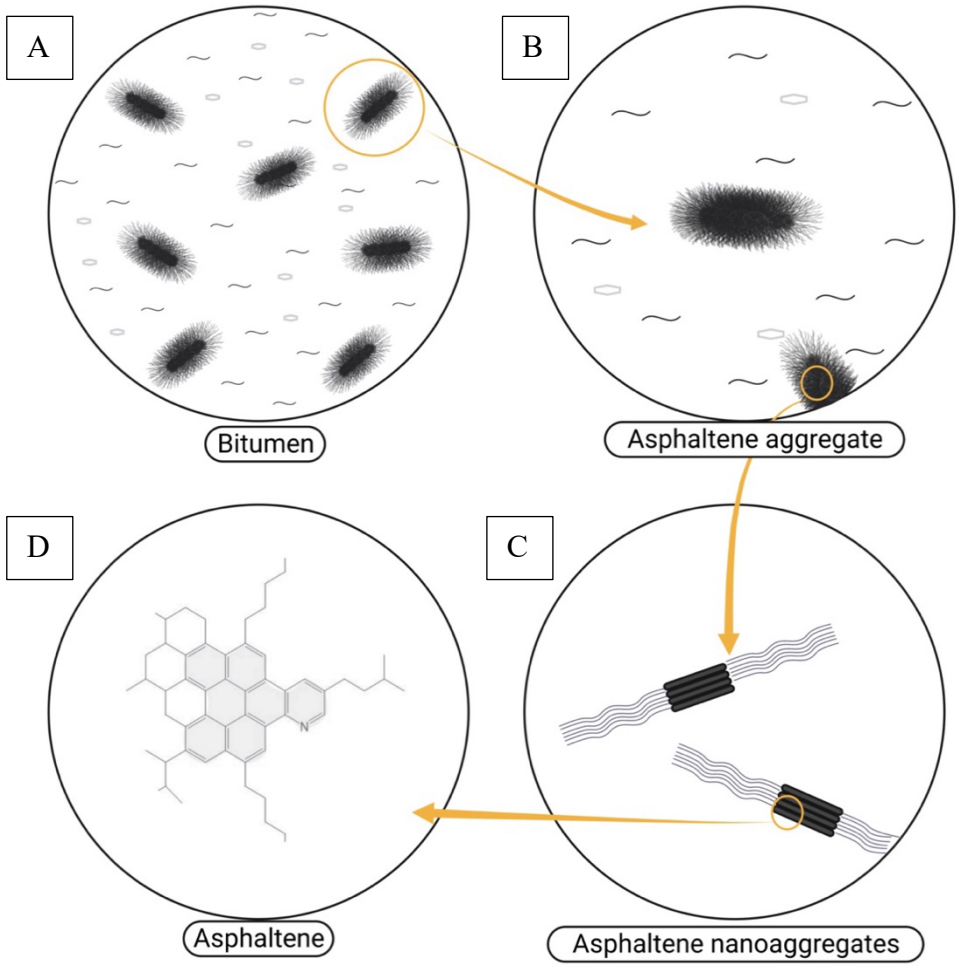

Figure 2.4: An illustration of the postulated colloidal structure of petroleum (e.g., in bitumen). A). a hypothesized colloidal structure of bitumen with all SARA fractions. B). asphaltene aggregates formed from the interaction between asphaltene and resins. C). asphaltene nanoaggregates formed due to self-interaction. D) One of the many proposed architectures for asphaltene molecules.

2.2.4. Saturates

Saturates are a colorless or lightly colored liquid. They consist of alkanes hydrocarbons, in paraffinic-naphthenic form. They are apolar and form the lightest fractions of petroleum

derivatives. They have almost no heteroatoms, and including linear, branched, and cyclic saturated hydrocarbons. [27, 28].

2.3. Aggregate structure of petroleum

Over the years, many proposals for microstructures for petroleum derivatives have appeared [1, 28]. It began with hypothesizing that asphaltenes were free carbon suspended in a maltene solution [28]. Back then, maltene was assumed to be a homogenous fluid. Later, by the method of chromatography, maltene was further divided into different fractions based on polarity and polarizability [1, 28]. After this era, a large group of researchers subscribed to the theory of a sol-type and gel-type material. Sols and Gels were differentiated based on their elastic response to loading. Further, in the 1970s, flocculation models of petroleum were developed [28, 32].

Later, Yen et al. [33] proposed a new microstructure for petroleum. The new model integrated a colloidal structure. This later came to be known as the Yen model. Over the years, the Yen model has been modified to accommodate recent scientific findings. Proposed by Oliver C Mullins, the iterated version of Yen's model later came to be known as the Modified Yen Model [33]. Today, it is understood that asphaltenes and resins interact with each other to form *asphaltene aggregates*. These aggregates are dispersed in saturates. Further, aromatics support the aggregates in dispersing them in saturates, see Figure 2.4. The phase stability, behavior, and ordering of the asphaltene aggregates are influenced by the concentration, entropy, and molecular dimensions of all the fractions in SARA fractions [28 - 30, 33].

Additionally, the size and stability of asphaltene aggregates can vary depending on the composition and properties of the petroleum derivative. Factors that can affect the size and stability of asphaltene aggregates include temperature, pressure, and the presence of other components such as metals, resins, and surfactants [28 - 30, 33]. The stability of asphaltene aggregates can also be influenced by the type and concentration of resins present. While some resins have a high affinity for asphaltene molecules and can help stabilize the aggregates, others can cause destabilization [28].

2.4. Function of asphaltene aggregates

In petroleum derivatives such as bitumen, the asphaltene and resin molecules are thought to be arranged in a complex network-like structure, which imparts unique properties to the material [1, 28-30, 33]. Thus, playing a crucial role in determining the properties and behavior of bitumen, such as viscosity, consistency, density, and stability.

2.5. Asphaltene growth and stability

There are various models that discuss asphaltene growth and stability. Some of these popular concepts are presented here.

Critical nanoaggregate concentration: As discussed, asphaltenes are polyaromatic (PHAs) with heteroatoms, i.e., they have functional groups of oxygen, nitrogen, and sulfurs on their surface. Due to their chemical structure, asphaltenes can engage in hydrogen bonds, dipole moment, van der Waals forces, and π-interactions [34]. In addition, the aromatic cores have an electron-rich π-system [34]. This can lead to the electrons interacting with the π-systems of other aromatic molecules to form non-covalent interaction called the π-effect [34, 35]. In asphaltene, this would mean that the molecules will self-interact to form stacks or agglomerates of asphaltenes [34-36]. These asphaltene-rich phases are formed early in the stage of petroleum. This asphaltene-rich phase is called *asphaltene nanoaggregate* and is theorized to be the preferred state of asphaltene molecules. An asphaltene nanoaggregate is estimated to be a stack of 10 molecules [28]. The concentration at which asphaltene molecules self-associate to form asphaltene nanoaggregates is called the *critical nanoaggregate concentration* (CNAC). Beyond this size, steric hindrance from the aliphatic sidechains dominates. Thus, this limits the growth of the stacks. Further, since resins have an aromatic core, there is potential for resins to stack with the asphaltene molecules [35].

Critical cluster concentration: When the structure of asphaltene restricts further growth, the rapid growth of asphaltene nanoaggregates hinders. When the local concentration of asphaltenes nanoaggregates increases, the nanoaggregates interact to form clusters. These clusters sterically bond to each other, and the concentration at which the clustering happens, is called the critical cluster concentration (CCC). CCC is theorized to be 10 times the CNAC. However, there are uncertainties around the actual size and scale of cluster formation. It is supported that these clusters are fractal, and unlike asphaltene nanoaggregates, the binding energy is said to be relatively small, leading to conclude that they are not formed by the crosslinking of the aromatic cores. The formation of the clusters could lead to phase separation in petroleum, causing flocculation [37]. The consequence of this is seen as fouling in pipelines and sedimentation in bitumen.

Critical instability index: On a macroscopic scale, some use the critical instability index (CII) to help equate the stability of asphaltenes. The CII is calculated from the ratio of the SARA fractions. The stability of the colloidal structure is assumed to be a delicate balance between the ratio of the sums of the volumes of saturates and asphaltenes to the sum of volumes of resins and aromatics, see eq. 1.

$$CII = \frac{Asphaltene + Saturates}{Resins + Aromatics} \tag{01}$$

If the petroleum has a CII below 0.7, it is generally considered as a stable. When the CII value is above 0.9, the colloidal structure in petroleum will destabilize. A various scenario can lead to stabilization or destabilization of the structure [38]. For instance, asphaltenes are solvable in toluene, xylene and other aromatic structures. The increase in aromatic content in petroleum will help form a stable dispersion in saturates. This leads to a ‘’bridged’’ structure of resin and asphaltene nanoaggregates dissolved in aromatics. When CII is low, it indicates that the asphaltenes are stabilized by dispersion in aromatics.

2.6. Bitumen

Bitumen is a petroleum derivative that is primarily used as a binding material in asphalt, which thereafter is used to construct roads. [1]. It is also a popular choice for applications in which long-lasting performance is required, such as roofing, waterproofing, and paving [1]. This is because of some of the advantages properties of bitumen are its viscosity, adhesion, hydrophobicity, elasticity, and insulation.

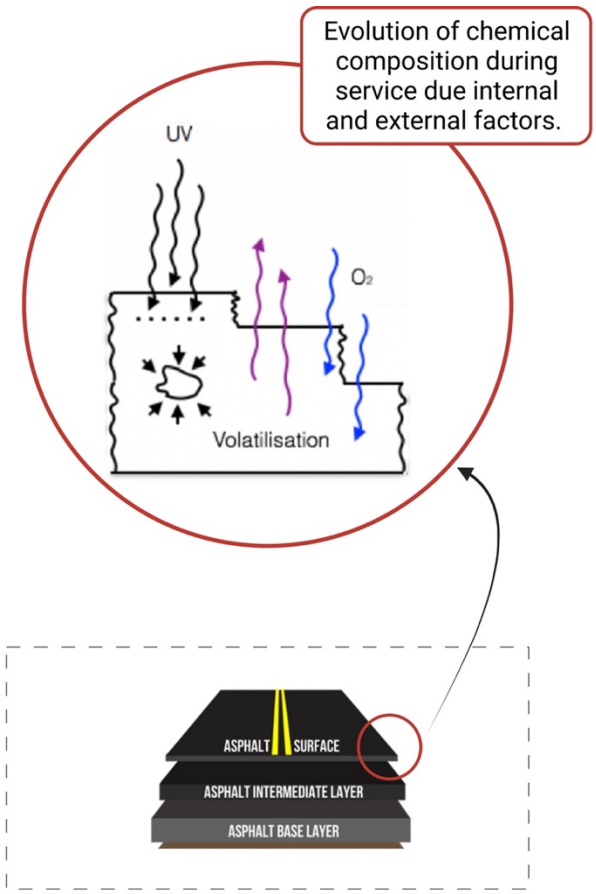

Figure 2.5: Potential evolution of the chemical composition of bitumen due to external and internal factors.

2.7. Bitumen processing

As shown in figure 2.1, during fractional distillation of crude, is the final distilled fraction [1, 18-25, 28]. The chemical nature of bitumen is discussed in detail in **papers 1, 2 and 4**.

To be used in roads, bitumen is mixed with stone aggregates to be used in asphalt [1]. The mix of bitumen can take place at different temperatures [1, 28]. The 3 popular mixing designs are hot mix, warm mix and cold mix. Hot-mix asphalt is used in roads that require heavy duty and cold-mix is used in lighter duty applications. It is performed at temperatures around 180°C. Warm-mix is performed at lowed temperatures to prevent oxidation of bitumen, at temperatures close to 130 °C. Lastly, cold-mix asphalt is usually mixed at room temperature with pre-mixed bitumen, aggregate and additives before being spread on the road surface. This type of asphalt is often used as a pothole repair solution. Another type of bitumen mixing is emulsions. It is sometimes considered as a form of cold-mix. The selection of the appropriate bitumen, aggregates and the mixing design varies depending on factors such as climate, traffic loadings and type of surface being constructed [1, 22, 28].

2.8. Dynamic nature of bitumen

Bitumen has a complex mixture of various hydrocarbons and reactive molecules, making it challenging to control chemical reactions in it during processing and service [1, 27, 28]. This complexity can influence the behavior and impact the stability of asphaltene aggregates. Additionally, during service the complex chemical nature of bitumen can also lead to change in the chemical composition, which can in turn, change the physical properties [1, 28]. Finally, during service bitumen can interact with UV light and oxygen in the atmosphere, it can also lose volatile molecules in it, and have the saturates and aromatics adsorb into stone aggregates, see figure 2.5 for an illustration of the evolution of bitumen during service.

2.9. Challenges of using bitumen in lab studies

Bitumen's chemical and physical properties can vary depending on the type of bitumen, its source, and environmental conditions [1, 28]. This means that the composition and concentration of the SARA fractions in it can vary. Further, during the blending of bitumen, bitumen from various sources can be blended together to obtain the desired physical properties. This adds to the challenge of understanding the composition of the SARA fractions in in. In a lab study it is crucial to assure reproducibility and understanding of the studied system, and this complex nature of bitumen reduces these fugues of merit.

Additionally, its physical properties such as viscosity, opacity, and viscoelasticity can mask or reduce our capacity to observe phenomena such as precipitation, agglomeration, and interactions in bitumen difficult to observe. So, it is equally important to reduce the influence of these physical properties to be able to study these phenomena experimentally.

In this thesis we studied the interaction between asphaltene aggregates and graphene derivatives in bitumen. Thus, to use bitumen in such a lab study, it is crucial to simplifying its chemical complexity so we can determine the interaction between graphene derivatives and asphaltene aggregates with higher accuracy. Therefore, we designed a model bitumen called the *asphaltene aggregate system* with fixed concentration and limited complexity for this study. We will discuss the different design factors of the model bitumen in **chapter. 5.** Furthermore, the synthetic bitumen produces more reproducible results that will help us understand their interaction and the factors that affect it.

3. Graphene and functionalization

Graphene is an atomic layer of a linearly arranged aromatic carbon structure [39-42]; see Figure 3.1. It has an sp2 hybridized orbital in the lattice, suggesting an orbital configuration of σ-bond in the bond axis with two lobes of a delocalized π-bond, and an sp3 hybridized orbital at the edge [40]. Due to this strong covalent bond and its 2D lattice arrangement, graphene it flat [41]. The electron structure of graphene that makes it a wonder material. This electron dynamics of graphene can be best described by the relativistic Dirac equation [43]. By this, the Fermi velocity of the electrons in the graphene is substituted by the speed of light. Hence the effective mass of the electrons vanishes, making them appear as massless fermions [44]. This lets graphene to have quantum anomalies such as the quantum hall effect [45], absence of localization [46], and ballistic transportation [47]. However, this same electron structure of graphene, makes it nearly chemically inert and insoluble in many organic solvents [48]. This limits the application in some cases such as in nanocomposites. As an alternative, graphene is chemically or physically modified to suit the application. This type of graphene

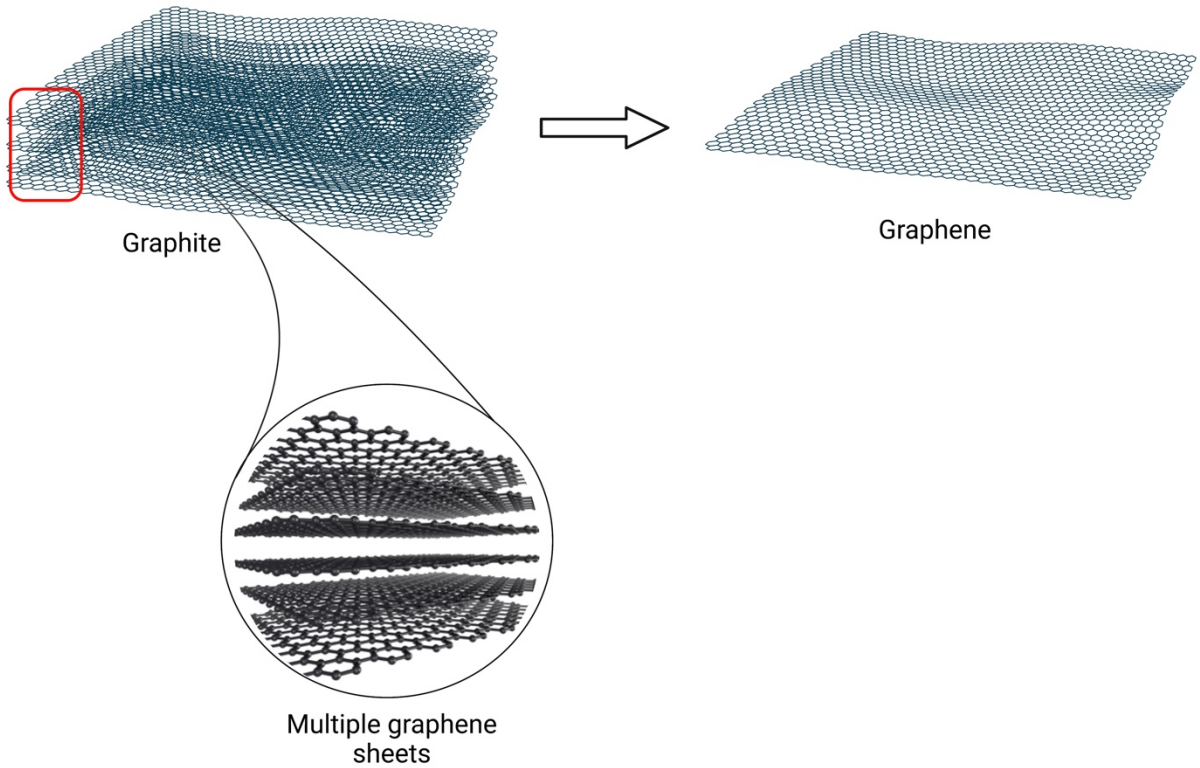

Figure 3.1: Illustration of graphite and graphene. Graphite is seen to have many layers of graphene sheets.

is categorized as a graphene derivative. Some of the graphene properties and applications are discussed in the appended **paper 4.**

3.1. Graphene derivatives

Graphene can be seen as a starting material for many carbon structures. For example, graphene monolayers can be stacked to form graphite, rolled in to form nanotubes, and wrapped to form buckyballs. Due to the sacristy of natural graphene and the high cost of monolayer graphene on the current market, low-cost alternatives such as *graphite nanoplatelets (GnP), graphene oxide (GO), reduced graphene oxide (rGO),* and functionalized graphene are used [48 - 55]. These graphene derivatives are widely used in research for many applications [2].

3.1.1. Graphene nanoplatelets

GnP is a few layers thick [54]. It contains multiple layers of atom-thick carbon sheets. This is a reasonably inexpensive alternative to pristine graphene as it provides similar surface conditions on a large scale. However, the thickness of GnP makes it opaque [51]. Further, it could also contain edge defects and heteroatoms depending on the production method. Nevertheless, GnP is also of interest to many researchers as it is used in labs to extract graphene layers using various exfoliation techniques, see Figure 3.2.

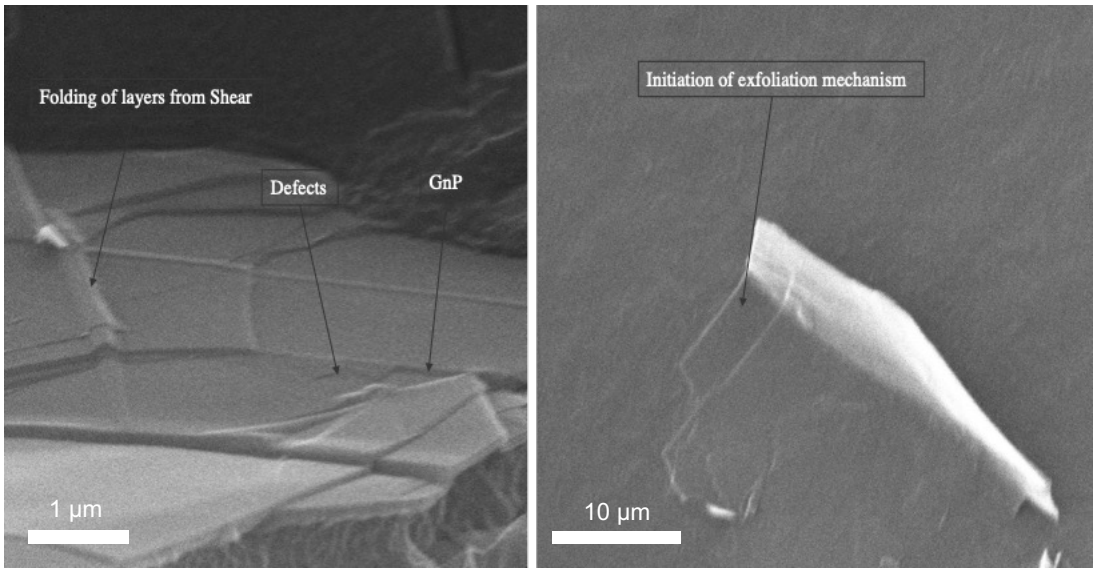

Figure 3.2: a) GnP on a polymeric substrate. It can be seen that GnP has structural defects. Due to in situ shearing of GnP in polymeric melt, GnP folding of sheets takes place. b) The exfoliation is non-uniform and a few layers thick by in-situ exfoliation.

3.1.2. Functionalised graphene

The functionalization of graphene is a chemical process of modifying its surface [56 -59]. This process transforms the surface characteristics, allowing the functionalized graphene to react with specific molecules, act as an interface in a nanocomposite, form bonds with polymers and more [56, 57]. The process is chemically achieved by attaching a chemical species (functional group) onto the surface of the graphene derivative. The type of functional group and its characteristics would vary the behavior of graphene. In principle, the selection of the functional group depends on the application of graphene [56, 59].

Furthermore, the attachment can be done both covalently and non-covalently [59]. Covalent functionalization includes nucleophilic and electrophilic functional groups [59], and non-covalent bonding primarily includes the bonding of cations, anions, or hydrogen to a π-electron on the surface of graphene [60-65]. *Thus, functionalizing graphene is similar to creating a painting on a blank canvas, where the graphene serves as the canvas and the act of functionalizing is like painting a piece of art on it. The type of functionalization and its characteristics depend on the scientist (artist) and the intended application (client).*

3.1.3. Graphene oxide

GO is a metastable form of graphene with induced defects [55, 58, 59, 66-69]. The defects are induced by incorporating oxygen. This transforms graphene from an sp2 hybridized to an sp3 hybridized state. In addition, transformation also modifies the planar structure of graphene [2]. The main difference between graphene and GO is that the latter is reactive. Further, the oxygenated carbon groups on the surface helps GO form hydrogen bonds and dipole moments in aqueous and organic mediums [66 - 69]. Finally, GO is an intimidate in many functionalisation processes of graphene [59]. This is because the reactive surface of GO can be used to attach functional groups onto it.

3.1.4. Reduced graphene oxide

When GO is elevated to higher temperatures the oxygen functional groups on its surface can decompose, which reduces GO and thereby reversing it to graphene. This graphene derivative is called rGO [70]. Although, in theory, the reduction of GO must provide graphene, it is not the case; rGO contains residual oxygen and other heteroatoms, as well as structural defects, see figure 3.3 [59]. These structural defects lower its quality when compared to graphene. Beyond high temperature, rGO can also be formed in the presence of reducing agents and electrical processes.

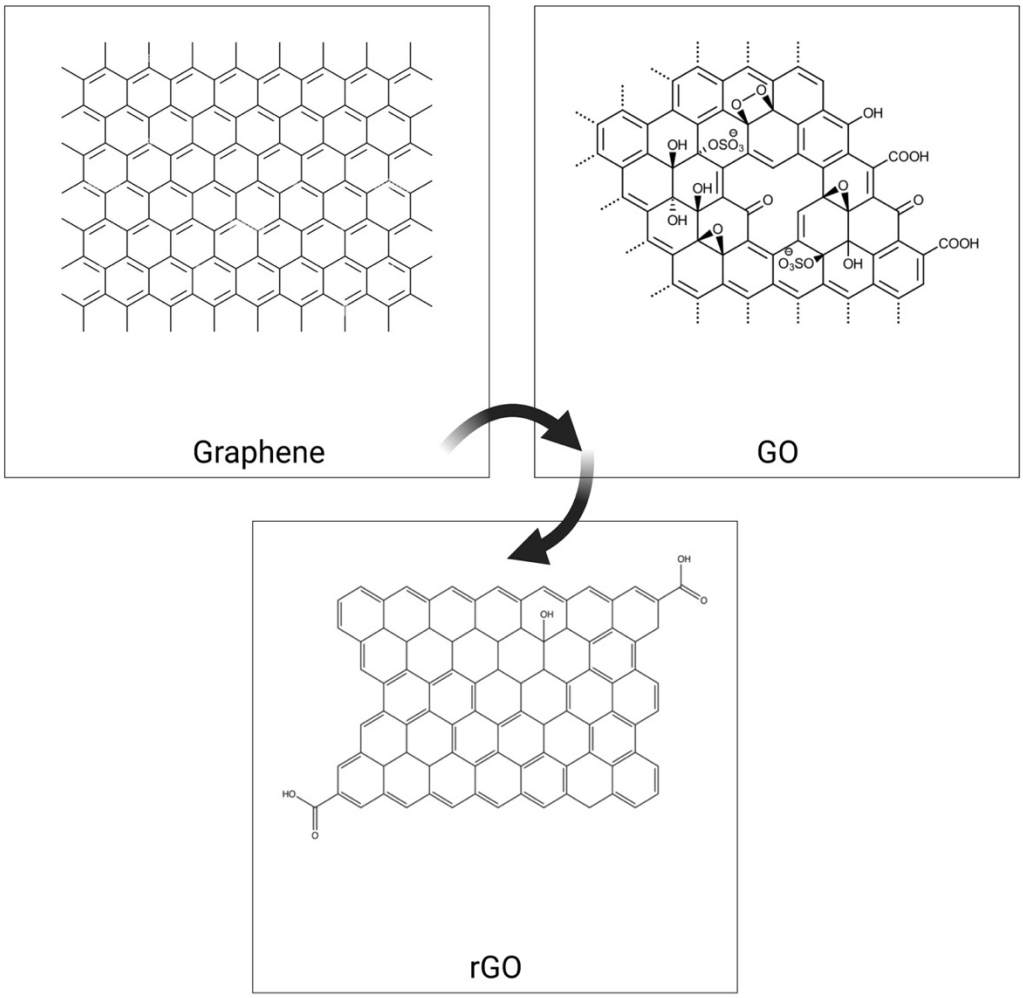

Figure 3.3: The figure illustrates theorized structures of graphene, GO, and rGO. Further, in the figure, graphene is transformed into GO, though modified hummer's method. Then GO is reduced to rGO.

3.2. Graphene functionalization

Functionalization can be achieved though many strategies such as chemical bonding through chemical reactions or bonding an ion via the π-electron [59]. Each strategy affects graphene's electronic and mechanical structure and has its own advantages and disadvantages [59]. For example, graphene has a delocalized π-electron cloud, which gives it its unique properties. However, functionalization leads to structural defects [2, 58, 59]. This can cause electrons and holes to be trapped at the structural defects due to the localization of electron density. Thus, resulting in a change of the electronic properties. For instance, the electrons are shared between the graphene and the functional group in covalent functionalization. The sharing of electrons results in an altering of graphene's electronic structure, electron density, and sp2 hybridized state [71]. In an electrophilic functionalization, the electron density increases due

to the addition of electron-withdrawal groups. Similarly, nucleophilic functionalization has an inverse effect on electron density due to the addition of electron-donating groups [59].

Nonetheless, both cases result in properties such as bandgap, electronic conductivity, electron mobility, charge distribution, electronegativity, and chemical reactivity being modified [2, 40, 58, 59, 71]. Likewise, in non-covalent functionalization, hydrogen bonding, ionic bonding, and van der Waals interactions are used to attach the functional group. Since electron sharing does not occur, sp2 hybridization is maintained. However, non-covalent functionalization can alter the electronic structure of graphene, thus, changing its electronic conductivity and chemical reactivity [59, 60-65, 72-76].

Besides the electron structure of graphene, the choice of the functionalization strategy and functional group can be based on the desired bond strength, performance of the nanocomposite or graphene, complexity and control of the synthesis process, and desired material performance [59].

For instance, covalent functionalization can often be a complex and time-consuming chemical process [77]. The surface preparation and the attachment of the functional group can be demanding. It could involve multiple steps, be expensive and use toxic chemicals, have controlled functionalization conditions, use complex post-processing to extract the functionalized graphene, and have low yield. However, covalent bonds are strong, making the corresponding functionalized graphene more stable and resistant to degradation. Another advantage of this functionalization strategy is that the process can be controlled, thereby allowing fine-tuning of the properties of graphene for specific applications. Finally, covalent functionalization can be used to introduce a wide range of functional groups, including both polar and non-polar functionalities, making it suitable for a wide range of applications.

Unlike the former, non-covalent functionalization can be a simple and rapid process that does not require specialized equipment or techniques [60 - 65]. It also helps the retention of the electrical conductivity of graphene to a great extent. Nevertheless, non-covalent bonds are weaker when compared to the former. Also, the simplicity of the functionalization reduces the ability to control and fine-tune the synthesis. Some of the functionalization strategies are given in figure 3.4. These interactions can occur through π–π interaction, cation–π interaction, anion–π interaction, graphene–ligand interaction, and H-π interactions [59]. Non-covalent functionalization can be used to attach polymers, small molecules, and proteins. It can also be used to prevent the agglomeration of graphene and make it soluble in poor solvents. For example, small polymer chains can attach to graphene through van der Waals interactions and sonication [71 - 73]. This deposition of polymers can shift the solubility of graphene sheets. In this thesis, we are interested in a form of non-covalent functionalization called Molecular Wedging, see figure 3.5.

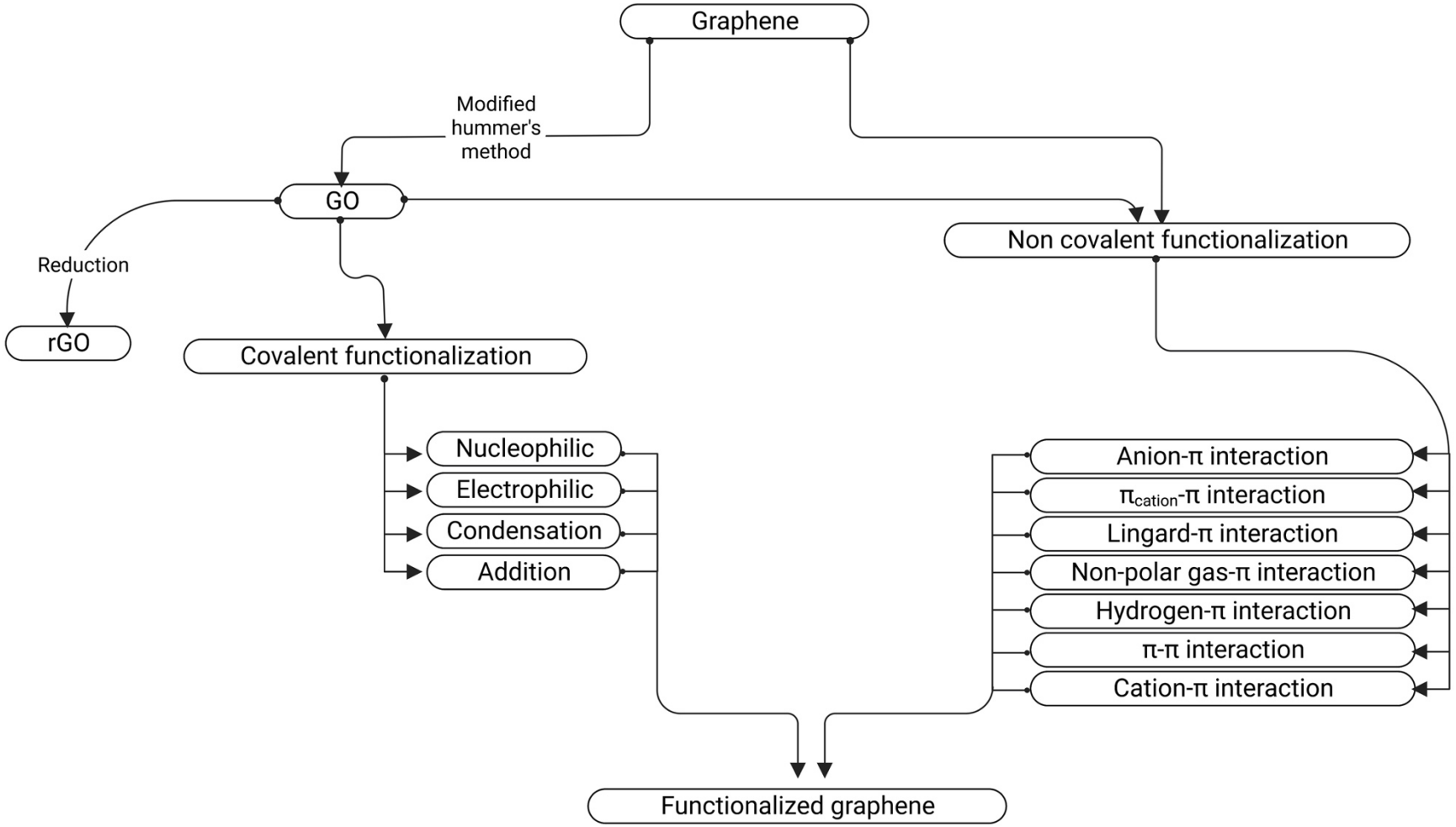

Figure 3.4: Flowchart about the strategies of graphene functionalization, oxidation and reduction. Graphene can be directly functionalized through non-covalent methods by utilizing the π-electron interaction. Graphene can also be oxidized through the modified hummer's method and then covalently functionalized with specific species depending on the application.

3.3. Molecular wedging

Molecular wedging (called Molecular wedging method in **papers 2 and 3**) is a non-covalent functionalization strategy [62]. In this method, small aromatic molecules (such as 1-pyrene carboxylic acid) are attached to the surface through π–π interaction. This is achieved through solvent-assisted swelling, physical wedging, and electrostatic interaction. Graphene exfoliation is also an outcome of this functionalization. An illustration of the steps involved in Molecular wedging is presented in figure 3.5. Besides organic molecules, the method can also be used to attach polymers, peptides, and dyes [59, 62]. The application of molecularly wedged graphene (MW-graphene) ranges from energy storage, sensing, and catalysis. In this thesis, we use MW-graphene in our model bitumen.

With this method the aromatic molecules are first dispersed in an appropriate solvent. In this thesis, we used a mixture of water and methanol. Following this, graphene is also dispersed in the solvent, and the mixture is sonicated. The sonication causes a slight separation of the graphitic layers, followed by a solvent-assisted swelling. This causes intercalation in graphene. *Intercalation* refers to the insertion of molecules or ions between the layers of a material, causing them to separate. The intercalation allows hydrophobic moiety of the aromatic molecule to interact with graphene layers through π–π interaction. At the same time, the hydrophilic moiety faces the solvent. Finally, the hydrophilic moieties repel each other due to their similar charge, which causes the graphene sheets to separate and exfoliate [62].

Factors such as pH, temperature, solvent, chemical nature of aromatic molecule, and charge induced by graphene in the solvent will play a significant role in successful functionalization [60- 65]. Thus, not all solvents will be "good solvents", and the solvent selection will depend on the desired aromatic molecule and the final chemical nature of the functionalized graphene [62]. We have discussed the choice of aromatic molecule and their impact on graphene in **papers 2 and 3**. Overall, molecular wedging is a simple, non-toxic, and cheap non-covalent functionalization strategy that requires only one molecule.

In the next chapter (**chapter 4)**, we discuss the how and why we use the functionalization strategy of molecular wedging, to use the potential of graphene in bitumen.

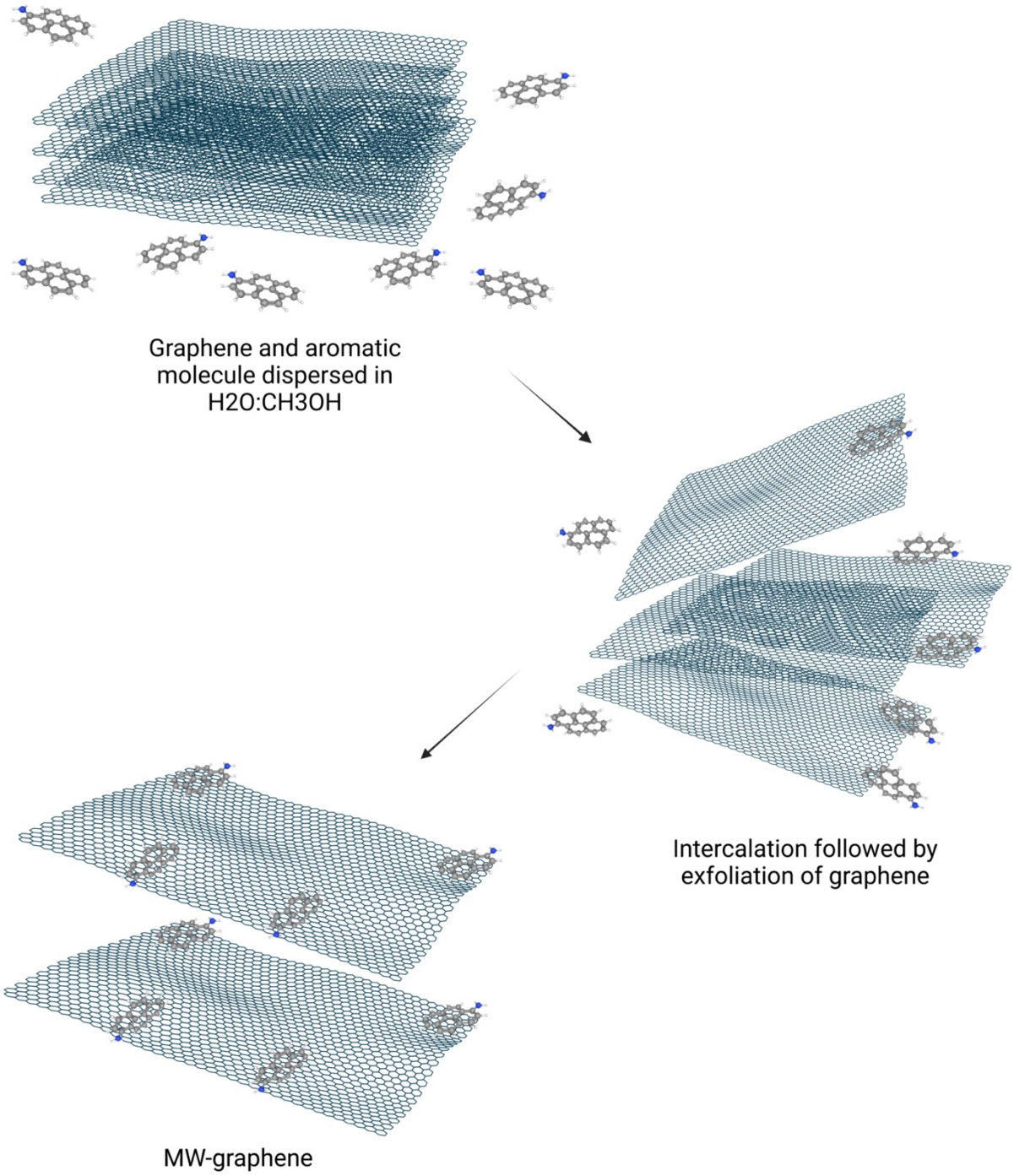

Figure 3.5: Steps involved in non-covalent functionalization of graphene by the Molecular wedging.

4. Functionalization of graphene for application in bitumen

In **Chapter 1**, we discussed the potential uses of graphene in bitumen. However, to effectively utilize the desirable properties of graphene, its electronic structure must be maintained. This can prove difficult because graphene, in its pure form, is nearly inert, making it difficult to disperse and stabilize in an apolar solvent like saturates (liquid phase of bitumen). To overcome this, the graphene must be functionalized to dispersal and stabilization in saturates while preserving its electronic structure. Additionally, we have to account for agglomeration without adding further chemicals.

4.1. Functionalization criteria use graphene in bitumen

- To self-stabilize graphene in saturates, its surface can be functionalized with hydrophobic functional groups or polymers, e.g., hexadecyltrichlorosilane or octadecyltrichlorosilane [78]. Such a process would involves converting graphene into GO and functionalizing it [59]. This process can alter graphene's electronic structure [39, 55, 59]. Additionally, the process can be expensive and requires a significant amount of chemicals.

- Despite functionalizing its surface, stabilizing graphene sheets over elevated temperatures or for extended periods of time can still be challenging due to its large aspect ratio and flexible structure. Furthermore, the chemical composition of bitumen is complex and. constantly changing (**refer to chapter 2 and 5**) [1, 28]. This can render the stabilization mechanism of the graphene ineffectively. Additionally, while using stabilizing agents (like surfactants or polymers) may appear logical, the complex and diverse chemical nature of bitumen might result in other molecules competiting for the same stabilizing agents [2, 28]. Finally, stabilizing and protecting graphene by coating it with a polymer will also alters its chemical structure or insulates it from direct interaction with bitumen.

- The selected functionalization strategy must also be sustainable. A simple method that allows for the reuse or recycling of solvents [77 ,79], have few steps, not use complex distillation or drying processes, and use non-toxic chemicals and solvents, is disable. Therefore, these design constraints limit the use of GO, restricting the options for solvents, functional groups, and many functionalization strategies.

- Ensuring phase compatibility is crucial between the functionalized graphene and asphaltene aggregates. In **paper 1**, we showed that introducing certain graphene derivatives can modify the phase stability of bitumen. The asphaltene aggregates give bitumen its unique properties, but the addition of functionalized graphene can disrupt their stability, leading to flocculation, phase separation, and ultimately, a negative impact on bitumen. To complicate matters, asphaltenes and the resins have a diverse chemical structure and composition (**refer to chapter 5**), which can vary from source to source [28]. This means that functionalized graphene must be compatible with all chemical configurations of asphaltene and resins [28]. Thus, designing a functionalized graphene to be phase compatible in bitumen is an important task.

- Finally, to ensure the desired properties of functionalized graphene in bitumen, it must remain chemically stable. The vast array of chemicals in bitumen could lead to chemical reactions, which could transform the nature of the functionalization on graphene. This, in turn, could negatively impact the interaction potential and stability mechanism of the graphene in bitumen. Therefore, it is essential that the functionalized graphene has a simple and predictable chemical composition.

These are some of the criteria that were evaluated during the selection of the functionalization strategy of graphene. It was evident that the best functionalization strategy was to utilize a simple functional group that does not require numerous chemicals or functionalization steps. Therefore, *molecular wedging* was seen as the best functionalization strategy. We discuss the criteria in more detail in **paper 4**.

4.2. Proposed Solution

Molecular wedging is a potential approach to functionalizing graphene for use in bitumen [62]. Despite being an untested method in this field, it aligns with the desired criteria and presents a straightforward and effective solution. We can the functionalized graphene produced through molecular wedging *MW-graphene*. This functionalization process requires

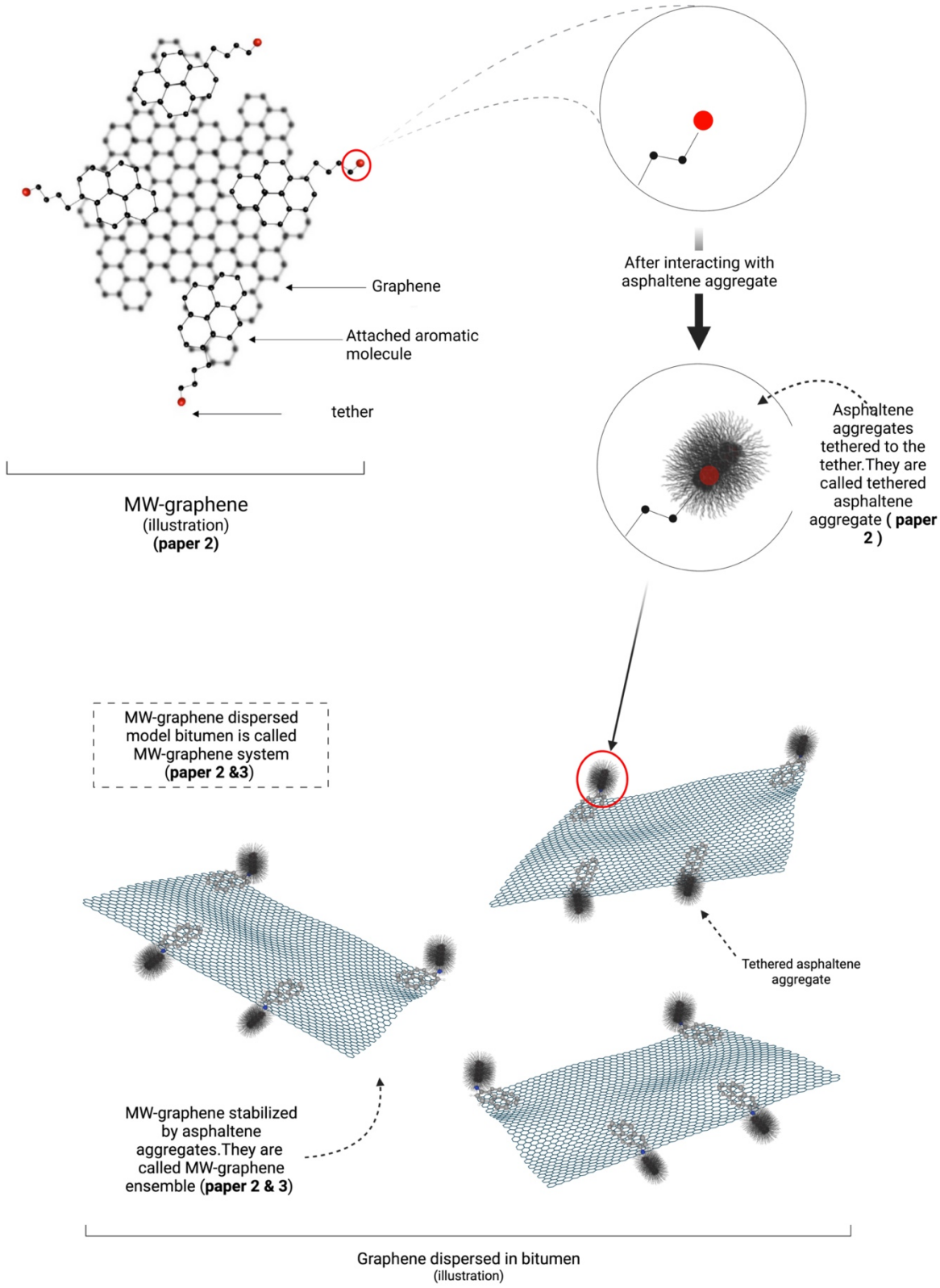

Figure 4.1: An illustration of asphaltene aggregates and MW-graphene interaction that will lead to stabilizing and dispersing graphene in bitumen.

only water and methanol, both of which can be recovered and reused on a larger scale. Moreover, the process only needs a single molecule for functionalizing graphene. Also, exfoliation, dispersion, and functionalization can be simultaneously achieved.

Thus, we propose that our MW-graphene functionalization strategy will be sustainable, naturally stabilize in bitumen, and improve the material properties of bitumen, and satisfy all our functionalization criteria. We have discussed the stabilization mechanism and the structure of the MW-graphene in detail in **paper 2**.

4.3. Hypothesised application of MW-graphene

Asphaltene aggregates are a key component of bitumen and play a significant role in determining its properties [1]. By modifying the structure of asphaltene aggregates using graphene, it is possible to alter the properties of bitumen. The interaction between MW-graphene and asphaltene aggregates will ensure this. Further, the interaction between the functional group on the surface of graphene and asphaltene aggregates, combined with the large surface area of graphene, can distribute asphaltene aggregates across the surface. This distribution of asphaltene aggregates has two main benefits.

Firstly, it could reduce the agglomeration of asphaltene aggregates, leading to a more stable distribution of these aggregates and thus an *inhibitor-like effect.* This is a new approach to using graphene as an asphaltene inhibitor.

Secondly, the MW-graphene might distribute asphaltene aggregates across the surface of graphene also helps to distribute the polymer tail (of asphaltene aggregate). These polymer tails reducing the probability of direct interaction between MW-graphene and might also help reduce agglomeration. In figure 4.1 we present an illustration of the potential interaction between asphaltene aggregates and MW-graphene.

Finally, the preservation of the electronic structure of graphene in MW-graphene, along with its potential interaction with asphaltene aggregates, will result in the distribution of highly thermally conductive nanoparticles in bitumen. This can help enhance the thermal conductivity of bitumen. We discuss the mutual stabilization and functionalization criteria in detail in **paper 3**.

4.4. Other functionalisation strategies

In this thesis, we explored multiple functionalization strategies. Some were even tested, not pursued due to it not meeting the design criteria or being less efficient compared molecular wedging. One of the strategies evaluated was functionalizing graphene with asphaltene. This

involved converting graphene into GO, then functionalizing it with epichlorohydrin. Later, binding asphaltene to this graphene's surface through a ring-opening reaction.

Also, we developed MW-GO (molecularly wedged GO) as a follow-up to the findings from **paper 1**. The results of this functionalization and its impact on functional groups are presented in **chapter 8.**

5. Asphaltene aggregate systems

In **chapter 2,** we presented the challenges of using bitumen in this study due to its chemical complexity and physical characteristics. This motivated us to use a model bitumen in this study. To make the model bitumen, asphaltene was extracted from bitumen and the appropriate solvent and surfactant were selected to disperse the asphaltene. We will discuss this process, the motivations for selecting the specific solvent and surfactant, and the limitations of the model bitumen in this chapter.

5.1. Asphaltene extraction

Asphaltenes precipitate in the presence of alkanes such as n-heptane due to their non-polar nature [28-29, 80]. This was the method by which asphaltene was extracted in this thesis. The exact procedure is discussed in **papers 1-3**. The properties, composition, and structure of asphaltenes can vary greatly depending on the source of the bitumen [28]. So, to embrace the complexity and ensuring that our results were as comprehensive as possible for all asphaltenes, we mixed bitumen from different sources, oxidized the mixture, and then extracted the resulting asphaltenes. This allowed us to create a mixture of different asphaltenes with a broader range of properties. Additionally, the oxidation process might have also altered the chemical structure of some of the asphaltenes, thereby further increasing the diversity of the extracted asphaltenes.

Figure 5.1 (A) shows the setup used for asphaltene extraction using a lab setup. The figure also shows the centrifuged and dried asphaltene. Due to the centrifugation, asphaltene appeared to be a black solid lump (5.1 B). This solid lump was investigated under electron microscope (5.1 C). Further, after redispersing it in toluene the solid lump immediately disappeared and was uniformly dispersed in toluene (figure 5.2A). As shown in figure 5.2(B), the dispersed asphaltene was observed under a bright field microscope. The same asphaltene was charactristized using XPS and FTIR and are presented in **paper 1**.

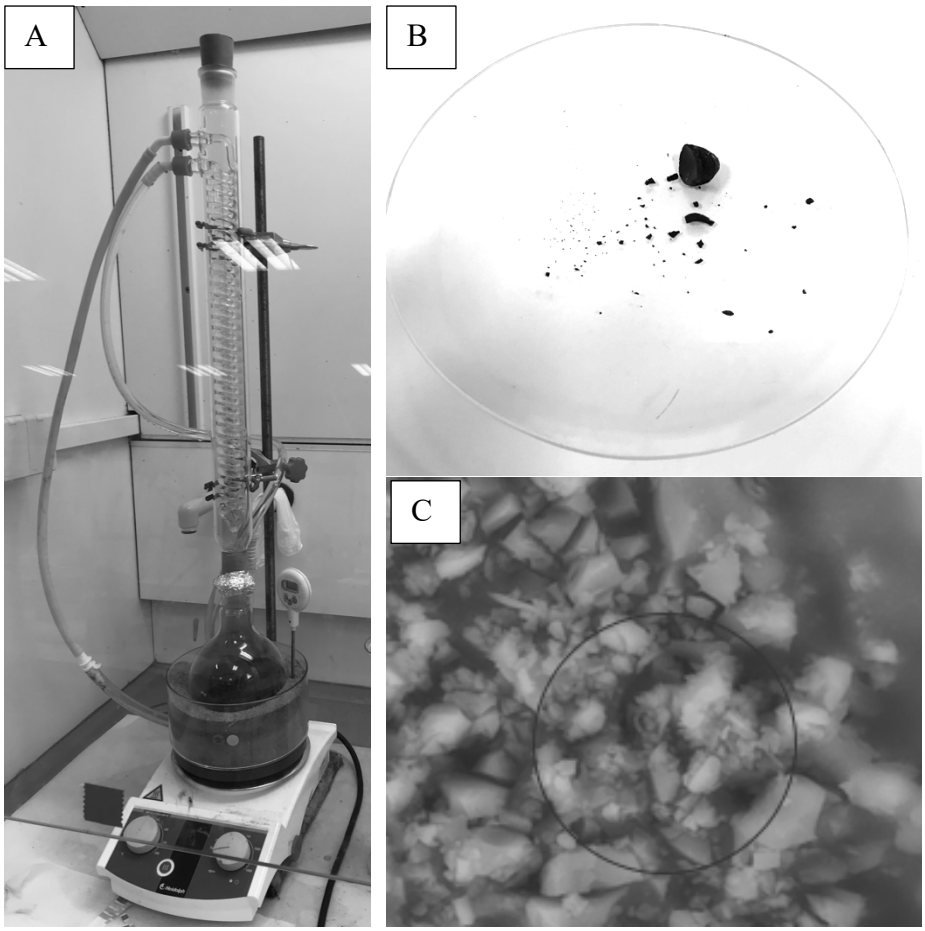

Figure 5.1: A) The set up for extraction of asphaltene from bitumen; B). The extracted asphaltene in the form of a solid lump after centrifugation and drying; C) The solid lump under an electron microscope.

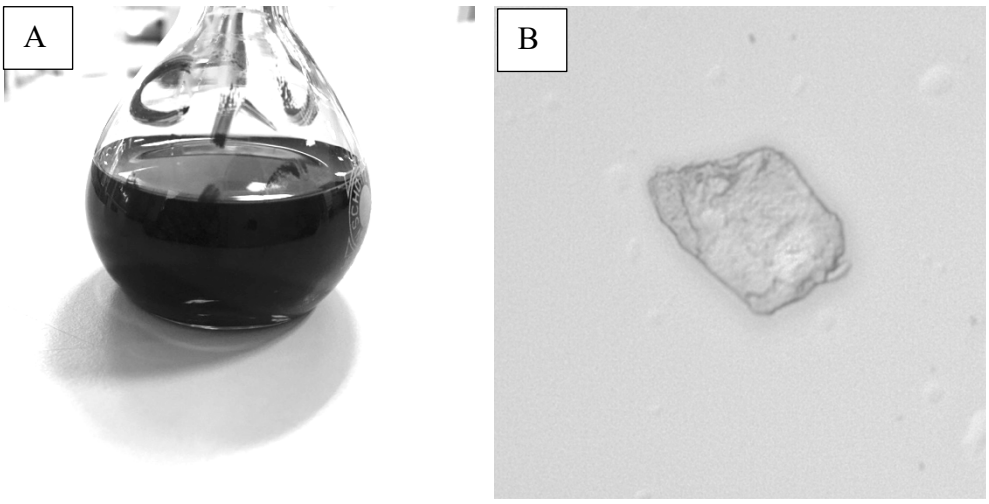

Figure 5.2: Left: The solid lump of asphaltene dispersed in toluene at a concentration of 5mg/ml; right: dispersed asphaltene nanoaggregate under brightfield microscope.

5.2. Selection of solvent

Asphaltenes can be dispersed in both organic compounds and oils [81 – 100]. However, the stabilization mechanism of asphaltenes in both is different. Organic compounds are more effective in dispersing asphaltenes than oils. This is because organic compounds can directly interact with the asphaltene and form a stable dispersion [81 - 88]. In contrast, asphaltenes are stabilized in oils using a surfactant or inhibitor [89 - 100]. The surfactant or inhibitor adsorb onto the asphaltene molecules and forms a protective layer around them, which can lowers the surface tension, and also prevents the asphaltene molecules from. The choice of solvent, either oil or organic compounds, can significantly affect the solubility and behavior of asphaltenes, surfactants, or graphene derivatives. Using oil and surfactant. would closely mimics the actual composition of bitumen, and provide a more realistic representation of bitumen. On the other hand, organic compound can facilitate us to isolate and investigation of the interaction between graphene derivatives and asphaltene.

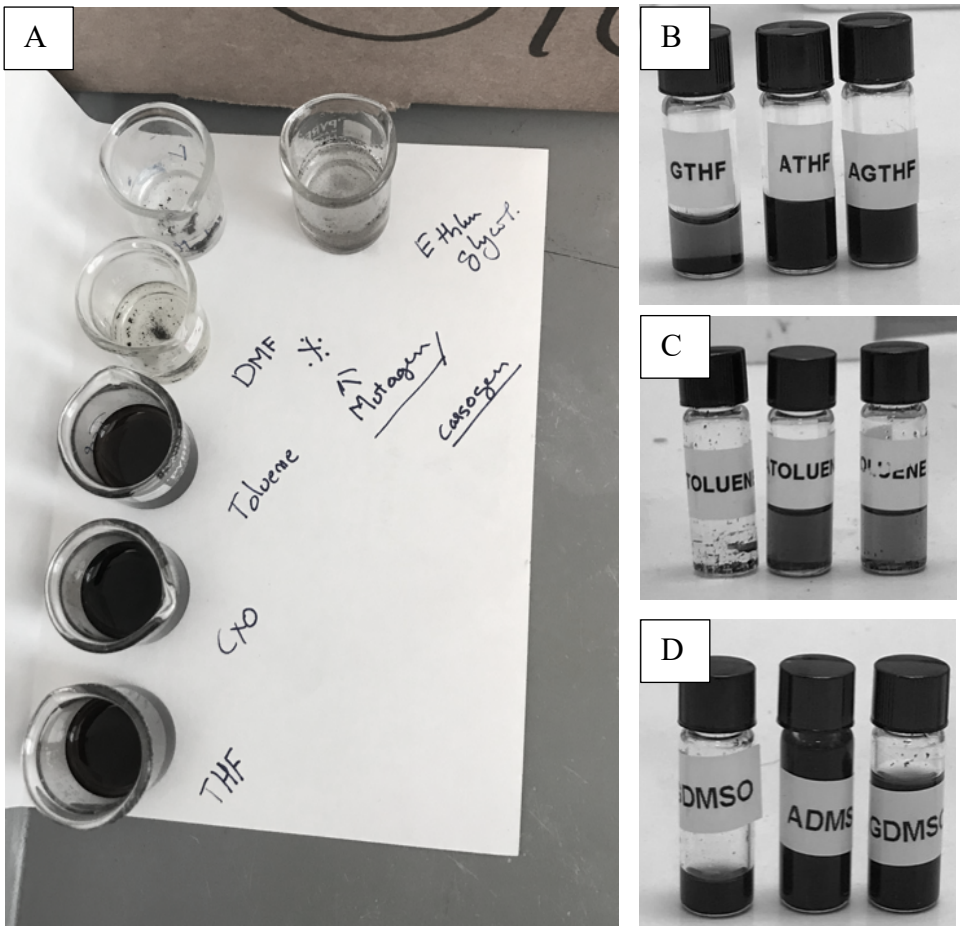

Figure 5.3: A). Asphaltene dispersed in various solvents; GO, asphaltene, and GO + asphaltene dispersed, respectively, in B). THF, C). toluene, and D). DMSO.

At the beginning of the thesis work, we evaluated both options, i.e., utilizing organic compounds or oils as a solvent. However, working with organic compounds posed more challenges than using oil.

We employed the widely used Hansen solubility parameter to determine appropriate solvents for asphaltenes. The Hansen solubility parameter (δ_T) considers hydrogen bonding (δ_H), dipole moments (δ_D), and dispersibility (Hildebrand solubility parameter. (δ_p) [88]. As shown in Table 3.1, we created a list of organic compounds, their solubility parameters, surface energy (Y_L^1), and the molar mass. The solubility parameters of asphaltenes in the literature vary widely, ranging from 18 $MPa^{1/2}$ to 25 $MPa^{1/2}$[88]. So we took an average of the solubility parameters. Next, we calculated their compatibility (solubility), and simultaneously reviewed their dispersibility for asphaltenes in the compatible organic compounds from the literature [81 - 88].

Table 5.1: Hansen solubility parameter, surface energy, and molar mass of various aromatic solvents.

Solvent	δ_D ($MPa^{1/2}$)	δp ($MPa^{1/2}$)	δ_H ($MPa^{1/2}$)	δ_T ($MPa^{1/2}$)	Y_L^1 (mJ/m^2)	Molar mass (g/mol)
Toluene	18.0	1.4	2.0	18.1	27.9	92.13
p-Xylene	17.6	1.0	3.1	17.9	27.9	106.17
Cyclohexanone	17.8	6.3	5.1	19.6	34.4	98.14
Tetrahydrofuran	16.8	5.7	8.0	19.5	26.7	72.11
N-N-Dimethylformamide	17.4	13.7	11.3	24.9	34.4	73.09
Carbon tetrachloride	17.8	0.0	0.6	17.8	26.3	153.82
Dichlorobenzene	19.2	6.3	3.3	20.5	35.7	147.00
Carbon disulfate	19.9	5.8	0.6	20.7	32.25	76.14
Cyclohexane	16.8	0.0	0.2	16.8	24.7	84.16
Dimethyl sulfoxide	17.4	13.7	11.3	24.9	42.9	78.13
Water	15.6	16.0	42.3	47.8	72.7	18.20
N-Methyl-2-pyrrolidone	18.0	12.3	7.2	23	44.6	99.13
Trichloromethane	17.8	3.1	5.7	18.9	26.7	149.19
Methanol	15.1	12.3	22.3	29.6	22.1	32.04

Table 5.2: The dispersibility of asphaltene and graphene in different organic compounds.

	Solvent	**Asphaltene** (mg/ml)	**Graphene oxide** (mg/ml)
1	Toluene	10.5	0.00157
2	P-Xylene	Good solvent (no data)	-
3	Cyclohexanonee	Good solvent (no data)	-
4	Tetrahydrofuran	1.7	0.00215
5	N-N-Dimethylformamide	5.2	0.00175
6	Carbon tetrachloride	2.93	-
7	Dichlorroobenzene	1.0	0.00191
8	Carbon disulfate	1.0	-
9	Cyclohexane	Good solvent (no data)	-
10	Dimethyl sulfoxide	-	Fair solvent (no data)
11	Water	-	0.0066
12	N-Methyl-2-pyrrolidone	-	0.0087
13	Triichloromethane	-	0.0013
14	Methanol	-	0.00066

The list of organic compounds and the dispersibility of asphaltenes in each solvent is presented in Table 3.2. As can be seen from figure 5.3(A), asphaltene was dispersed in various solvents to verify the calculated dispersibility.

Depending on the functionalization, graphene derivatives can be both hydrophilic and hydrophobic. Thus, a good solvent for asphaltenes might be a bad solvent for a graphene derivative. As an example, we have also provided the dispersibility of GO in different solvents [101]. This investigation showed that a partly suitable solvent for both asphaltenes and GO was tetrahydrofuran (THF), see figure 5.3 (B). However, while we could disperse both GO and asphaltenes in THF and obsessive their interaction, it was evident that this approach would be difficulty during graphene functionalization. It was also evident that the interaction between graphene derivatives and asphaltene in such a solvent is not represent what would be expected in bitumen. Thus, the solvent approach was abandoned. Further, most solvents that can disperse asphaltenes are toxic and can have long-term effects on human

health; thus, they were considered dangerous to use in the lab and during characterization. Both were also dispersed and observed in toluene (5.3 B) and DMSO (5.3 C).

Figure 5.4: Asphaltene, GO, and both asphaltene + GO dispersed in saturates + DBSA.

After weighing the available options, we decided to use group-II base oil (**paper 1**). Although group-II base oil is a close approximation of saturates, some differences exist. Saturates are composed of a mixture of non-aromatic linear, branched, and cyclic alkanes, with a small proportion of naphthenic hydrocarbons and trace amounts of other organic compounds. Group-II base oils also contain non-aromatic hydrocarbon compounds, but they are highly refined, narrowing the range of hydrocarbons and reducing impurities. This refining process can also remove naphthenic hydrocarbons and aromatic molecules, which are found in saturates, leading to a lower viscosity. The reduction in viscosity is welcomed as it makes it easier to observe precipitation, as the effect of viscosity on precipitation is minimized. The FTIR spectrum of the oil is presented in **paper 1**. Finally, we recognize the tradeoff of using group-II base oil and paraffin oil, instead of pure saturates.

5.3. Stabilization of asphaltene in model bitumen

In bitumen, the polar functional groups on both resins and asphaltenes interact, resulting in the stabilization of asphaltenes [1, 28]. Many factors can influence their strength [1, 28].

Using these natural resins in the model bitumen would lead to a lack of control and consistency in our research [28]. For instance, resins have a complex chemical structure, making them unpredictable and harder to work, consequently affecting the ability to reproduce the results. For instance, if resins interact poorly it would lead to separation and reduced effectiveness of asphaltene aggregate formation. On the other hand, a strong interaction between resins and asphaltenes can lead to excess asphaltene aggregates, accelerating the precipitation [1, 22-24].

Furthermore, resins can sometimes destabilize asphaltene aggregates by acting as a surfactant, solvent, or by forming complexes with asphaltene. As a surfactant, it reduces the surface tension of the bitumen, causing the asphaltene aggregates to break apart. In some instances, if resins act as a solvent, the asphaltene aggregates can dissolve and disperse. Finally, the formation of complexes reduces the stability of the asphaltene aggregates [1, 22-24, 28, 89]. Finally, resins can also prefer to interact with other resin molecules, thereby acting as a barrier between the asphaltene nanoaggregates [28]. Overall, the interaction between asphaltenes and resins is complex, affecting the accuracy and reproducibility of the results of our research.

Due to all these reasons, from the perspective of this research, we decided to use dodecyl benzene sulfonic acid (DBSA). DBSA is an amphiphile with a hydrophobic tail and a hydrophilic head. Numerous studies have shown how and why DBSA is an excellent bitumen surfactant [89-100]. Unlike resins, DBSA is theorized not to engage in peptization behavior with asphaltene but rather act as an inhibitor [89 - 95]. It also has many advantages over resins due to its simple chemical structure, making it easier to handle and make predictions its the interaction with asphaltene [89 - 95]. So, using DBSA will help control the model bitumen's uncertainties. Figure 5.4 shows asphaltene and GO dispersed in saturates (group II base oil) and DBSA. Also, the FTIR spectrum of DBSA is presented in **paper 1 and 3.**

5.4. The asphaltene aggregate system

The model bitumen developed in this thesis is called an asphaltene aggregate system. It was used to isolate and study the interaction between graphene and asphaltene aggregates. We describe this system in detail in **papers 2 and 3.** The asphaltene aggregate system used in **paper 1** has a composition of 5% asphaltenes, 5% DBSA, >90% saturates.

Group-II base oil (SR60 from Chevron) is used in **papers 1 and 2** as the saturates, and paraffin oil (from sigma) is used as saturates in **paper 3**. The FTIR spectrum paraffin oil is presented in **paper 3**. Since aromatics are theorized to engage in more complex interactions with asphaltene aggregates, we did not use any aromatics. The ratios of the various fractions were selected based on literature, where some researchers have had confirmed the formation of asphaltene aggregates in saturates. Finally, figure 5.5 illustrates the difference between asphaltene aggregate system and bitumen.

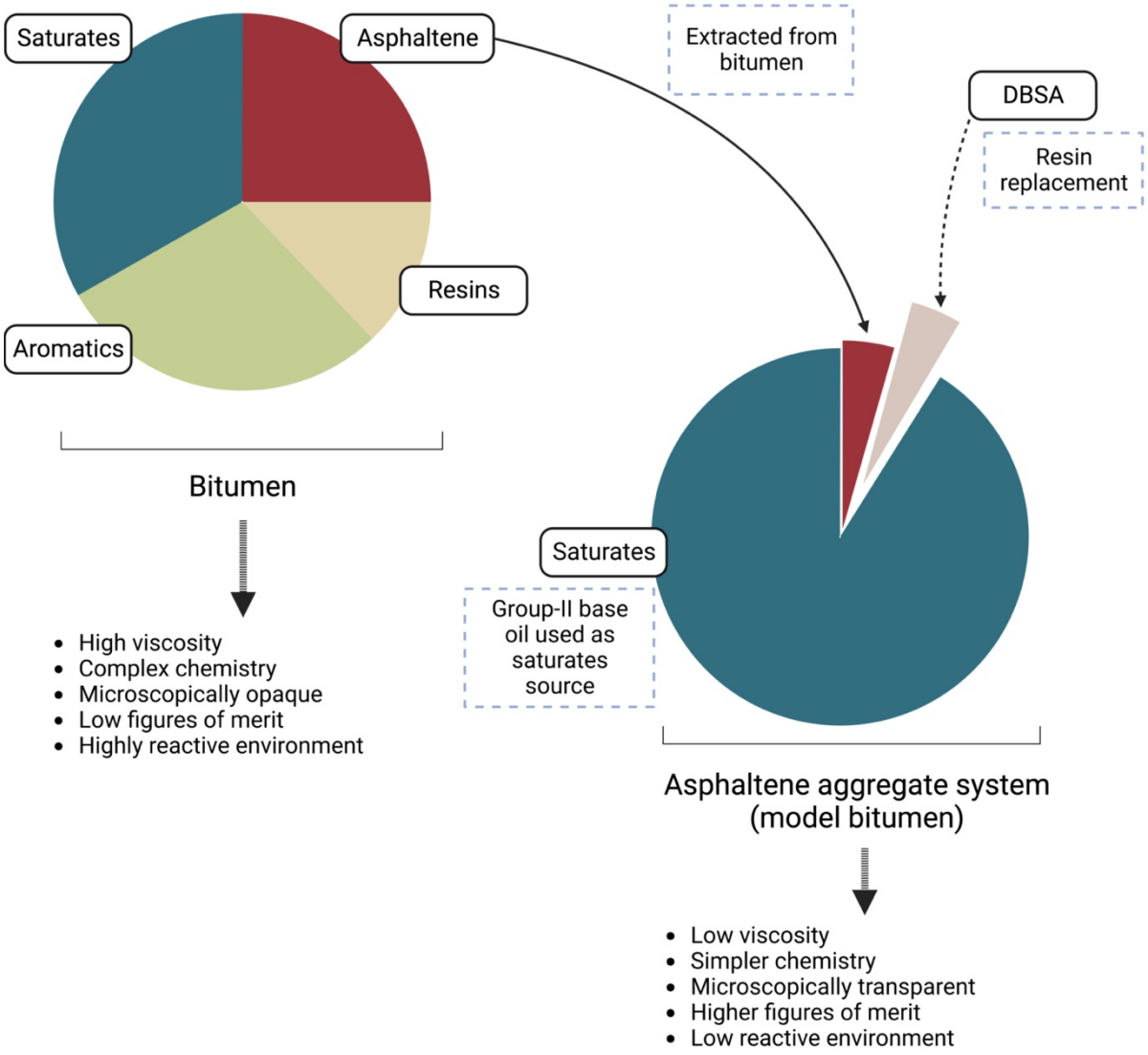

Figure 5.5: Illustration of the difference between bitumen and asphaltene aggregate system.

5.5. Limitations of using the asphaltene aggregate system

The asphaltene aggregate system used in this thesis is synthetic bitumen that we developed as a model system. This approach has its limitations. These limitations come from our attempt to reduce the chemical complexity and variables that can reduce the accuracy and reproducibility of our results.

The stabilization mechanism of asphaltene aggregates in our asphaltene aggregate system have some differences from bitumen. Furthermore, the roles of each fraction of bitumen and the physical nature of asphaltenes are also unknown; thus, the findings of this thesis might be affected by these factors when adapting the results to bitumen. Hence, due to such reasons

the conclusions formed in this thesis might require additional testing and characterization to accurately reflect the actual behavior of graphene in bitumen, particularly concerning the precipitation pattern in the complex and dynamic nature of bitumen.

All of the discussed reasons can limit the transferability and generalizability of our findings. Nonetheless, bitumen has a complex chemistry and stabilization mechanism that is not fully understood, and so, studying the interaction between graphene and asphaltene aggregates in bitumen will also be equally limited, as discussed in **paper 1**.

6. Characterization techniques

Characterization techniques utilized in this thesis can be categorized into microscopy, spectroscopy, diffraction, rheology, thermal analysis, and chromatography. The characterization techniques were selected based on their ability to provide information about the interaction behavior of graphene derivatives and asphaltene aggregates. For the validation of results, complementary techniques were used.

6.1. Microscopy

6.1.1. Scanning electron microscopy

Scanning electron microscope (SEM) is a form of high-resolution microscopy that uses electrons as a probe. It is used when detailed information about the structure of the material is needed. As shown in figure 6.1, an SEM has an electron gun, electron optical system and electron analyzer. The electron gun can be a high energy source of electrons; this source can be tungsten-hairpin (T-h), a LaB_6 source or a field emission source (FES). While the high energy source has an energy spread of 3 eV, the FES source has a range of 0.3 eV [102]. Rayleigh resolution is a major limiting factor for microscopy studies. It is the smallest distance at which two objects can still be resolved as being separated. Thus, the resolution limit (r) of a microscope is proportional to the wavelength (λ) and the numerical aperture (NA).

$$r = \frac{0.61\lambda}{NA} \tag{01}$$

So, for a bright-field microscope, the resolution highly depends on the source of light, which is between 0.4 μm and 0.7 μm [102]. In SEM, one could describe the source with the de Broglie resolution, with approximating the resolution to be about 1 nm for 30 kV [103]. However, th intersection volume is typically around a few nanometer. An advantage of SEM when compared to other electron microscopes (such as transmission electron microscopy) is its ability to maintain its depth of focus compared to a special resolution. The depth of focus is the ability of the instrument to maintain a focus across a field of view, regardless of the surface roughness. The region of effective focus is called D. It is within the plane of optimum focus and

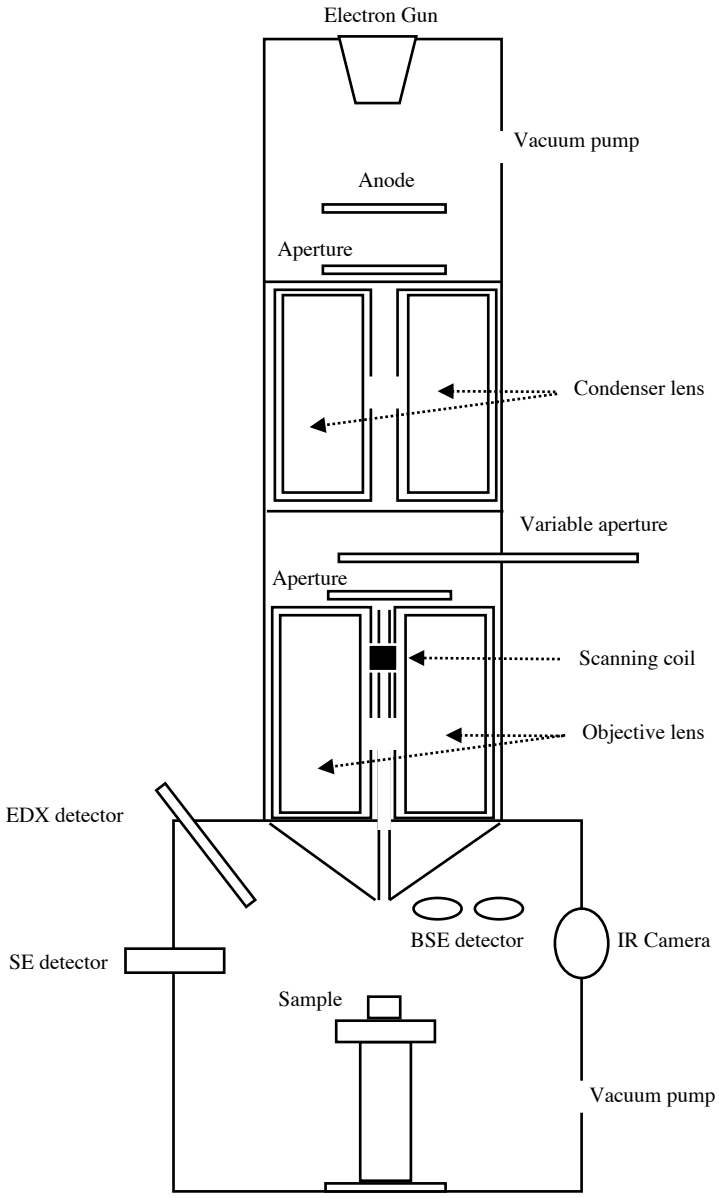

Figure 6.1: Schematic representation of a SEM.

$$D \approx \frac{2r}{\alpha} \tag{02}$$

where α is the beam divergence, so, this is maintained by either reducing the magnification of the divergence angle.

Surfaces of samples have multiple electron energy range, i.e., auger electrons, secondary electrons, backscattered electrons. Following this, the interacting electrons generate characteristic x-rays and continuum x-rays. It could be said that interacting with different kinds of regions will provide different radiation. The information retrievable from each region is proportional to the atomic number, angle of incidence and accelerated voltage. In SEM, the

two primary electron regions used are with backscattered and secondary electrons. While the former is used to attain compositional contrast, the latter provides topological contrast. Secondary electrons are low energy electrons. Surface chemistry can cause a potential barrier for secondary electrons, and surface morphology can lead to absorption of secondary electrons. Depending on the atomic number, the number of backscattered electrons varies, they are directly proportional. This type of elastic scattering is independent of accelerated voltage, unlike secondary electrons [103-104].

For this study, SEM was used to attain a close imaging of the larger structures of the particles in **paper 1**.

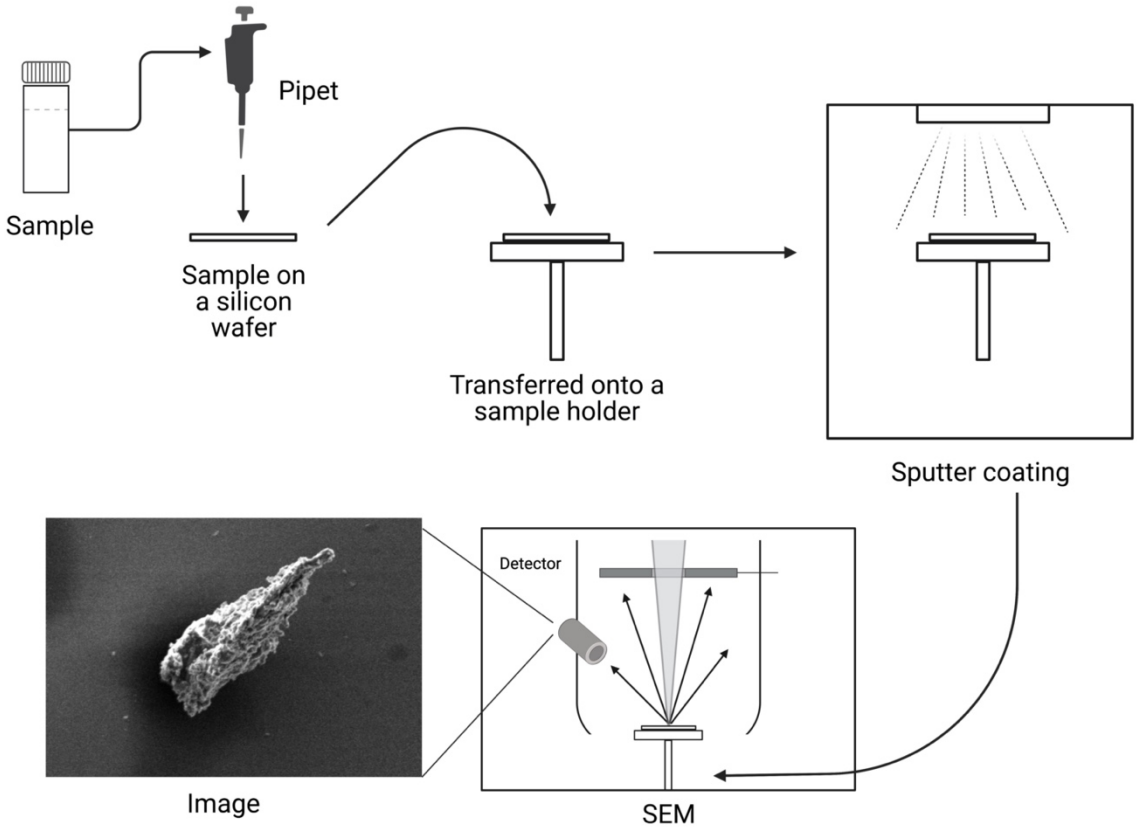

Figure 6.2: Schematic representation of the sample preparation and the electron microscopy image is shown.

An example of the sample and a microscopy image is presented in figure 6.2. The figure shows the procedure used in this thesis to prepare samples for SEM. Some samples are nonconductive and thus will not provide a good image in SEM due to surface charging, in those cases, the sample is sputter coated with gold or platinum to improve contrast. The samples, in the thesis, were transferred to a silicon wafer and then sputter coated with platinum before viewing it under a SEM.

6.1.2. Transmission light microscopy/ brightfield microscopy

Brightfield microscopy is a simple optical microscopy technique [102]. In brightfield microscopy, a sample is placed on a glass slide, and illumination is transmitted through it. The illumination source is generally white light. Further, the contrast in the sample image is caused due to the refractive index of variations in the sample [102]. The technique can be used in ambient light and pressure and is a powerful tool for observing the features in colloidal systems. Additionally, options such as polarized light, false coloring, and phase contrast can be used to differentiate features on samples [102, 105]. An illustration of the microscope is shown in figure 6.3. The figure shows the how the light is illuminated through a sample and passed through lenses and collected and transmitted to a computer. The figure also presents the difference between normal light and polarized light. In brightfield mode, the absorbance of light gives the contrast, and in the phase contrast mode, the real part of the refractive index gives rise to the contrast in the sample.

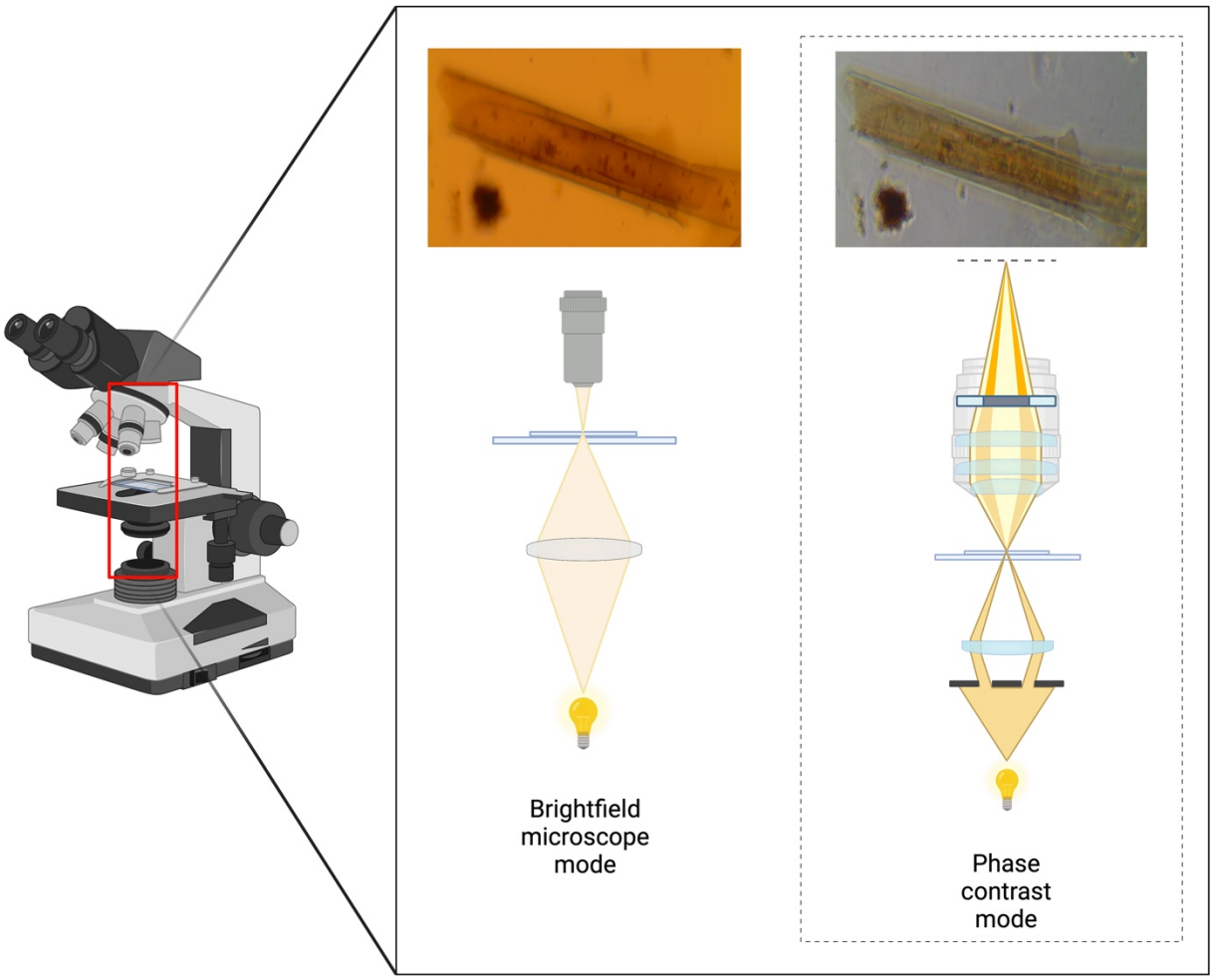

Figure 6.3: Schematic representation of a brightfield microscope. The figure also shows MW-graphene ensemble in brightfield and phase contrast mode.

It was used in **papers 1,2, and 3.** The technique was very helpful in observing structures and structural changes over time. This included, observing phase separation in **paper 1**, formation and growth of stable ensembles in **paper 2**, and observing stability of all 4 systems in **paper 3**.

6.2. Spectroscopy

4 types of spectroscopies were used in this thesis, 3 are discussed in this subheading while the last is acknowledged in section 6.6.

6.2.1. Fourier transform infrared spectroscopy

Fourier transform infrared spectroscopy (FTIR) was used as a powerful tool [106]. The results from this technique provide information about the molecular structure, bonds, functional groups, compound length, degree of crystallinity and contaminations. Thus, most often, it is used as a rapid tool to analyze organic compounds. The technique generally has three modes of function, transmission, attenuated total reflection (ATR), and diffuse reflectance (DRIFT). Depending on the characterization output, state of matter and thickness of the sample, the appropriate mode is selected.

Samples are required to be ‘‘active’’ in order to be able to characterize them by this method [107]. This is so because the fundamental working of the technique requires a sample consisting of molecules with dipole moment. By theory, a molecule with no dipole moment will not be able to absorb the infrared rays. It is well established that molecules absorb photons. In the electromagnetic spectrum, the photons in the energy range of infrared are known to be absorbed by many molecules. For organic studies, this is significant because the wavenumber of the absorbed photons corresponds to the vibrational wavenumber of the molecular bond between the atoms.

The energy source in FTIR studies is infrared light [106]. Every object radiates light in the infrared region. Infrared has a wavelength between 1-100 microns, which is between visible light and microwave. The primary source of infrared radiation is thermal radiation. Infrared spectrum can be divided into three regions: near, mid and far (10 μm to 1 mm). Near infrared is closer to visible light and far infrared is closer to microwave.

In FTIR, when atoms or molecules are energised, they vibrate, and these vibrations occur at fixed frequencies called natural frequencies. If a beam of photons is bombarded on a molecule, and the applied frequency of the photons is equal to the natural frequency, then the vibration of the molecule will be amplified. This vibration is analogous to spring with two atoms acting as weights and the bond that forms between the two atoms acting as a spring. Since the natural frequency of each bond is unique, the absorbed wavelengths act as an indicator of the identity of the bonds present in the molecule [108, 109].

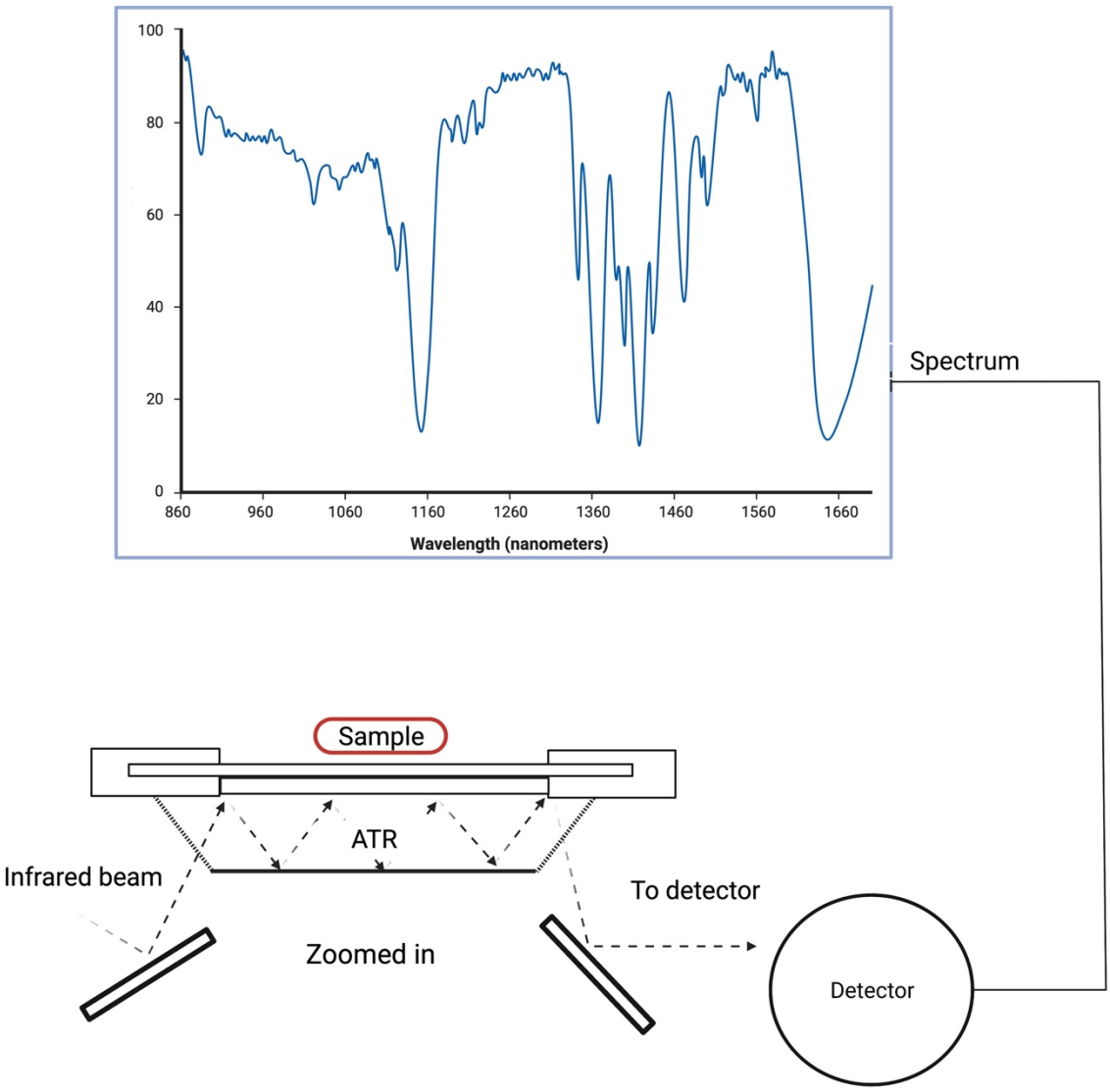

Figure 6.4: Schematic representation of a reflectance setup for a FTIR in the ATR setup. In it, the incident ray is bounced back and forth between sample and the ATR crystal, before refracting towards the detector. An example of the spectrum is shown in the figure.

A typical instrument has a heat source as the source of the infrared light. The light from this source is then passed through an interferometer. ATR mode is used in this study and (figure 6.4) With the ATR mode, the incident beam is directed towards a diamond crystal; the sample is placed on the crystal that absorbs the waves. The wave is internally reflected through the crystal back to the sample several times before it is transmitted out of the sample towards the detector [96]. In this study, the spectra of GO, purchased chemicals, and the extracted asphaltene, were measured using FTIR in papers **1 and 3**.

6.2.2. X-ray photoelectron spectroscopy

X-ray photoelectron spectroscopy (XPS) is a surface analytical technique [110]. It has high sensitivity and can be used to understand the elemental composition, chemical state, and electronic structure of compounds [111]. The technique is highly effective as a surface technique and can provide information up to 6 nm.

XPS works by releasing a photoelectron from the outermost orbital of an atom using X-rays [110]. When X-rays are shot on an atom, they absorb this energy until the kinetic energy of the electrons, and above it they eject the outer orbital electron with a fixed kinetic energy. This ejected electron is called a photoelectron. The energy of each ejected electron is characteristic of an element. Thus, the element and its state can be identified using the kinetic energy of the ejected electron, the number of released electrons, and the energy of the X-rays at the determined wavelength [110]. Hence, X-rays are used with characteristic energy that is above the kinetic energy required to release the electron from the orbital, refer to figure 6.5 for an example and an illustration of the electron orbitals and ejected photoelectron. The analyzed data is generally expressed in terms of binding energy. The binding energy is calculated from the measured kinetic energy.

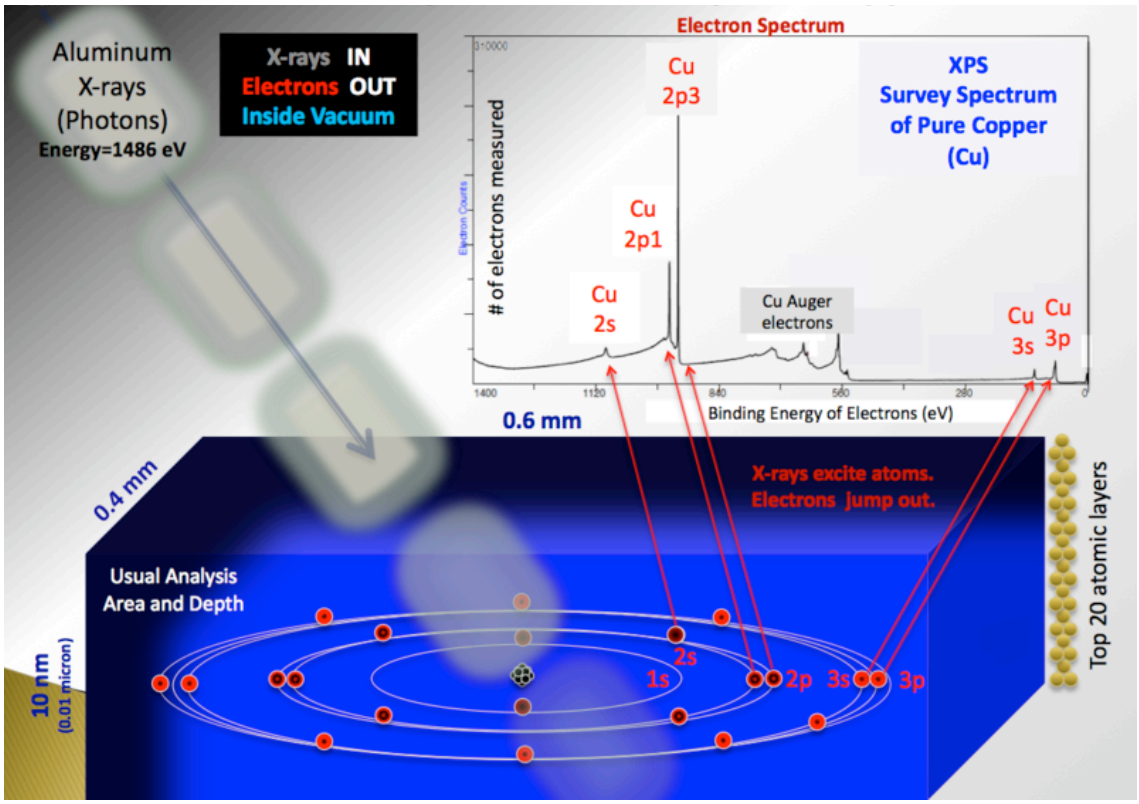

Figure 6.5: Schematic representation how the incoming energy interacts with the electrons on the outer shell of an atom, in XPS.

$$e_{binding} = e_{photon} - (e_{kinetic} + \phi) \tag{03}$$

where, ($e_{binding}$) stands for the binding energy, (e_{photon}) is the energy of the emitted X-rays, and ($e_{kinetic}$) is the kinetic energy of the ejected electron measured by the instrument. Also, the Φ is the adjustable instrumental correction factor.

The setup of an XPS is shown in figure 6.6, where an X-ray source, sample, lens, an analyzer, and a detector can be seen [110]. In an XPS setup, the source of X-rays is generally, a metal such as aluminum (Al) or magnesium (Mg). The electrons of an electrode source strike the metal, and this process causes the Kα X-rays from the metal to be emitted [112]. It is this source of X-rays that is targeted toward the sample. The choice between aluminum and magnesium is decided based on the desired energy, sensitivity, and resolution [112].

The measurements can comprise conductive and nonconductive samples. Depending on the conductivity of the sample, different sample preparation techniques should be used. Here, the method for preparing nonconductive samples is discussed. Due to the techniques' sensitivity, the samples must be cleaned of any surface contamination. With samples such as graphene derivatives, we clean and sonicate the sample in the appropriate solvent, such as methanol. Methanol is chosen because it can evaporate after deposition and will not bind to graphene derivatives, unlike water. After sonication, the graphene derivative is deposited on a silicon wafer. After deposition, the sample is dried to remove any residual methanol. Following this, a thin layer of conductive carbon is deposited on the surface of the sample. The most popular way to do this is via sputtering or carbon evaporation. Finally, the instrument is calibrated with C1s spectra of sp2 hybridized carbon for graphene derivatives.

After the X-rays are shot on the sample the photoelectrons are emitted. However, the ability of the photoelectron to be detected by the instrument depends on many factors, such as the kinetic energy, escape depth, chemical sensitivity, and surface sensitivity of the sample [112]. As mentioned, kinetic energy is the determinate energy that must be exceeded for an electron to escape the atom. After escaping, the photoelectrons must travel within the sample before reaching the surface and towards the analyzer [112]. During this journey, the photoelectrons can be absorbed by another atom in the sample. This traveling distance within a sample before escaping the sample is called escape depth. The escape depth is proportional to the energy of the photoelectrons. This implies that high-energy photoelectrons can travel a longer distance and, thus, can provide information about the bulk of the sample [112].

As seen in figure 6.6, a lens is used to concentrate the photoelectrons toward the analysis. This improves the signal-to-noise ratio and the resolution of the photoelectrons. From the lens, the photoelectrons pass through the entrance slit. It has a small opening that allows the photoelectrons to pass through to the analyzer. The slit can be used to control the intensity of

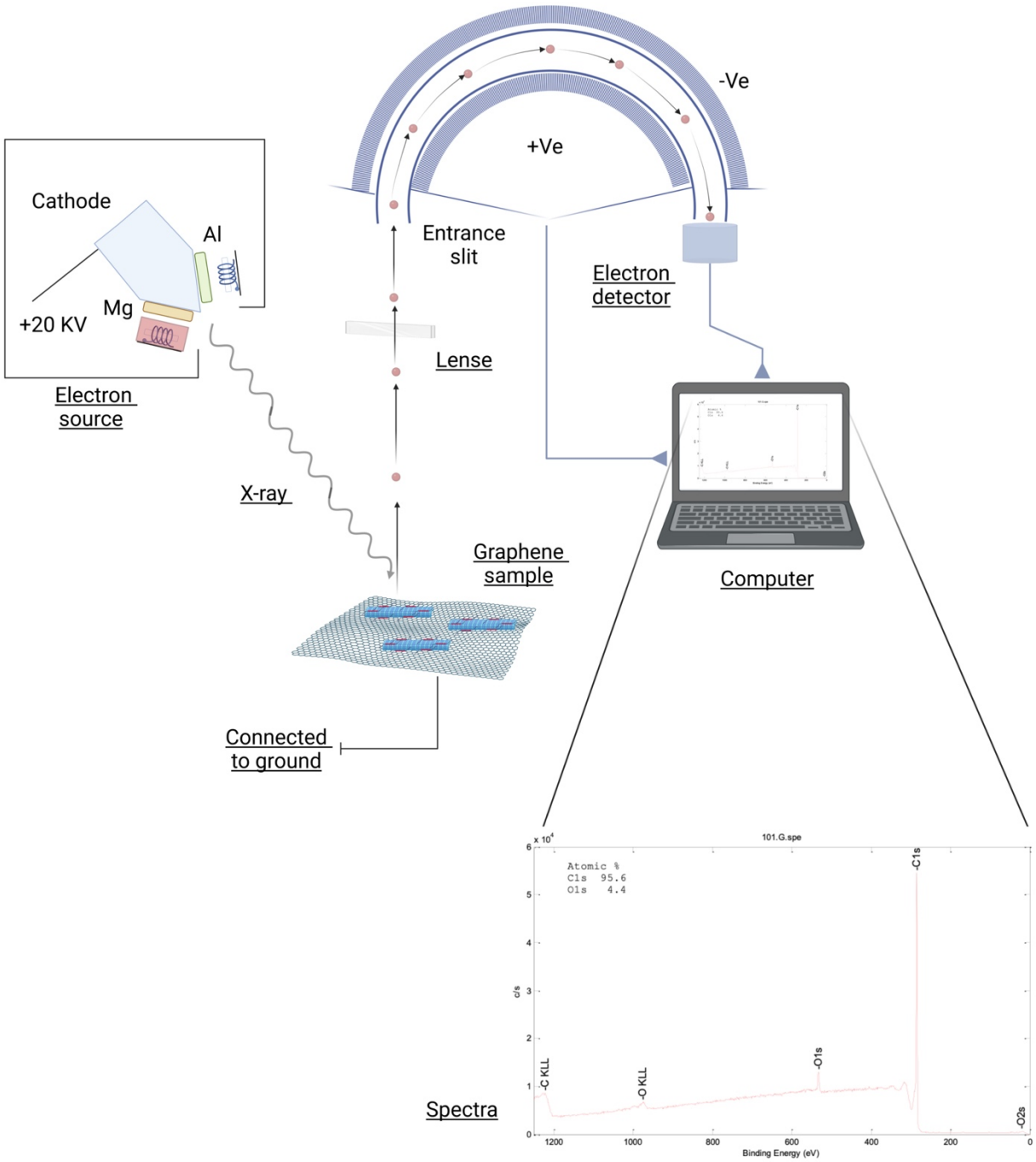

Figure 6.6: Schematic representation the XPS setup. The figure shows how an emitted photoelectron is collected by the detector to analyze the surface chemistry of the atom.

the photoelectrons. It can also limit the angular spread of the emitted photoelectrons, improving the measurement's energy resolution [110-112].

Before reaching the detector, the emitted photoelectron journeys through an analyzer. The analyzer is a hemispherical tunnel with a series of concentric rings that are charged to different potentials [112]. During its journey through the analyzer, the photoelectrons experience a combination of repulsive and attractive electric forces that are caused by the hemispheres. This causes them to have a curved trajectory. Thus, the curvature of the path is determined by the kinetic energy of the photoelectron and the electric field inside the analyzer. This helps separate the photoelectrons based on their kinetic energy. In addition, carefully controlling the electric field inside the detector helps analyze photoelectrons of specific kinetic energy [112].

Finally, the photoelectrons reach the detector that is in the end of the analyzer. The detector has high sensitivity and resolution, and can distinguish between photoelectrons with slight differences in kinetic energy. The obtained data can then be a board scan for the entire sample or a narrow scan for a specific element [112]. By comparing the binding energy against a known database will help deduce a deeper understanding of the sample surface [112]. In **papers 1,2, and 3**, we used XPS as a tool to identify the surface chemistry of GO, MW-graphene, asphaltene, and the precipitates.

6.2.3. Ultraviolet-visible spectroscopy

Ultraviolet-visible Spectroscopy (UV-Vis) is an analytical technique that can be used to study the interaction of light with matter in the ultraviolet, visible light, and near infrared regions [113]. During the interaction, the sample either absorbs or transmits the incoming light. The collected light is then analyzed, and an absorption spectrum of a sample is created. The spectrum provides information about the electronic structure and composition of the sample. UV-Vis is valuable for determining the concentration of a substance in a solution. Using the Beer-Lambert law,

$$A = \varepsilon l c \tag{04}$$

In it, (A) is the absorbance, (ε) is the molar attenuation coefficient, (l) is the optical path length, and (c) is the concentration. The equation can be used to determine the concentration of a suspension in the solution.

The measurements can be performed using either a single-beam or double-beam setup [113]. The sample is exposed to light in a single-beam setup, and the resulting absorption spectrum is recorded. Whereas in a double-beam setup, the light is split into two beams. One beam passes through a reference material while the other passes through the sample. Later, the beams are recombined. In the double-beam setup, the reference beam is subtracted from the sample beam during the measurement. Often, the solvent is used as the reference beam. This helps identify the spectra produced by the sample in the solvent. However, in a single-beam

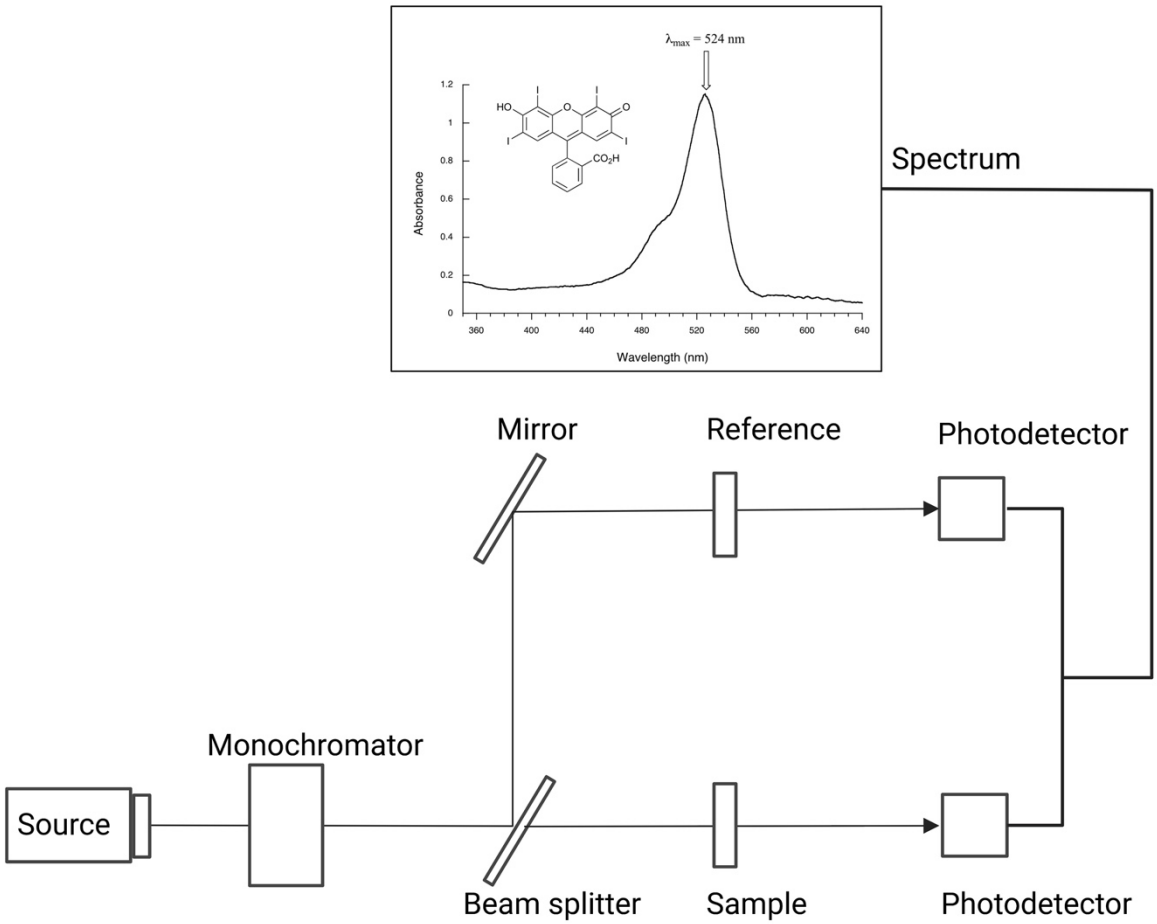

Figure 6.7: Schematic representation of an UV-Vis instrument with a double beam setup. It also provides an example of an spectra of a molecule.

setup, the subtraction of the solvent has to be performed manually, post measurement. The double-beam setup and an example of a spectrum is presented in figure 6.7. It shows the various parts of a UV-Vis spectrometer. The instrument has a source for the light and a monochromator to select and transmit a mechanically selected narrow band of wavelengths of light. This beam is then split and transmitted through the sample and the reference, and finally collected at the photodetector.

In **paper 3**, we use a double-beam setup to measure the precipitation in our samples. For this, we use paraffin oil as the reference. The signal from paraffin oil is subtracted by the instrument.

6.3. Diffraction

3 types of diffraction methods are used in the thesis. Two are discussed in this section while the 3rd is acknowledged in section 6.6.

6.3.1. X-ray Diffraction

X-ray diffraction is a characterization technique that works in the principle of constructive interference [114-117]. In liquids and solids, the average interatomic distance is between 1-3 Å. If the structure of a crystalline material has to be determined, then the wavelength of the radiation must be similar to the spacing between the crystal's atoms [114]. X-rays fit into this criterion as they have a range from 0.1 Å to 100 Å [114]. X-rays are short wavelength electromagnetic radiation that is produced as a consequence of a deceleration of high energy electrons or by the transition of the inner orbital electrons in an atom.

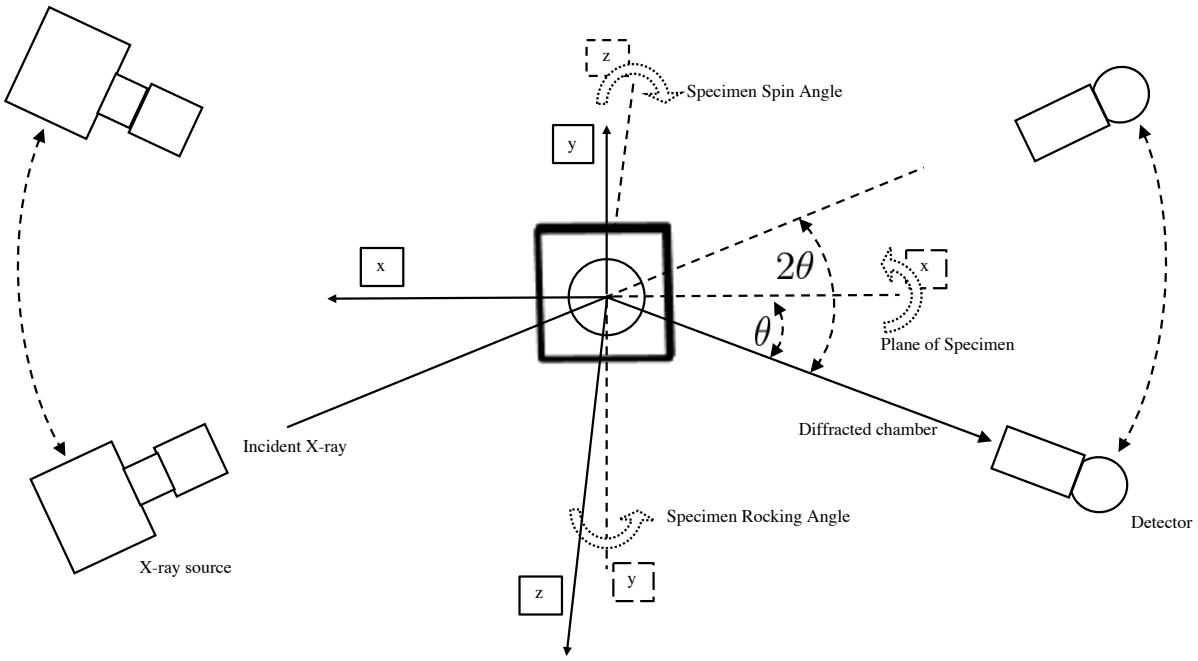

Figure 6.8: Schematic representation of an XRD setup

Near monochromatic intense (Kα) X-rays are the most common type of radiation used in XRD [114]. The penetration depth of X-rays used is proportional to the wavelength of the source. Target metals such as Mo, Cu, Co, Fe and Cr are used as the radiation source. The X-rays released from the source is passed through carefully packed metal plates called collimator. The collimator has a small gap that allows a narrow beam of X-rays to pass through. This narrow beam of X-rays is then bounced off a monochromator that absorbs the undesirable wavelength by allowing only the required wavelength to pass through. A schematic representation of an XRD setup is shown in figure 6.8.

The beam of X-rays that act as the primary source interacts with the electrons in the crystal. The energy of the X-ray that interacts with the electrons is not sufficient to eject the electrons. This interaction causes the X-ray to undergo elastic scattering [117]. During elastic scattering, the electrons start to oscillate, which in turn transforms the electrons into a secondary source. The atoms act as a periodic array of radiation source. When two wave sources interact constructively, they amplify the intensity of the final beam while the opposite causes the wave to cancel out [117]. The technique was used in **paper 1** to study the adsorption of asphaltene to GO.

6.3.2. Small angle. X-ray scattering

Small-angle X-ray scattering (SAXS) and XRD are related but distinct techniques. They both utilize X-ray sources to probe the structure of materials at different length scale [118]. While XRD is useful in studying a material's crystal lattice and atomic, SAXS provide information about the order, size, and shape of large structures in materials [118]. Thus, while XRD probe the structure correction between neighboring atoms, SAXS probes fluctuations in electron density in the studied material, i.e., structural inhomogeneities on different length-scales. The setup of a SAXS instrument is presented in figure 6.9. As shown in the figure, SAXS has an X-ray source, X-ray optics, and a detector. When incident X-rays interact with the electrons in the sample, this causes the electrons to scatter in different directions. The scattered X-rays can be represented by their momentum transfer [118].

The momentum transfer (q) is given by the scattering angle and the wavelength of the X-rays. It can be described using the following equation:

$$q = \frac{4\pi}{\lambda} * sin\frac{\theta}{2} \tag{05}$$

where, (θ) is the scattering angle of the X-rays and λ is the wavelength of the incident X-rays.

Unlike XRD, the scattering angles of SAXS are typically comparatively small. This implies that XRD provides information in a q range of 0.5 $Å^{-1}$ to 30 $Å^{-1}$ and SAXS provides information in a q range from about 0.001 $Å^{-1}$ to 1 $Å^{-1}$. From the scattering, we obtain intensity of the scattered X-rays as a function of q. To obtain detailed information from SAXS, the data has to be modeled. This helps determine the size, shape, and arrangement of scattering object in the sample [119].

The equation that describes the scattering intensity in SAXS is:

$$I\,(q) = (\Delta\rho)^2\, V * P(q) \tag{06}$$

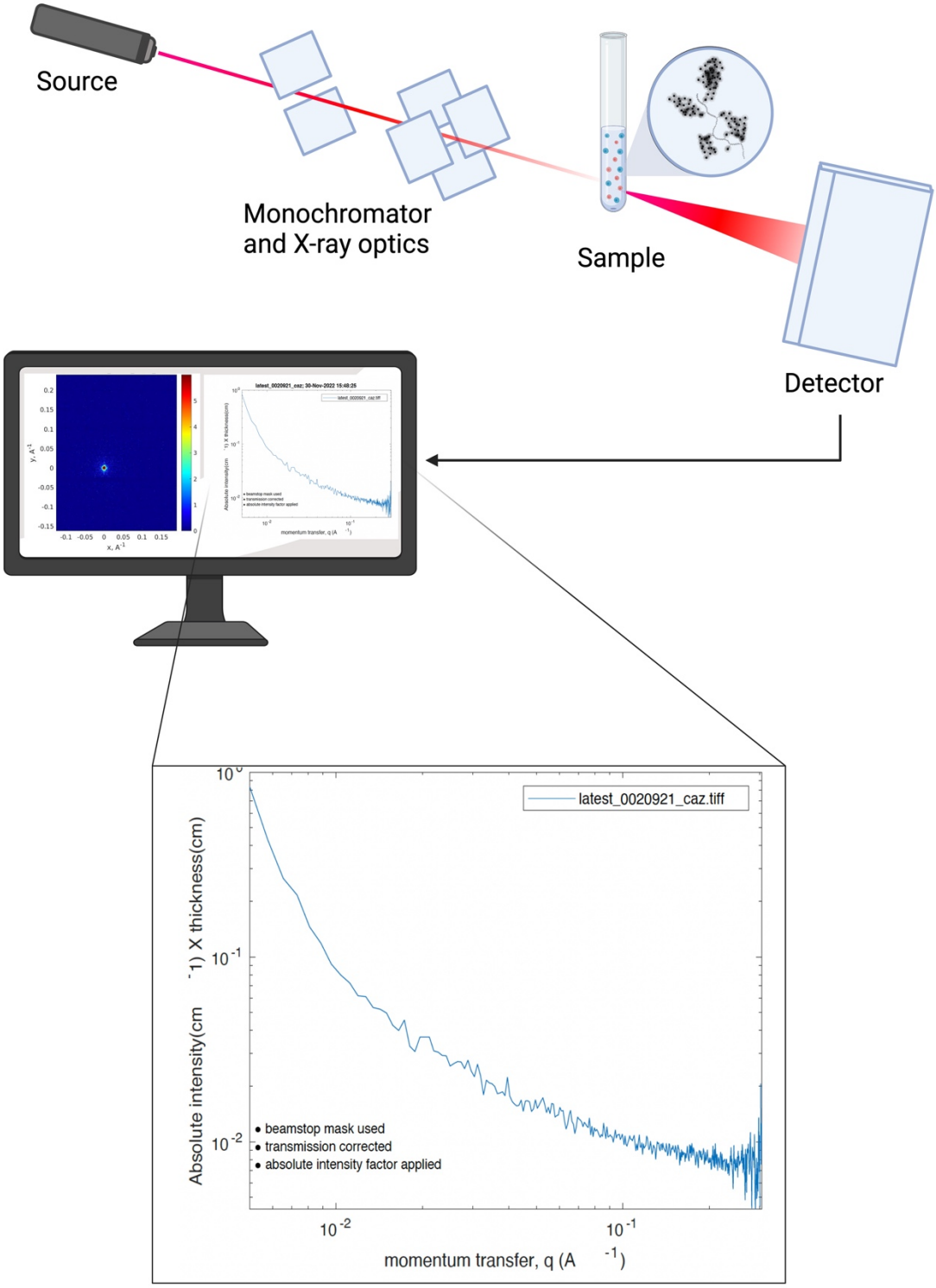

Figure 6.9: Schematic representation of an SAXS setup

In the equation, I(q) is the scattered intensity as a function of q, (V) is the volume of the scattering object, (Δρ) is the contrast factor between the electron density of the scattering particles and the surrounding medium, and (P(q)) is the form factor.

The form factor describes the size and shape of the particles in the sample, and it can be calculated using models that describe the scattering from such objects. For instance, it can be a single spherical particle or a collection of particles with a wide size distribution [118]. An appropriate model has to be selected to obtain a correct understanding of the system. Another important information that can be obtained besides P(q) is the structure factor S(q). S(q) describes the distribution of particles and their interparticle interaction [118]. The scattering intensity can therefore also be expressed as:

$$I(q) = P(q) * S(q) \tag{07}$$

A SAXS capillary and capillary holder is shown in figure 6.10. The figure also shows the how the prepared sample were prepared for measurement.

In this thesis SAXS is used in **paper 2**. It is used to detect the scattering intensity at q= 0.005 $Å^{-1}$. This was done in order to study the aggregation and precipitation phenomena in the samples due to the introduction of hexane.

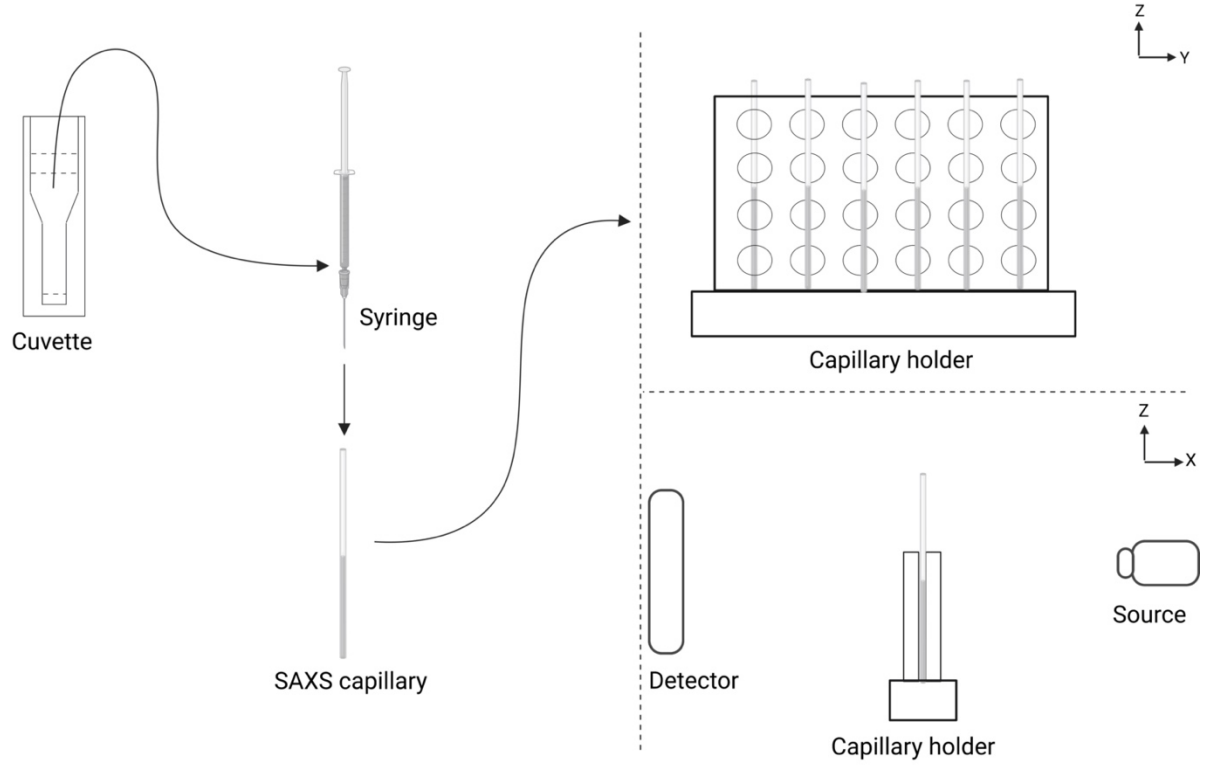

Figure 6.10: Schematic representation of the sample preparation for SAXS.

6.4. Dynamic shear rheology

Rheology is a powerful tool to study the behavior of liquids, colloids, and viscoelastic fluids [120 - 122]. A sample's rheological behavior is directly influenced by its microstructure [28].

In general, samples are sheared in a narrow gap between two surfaces in a rotational rheometer. As a result, the viscosity and viscoelasticity of a material can be studied. *Viscosity* is the magnitude of internal friction in a fluid and is defined as the ratio of the shear stress and the shear rate. Furthermore, *viscoelasticity* is the material property that exhibits viscous and elastic characteristics when undergoing deformation. Key factors that influence measure the material properties, such as viscosity and viscoelasticity, are the geometry and dimensions of the surfaces. The most common surface geometries are concentric cylinders, parallel plates, and cone and plate. In a rheometer, either both or just the upper surface can be a moving part. In

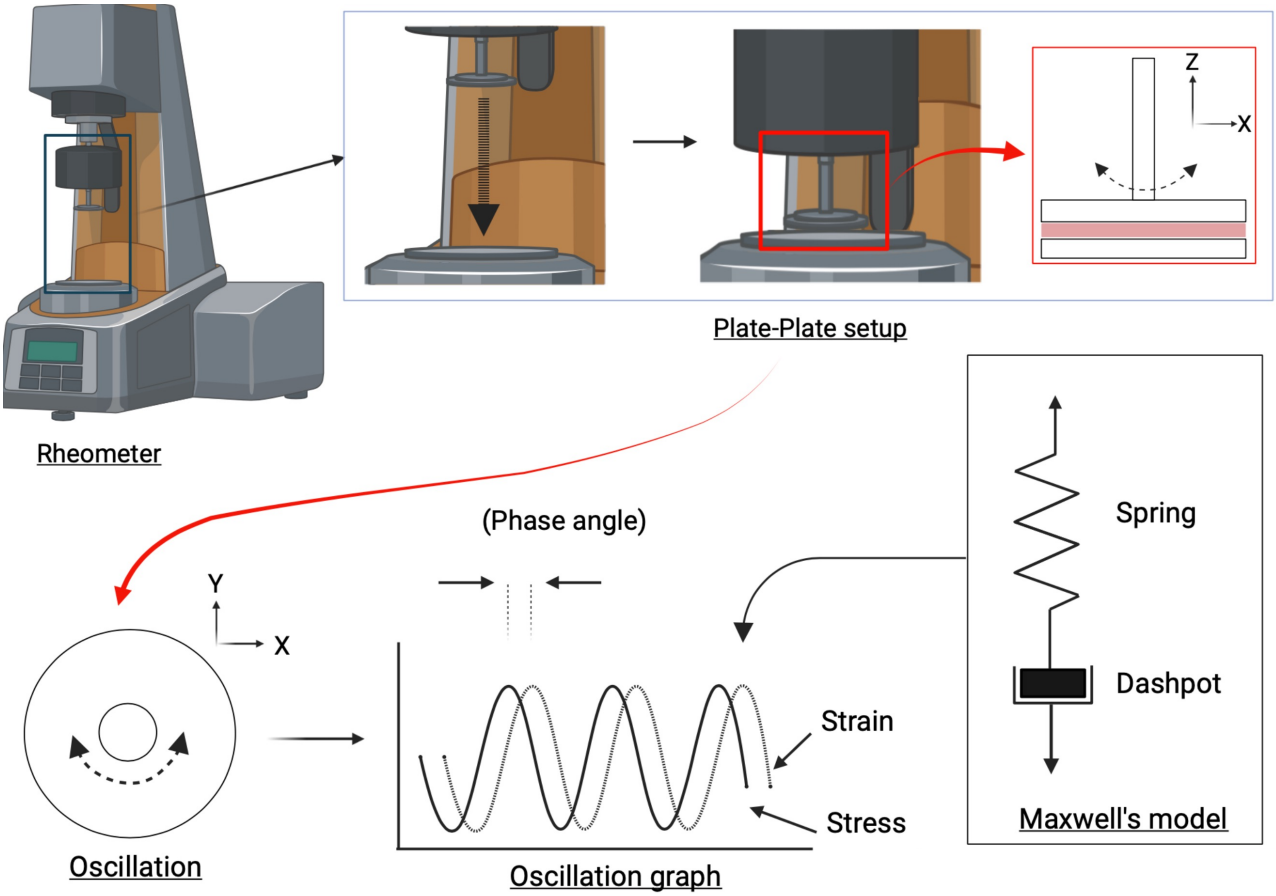

Figure 6.11: Schematic representation of the plate-plate setup. The stress to strain response from a DSR is in phase difference with each other. This behavior is best represented with Maxwell's model of viscoelasticity.

the latter case, the upper geometry is attached to the driving motor, which functions with an air bearing that rotates under the conditions provided for the experiment.

The surface is rotated at a known shear rate for viscosity measurements, with the sample between the two surfaces. When the surface rotates, the sample's resistance to shear (force) is recorded. This provides the shear stress, which provides information about the viscosity. In the case of viscoelastic measurements, the top surface oscillates with a predetermined frequency (angular deflection) or amplitude (torque).

When a sinusoidal stress is applied to a sample under oscillation within its linear viscoelastic region, the material can respond to this with a response strain that is out of phase with the applied strain. This phase difference is called the phase angle. Thus, it is defined as the phase difference between the applied stress and strain. For a solid, the phase angle is 0°, and for a purely viscous liquid, it is 90°. Anywhere in between, the response is viscoelastic. A representation of the oscillation measurement is displayed in figure 6.11.

In an oscillation measurement, the ratio of the resulting stress to the applied strain is called the complex shear modulus, G*.

$$G^* = G^{'} + iG^{''} \tag{08}$$

The in-phase component of the complex shear modulus is called (G') and the out-of-phase component is (G')'. The ratio of G' to G'' is called the loss tangent.

$$tan(\delta) = \frac{G^{'}}{G^{''}} \tag{09}$$

The in-phase component is called storage modulus and a representation of the energy stored in the sample. It is the cosine of the phase angle multiplied with the complex shear modulus.

$$G^{'} = G^* cos(\delta) \tag{10}$$

On the other hand, the out-of-phase component is called the loss modulus and it is defined as the sinusoidal component of the phase angle multiplied with the complex shear modulus. Loss modulus provides the information about the deformability of the sample.

$$G^{''} = G^* sin(\delta) \tag{11}$$

Further, the storage modulus and loss modulus are not analogues to elastic and viscous components of the complex shear modulus but rather, both storage modulus, and loss modulus

carry part of the elastic response. While loss modulus is the out of phase response, over time, the out of phase component could also show delayed elastic response.

Finally, the ratio of the complex shear modulus to the angular frequency will provide the complex viscosity of the material.

$$\eta^* = \frac{G' + iG''}{\omega} \tag{12}$$

Similar to the complex shear modulus, the complex viscosity also be calculated. It too can be divided into real and imaginary components. The ratio of the storage modulus to the angular frequency provides the real component of the complex viscosity and the ratio of the loss modulus to the angular frequency provides the imaginary component of the viscosity.

$$\eta^* = \eta' + i\eta'' \tag{13}$$

In this thesis, a plate-plate setup has been used. 25 mm and 8 mm diameter plates were used in this thesis. The gap for measurements for the 25 mm plates was 1 mm and for the 8 mm plates the gap was increased to 2 mm. In this thesis, the temperature was varied from 4° C to 88° C. The plates were made from stainless steel. Stainless steel is used as it has a low coefficient of thermal expansion and good heat-transfer coefficient. An environmental chamber was placed on top of the plates. This chamber controls the sample at the desired temperatures. The technique was used in **paper 2**.

6.5. Differential scanning calorimetry

Differential scanning calorimetry (DSC) is a thermal analysis technique [123]. It is used to analyze the thermal behavior of materials. It is a powerful tool that can help understand the phenomena giving rise to thermal response during cooling or heating, chemical reactions, phase transformations, degradation of the molecular structure of polymers, crystallization, and melting [123]. DSC measures the heat flow (ΔH) as a function of temperature. figure 6.12 shows that a DSC setup utilizes a reference and a sample.

First, the material of interest is filled in the sample crucible, while the reference crucible is usually kept empty. Both crucibles are generally made of metals with known thermal conduction, such as aluminum. The crucible used in DSC can come in varying volumes that range from a few micrograms up to a few milligrams. Later, the crucibles are placed in a temperature-control chamber. This setup is, in turn, connected to a heat flow sensor that detects difference in the heat flow between the sample and the reference [123].

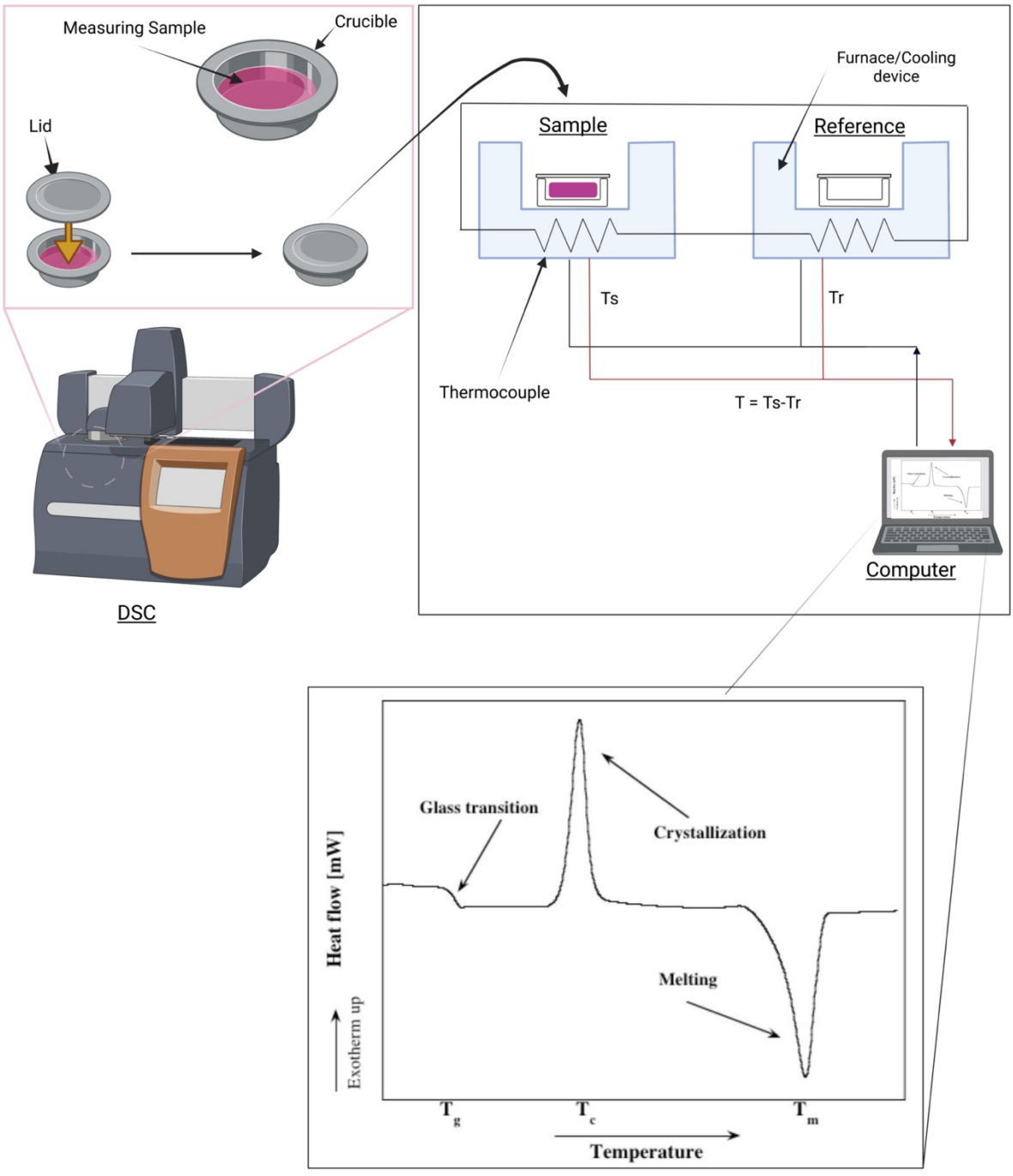

Figure 6.12: Schematic representation of a DSC. The left presents a representation of the instrument. Above it, a schematic of the sample perpetration is presented. On the right, the schematic of the technique is presented.

The temperature sensor is essentially a thermocouple. It measures the change in temperature in the two crucibles in the form of voltage. Further, the heat flux sensor is a setup of two temperature sensors that are placed under the crucibles and is a thin plate that conducts heat

between the two sensors. The sensor measures the heat flux that is caused by the temperature difference between the two sensors during measurement.

The DSC must be calibrated before conducting any measurements. The calibration process typically uses standard materials such as sapphire and indium. The processes performed to calibrate the heat capacity, melting point, and enthalpy.

During experiments, the air in the chamber is purged with nitrogen and helium gases. This is done for three reasons. First, during a thermal cycle, some samples might undergo oxidation or degradation in the air. Purging the chamber with nitrogen or helium can prevent such reactions [123]. Secondly, air can have varying thermal conductivity due to the presence and varying density of gas molecules in the chamber. This variation can cause errors and anomalies in the measurement [123]. The thermal conductivity can be corrected by purging the chamber with one of the two gasses. [123].

The heat balance equation is the underlying equation that governs the function of a DSC [123]. The equation compares the heat flow rate (dQ/dt) to the temperature difference between the sample and reference holders, as shown below:

$$\frac{dQ}{dt} = Cp * \frac{dT}{dt} \tag{14}$$

Where (Cp) is the specific heat capacity of the sample or reference pan. We used DSC in **papers 2 and 3** to observe the thermal response of the systems over elevated temperatures. To evaluate the thermal stability MW-graphene ensembles, all measurements were performed in heating mode from -80 to 150 °C. Finally, a typical DSC graph is shown in figure 6.12. It shows important features such as glass transition, crystallization, and melting.

6.6. Other techniques

Other techniques were also used in this thesis. These include dynamic light scattering, Raman spectroscopy, and thin-layer chromatography-flame ionization detection. These techniques were used to compliment the main research findings.

6.7. Techniques used in the thesis

In this thesis, we used various characterization techniques. Figures 6.13 and 6.15 provides a compilated understanding of the various techniques used in **papers 1-3, and also the additional study**.

It also provides a compilation of what samples were used, and how they were prepared in **papers 1-3**, respectively.

Further, the different techniques used in **paper 1 and 2**, the motivation for using it, and the expected outcomes are discussed in the respective papers. Further, the detailed explanation of the sample preparation and the measuring conditions are also discussed in **papers 1-3**.

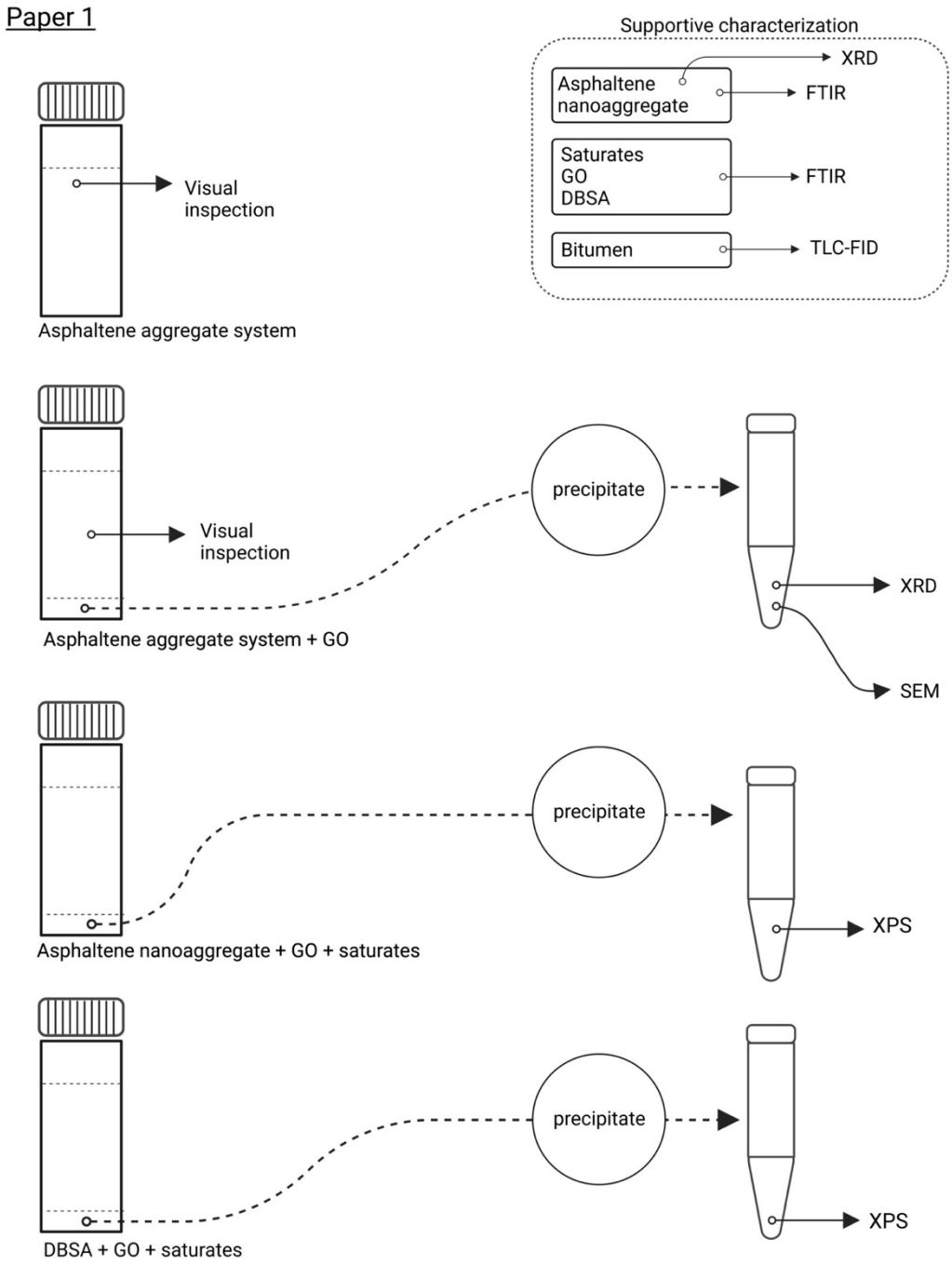

Figure 6.13: Schematic of the different characterization techniques used in **paper 1**. The samples were prepared in glass vials. Later, for extracting the precipitate, the samples were transferred to Eppendorf tube, centrifuged, dried, and then used for measurements.

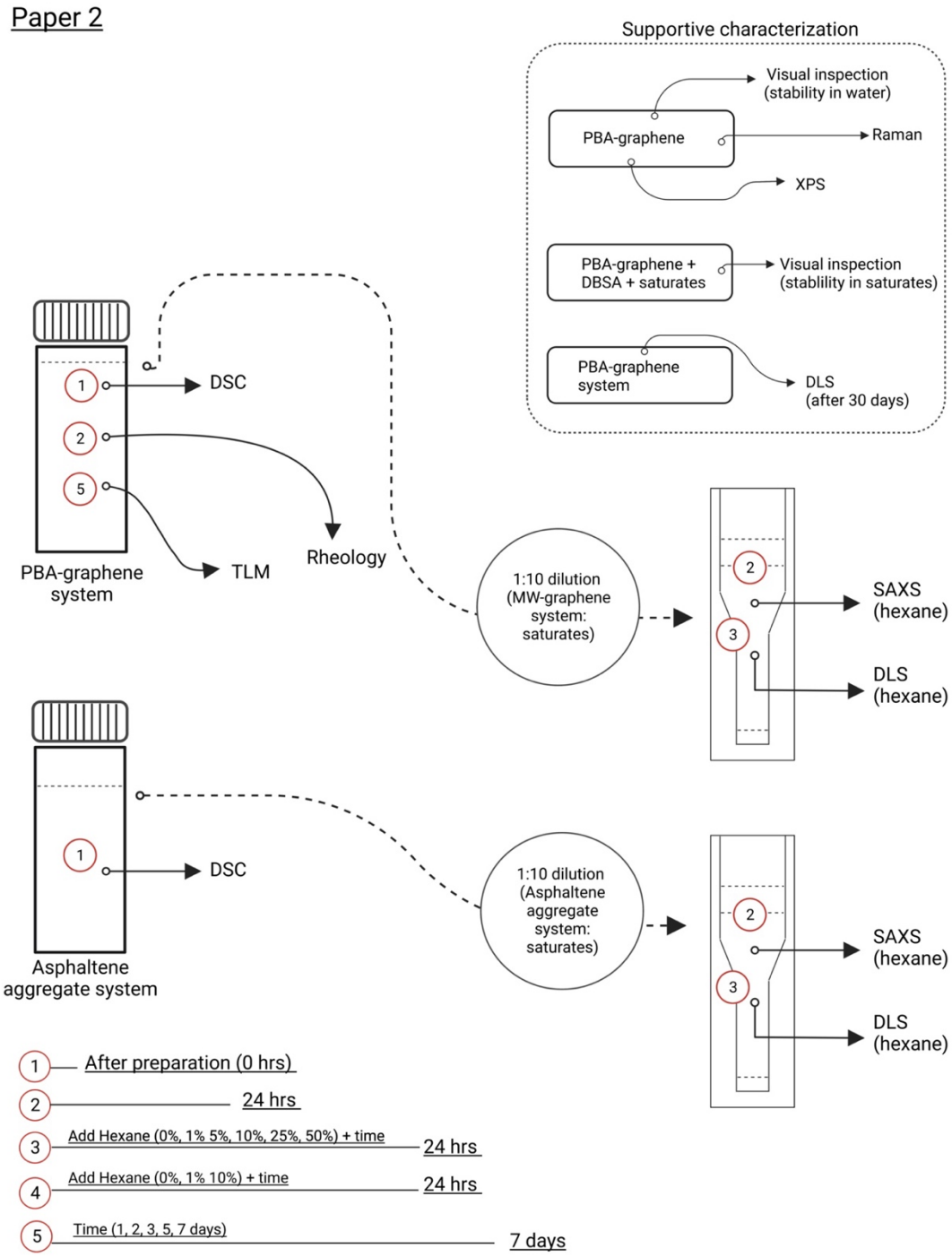

Figure 6.14: Schematic of the different characterization techniques used in **paper 2**. The samples were prepared in glass vials. Later, for some measurements some samples were diluted and transferred to disposable cuvettes and used for measurements.

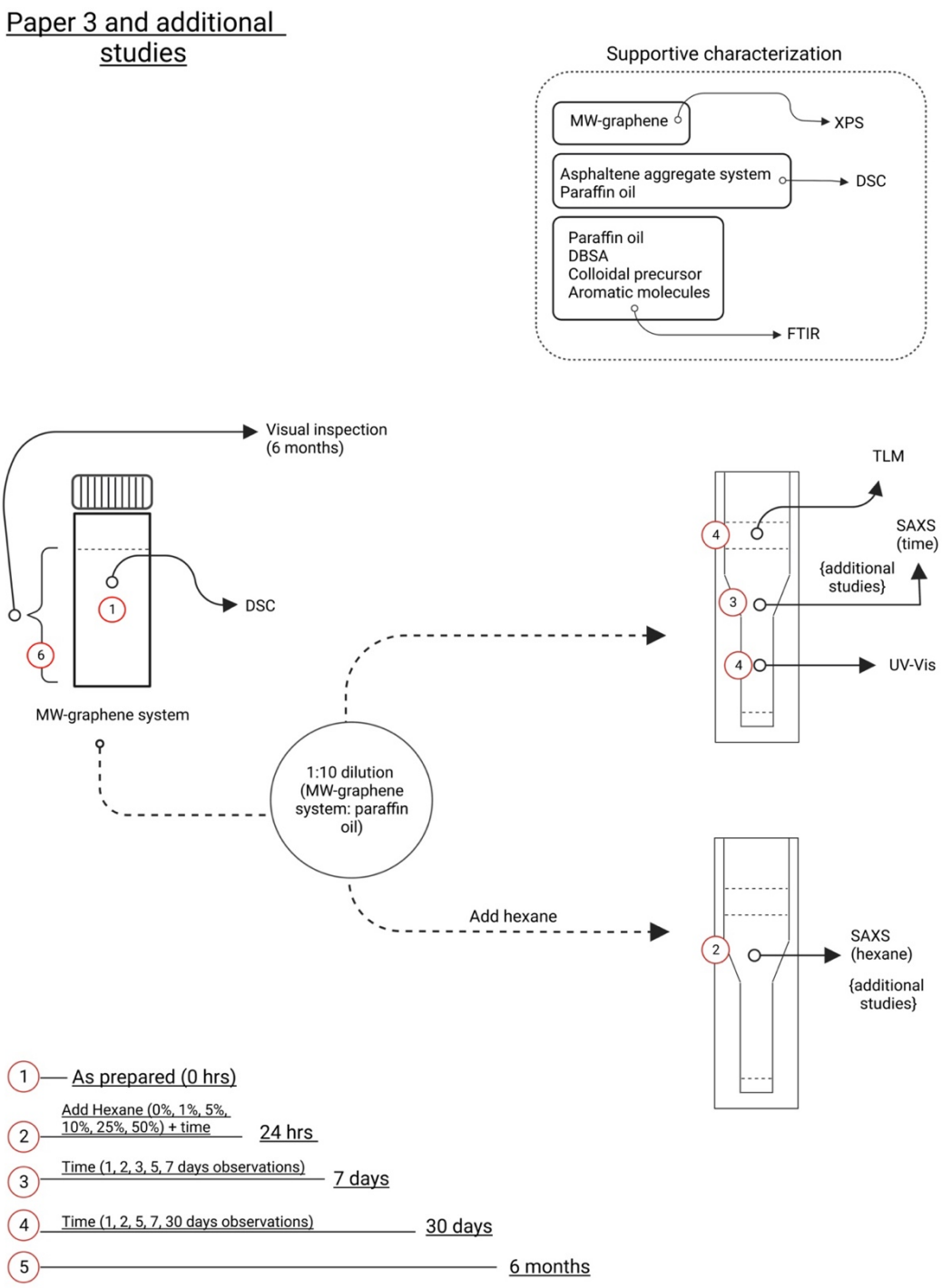

Figure 6.15: Schematic of the different characterization techniques used in **paper 3** and additional studies. The samples were prepared in glass vials. Later, for some measurements some samples were diluted and transferred to disposable cuvettes and used for measurements.

7. Results and discussion

The results of the papers are discussed in this chapter.

7.1. Paper 1: Interaction between GO and asphaltene aggregates.

Several research publications have employed graphene and its derivatives as additives to improve the properties of bitumen, as well as demulsifier in bitumen-water emulsions. To deepen our understanding of the relationship between graphene derivatives and bitumen, we conducted a study in which we developed a model bitumen system consisting of an asphaltene aggregate system. This model system allowed us to isolate and examine the interaction between the asphaltene aggregates and graphene derivatives, without the influence of a too high viscosity or other chemical interactions. Further, we functionalized GO and used it as the derivative in this study. Our investigation focused on exploring the interaction between the asphaltene aggregate system and GO. For the study two systems were used, a). without GO b). with GO, refer to figure 6.13 for further referenced.

We employed visual inspection, centrifugation, and microscopy to observe both systems (with and without GO). Our findings revealed that the asphaltene aggregates were immediately destabilized upon addition of GO. Initially, the asphaltene aggregate system appeared as a uniformly blown colored liquid, as seen in Figure 7.1b. However, upon introducing GO, the brown coloration began to precipitate, leaving behind only the saturates, which was clearly evident in Figure 7.1e. Furthermore, when subjected to centrifugation, the asphaltene aggregate system remained stable, whereas the system with GO precipitates completely. Additionally, during the microscopy investigation using brightfield microscope, we also observed phase separation, as seen in figure 7d.

We performed multiple attempts to redisperse the precipitate, but the effect was irreversible. Thereafter, the precipitate from the centrifugation was collected and dried. We preformed SEM on the precipitate and observed many particles, with lighter contras, on the precipitated on the surface of GO. The EDX analysis showed that the features had high concentrations of heteroatoms such as oxygen, sulfur, and nitrogen.

In order to determine the chemical composition of the precipitate, we utilized XPS. Two distinct samples were prepared for analysis: one containing GO and asphaltene and one containing GO and DBSA. This was necessary to prevent signal overlap between DBSA and asphaltene. The obtained spectra clearly showed that both asphaltene and DBSA were absorbed onto the surface of GO, confirming that the adsorbed structure was indeed asphaltene aggregates. Furthermore, these results provided strong evidence that the

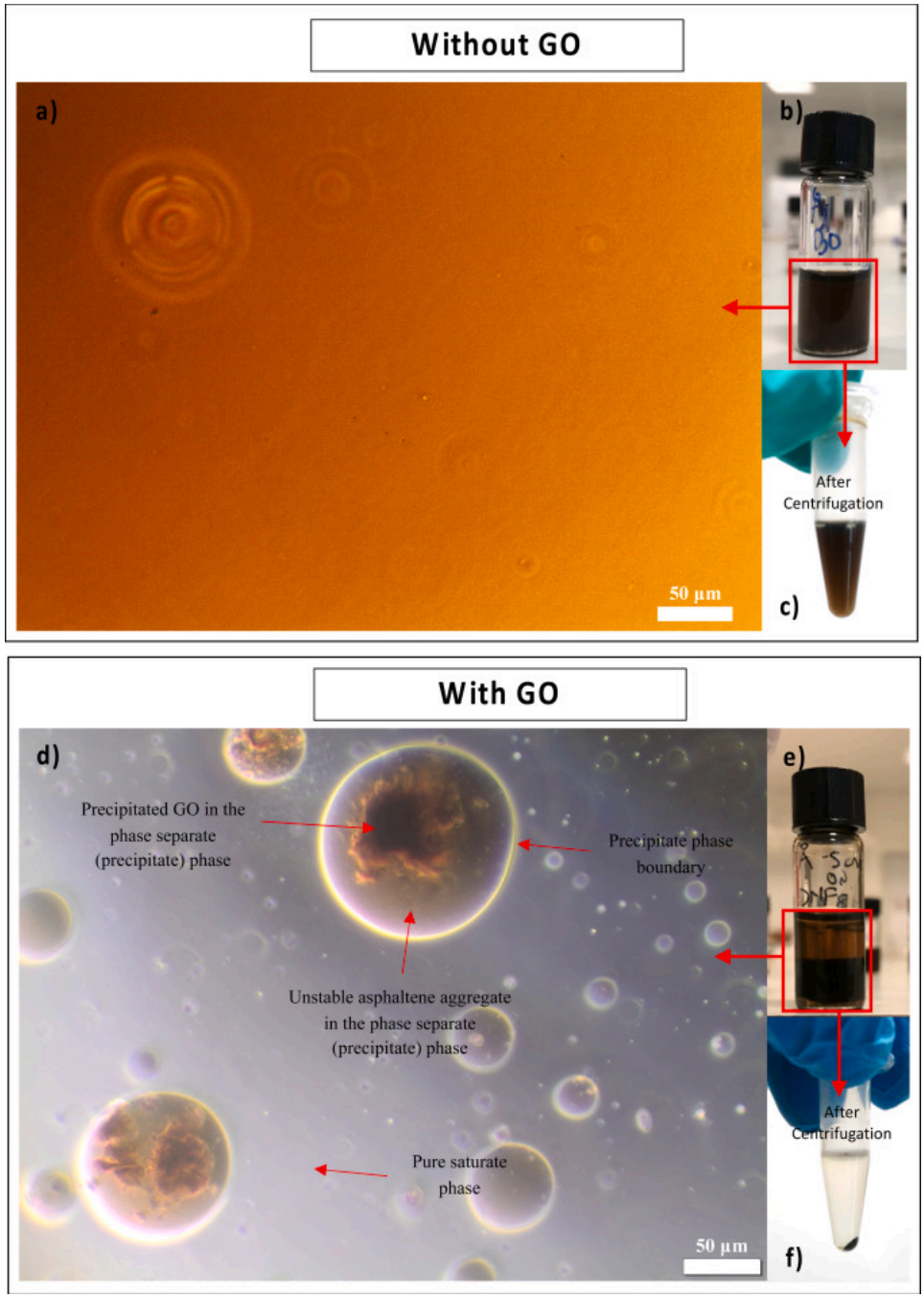

Figure 7.1: Transmission light microscopy images of asphaltene aggregate and precipitate (asphaltene aggregate with GO). a) Asphaltene aggregates can be seen as the circular fringe pattern (ripples) in the image. Due to the size of the asphaltene aggregate, it was imaged using polarized light filter. b) Stable asphaltene nanoaggregate dispersed in micelle precursor. c) After centrifugation, asphaltene aggregates solution without GO were still stable. d) The precipitate (after the introduction of GO) was imaged under phase contrast. Large structures were observed. The glowing ring around the structures is the boundary between the phase separated structure and saturates. e) After introduction of GO to the asphaltene aggregate solution. f) After centrifugation, the precipitate in figure 7.1e and the suspension can be seen to precipitate completely.

introduction of GO triggered the precipitation and phase separation observed in the asphaltene aggregate system. It was finally concluded that this behavior could be attributed to the presence of functional groups on the surface of GO, such as hydroxyl and ether groups, which induce phase separation.

7.2. Paper 2: Interaction between non-covalently functionalized graphene and asphaltene aggregates.

As a successor to the findings of **paper 1**, we developed a solution to overcome the detrimental effect and for effectively dispersing graphene in bitumen. In **paper 1**, we hypothesized that these functional groups, including hydroxyl and ether, could lead to asphaltene precipitation. To address this, we non-covalently functionalized graphene with butyric acid (-COOH). We assumed that in the presence of asphaltene aggregate, the -COOH group can undergo protonation, allowing it to bind with asphaltene aggregates. Therefore, the functional group was expected to embed itself in the asphaltene aggregate. We called the -COOH group on PBA-graphene was called a *-COOH tether*. Using XPS and visual inspection, we confirmed the successful functionalization of PBA-graphene.

After functionalization, we dispersed PBA-graphene in the asphaltene aggregate system. We used transmission brightfield microscopy to study their interaction. As predicted, PBA-graphene interacted with asphaltene aggregates to form an ensemble structure. This was called a *PBA-graphene ensemble*, see figure 7.2. The structure of the PBA-graphene ensemble and its evolution over time was also observed.

We utilized SAXS, DLS, and DSC to investigate the response of the PBA-graphene ensemble to as a function of increasing in hexane concentration and temperature. Our study found that the novel ensembles exhibited similar stability and stabilization mechanisms as the asphaltene aggregates. Both systems underwent initial agglomeration, destabilization, and precipitation as the hexane concentration increased. The similarity in the stability was attributed to the tethered asphaltene aggregates that stabilize the PBA-graphene ensemble.

Additionally, we discovered that asphaltenes were crucial to the formation and stabilization of the PBA-graphene ensemble. Furthermore, asphaltene aggregates formed a network structure, overtime, around the PBA-graphene ensemble. Finally, the PBA-graphene ensemble was always formed irrespective of the shape and structural defects, such as tears or bends on PBA-graphene.

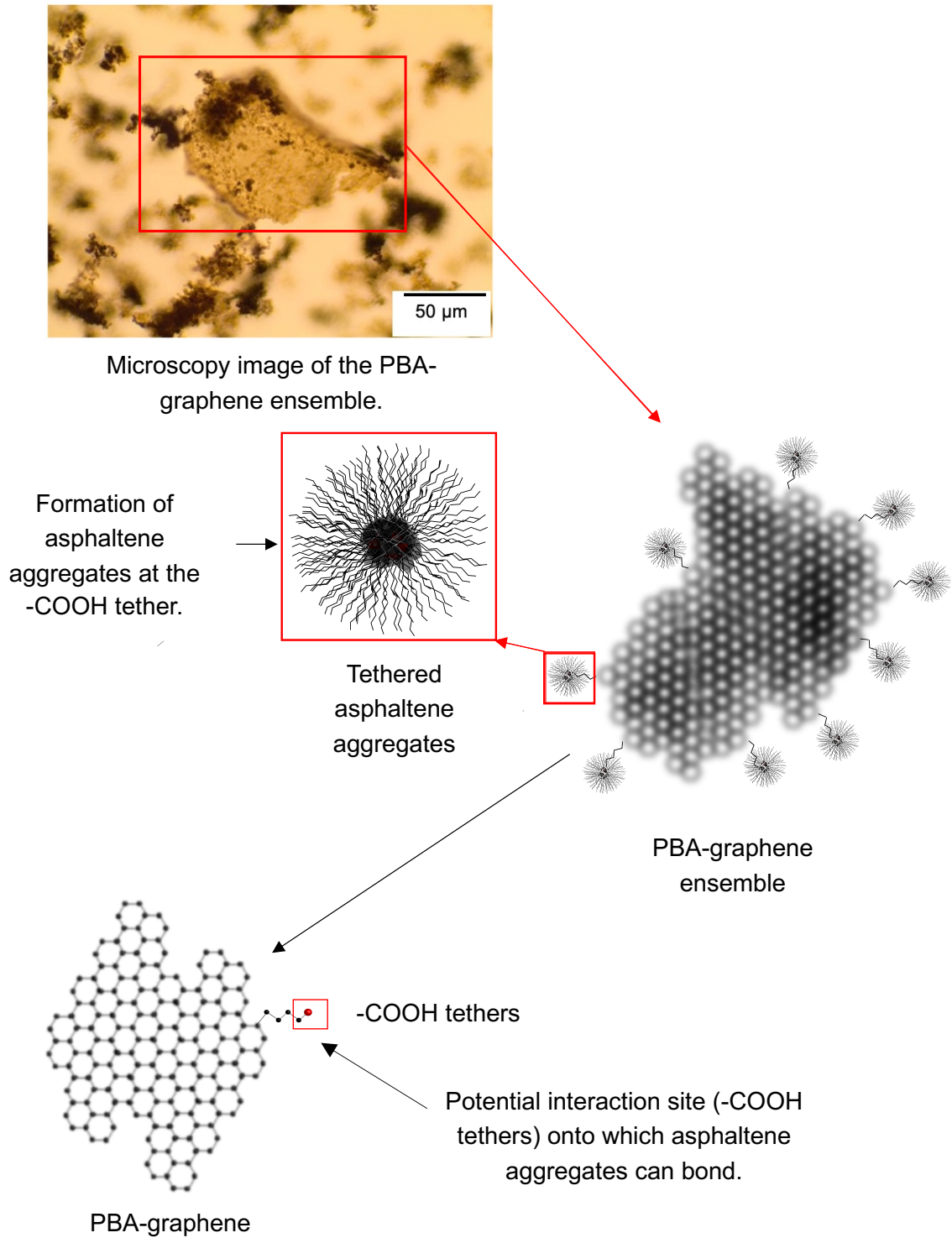

Figure 7.2: Schematic structure of the PBA-graphene ensemble based on the microscopic image shown in the top of the figure, i.e., the PBA-graphene with the asphaltene aggregates formed at the -COOH tethers. It should be noted that the structure of the asphaltene aggregates illustrated in the figure is only for an illustrative purpose.

7.3. Paper 3: Augmenting the stability of asphaltene aggregates using non-covalently functionalized graphene.

In **Paper 2**, we introduced a novel structure named the PBA-graphene ensemble and demonstrated the role of asphaltene in forming these structures. Our findings also showed the similarities between the PBA-graphene ensemble and asphaltene aggregates in terms of their stabilization mechanisms and thermal responses. Following this, we wanted to understand the impact of the tether and the underlying factors that influence its ability to form ensembles with asphaltene aggregates. Thus, we employed four molecules to non-covalently functionalize graphene: 1-pyrene boronic acid (PBrA), PBA (as studied in **Paper 2**), 1-amino pyrene (PAM), and 1-pyrene sulfonic acid (PSA). We selected these four aromatic molecules based on their pka value. Further, we refer to the four functionalized graphene as MW-graphene, with their corresponding ensemble known as the MW-graphene ensemble.

We used the same conditions to functionalize all four MW-graphene. After functionalization, we conducted XPS on all samples to confirm the functionalization's success and determine

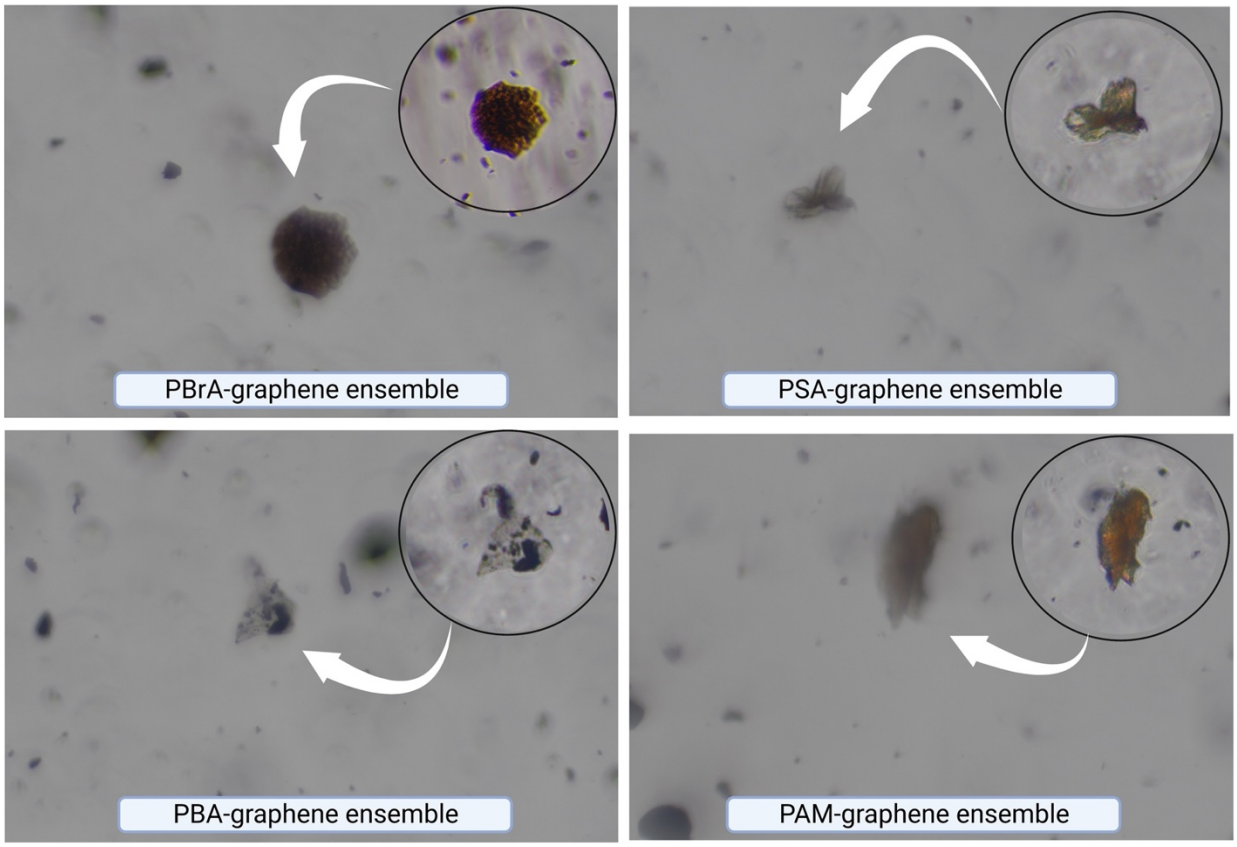

Figure 7.3: The brightfield image of each MW-graphene ensembles that was formed in each system is presented. Inset: the same MW-graphene ensemble in polarized light mode.

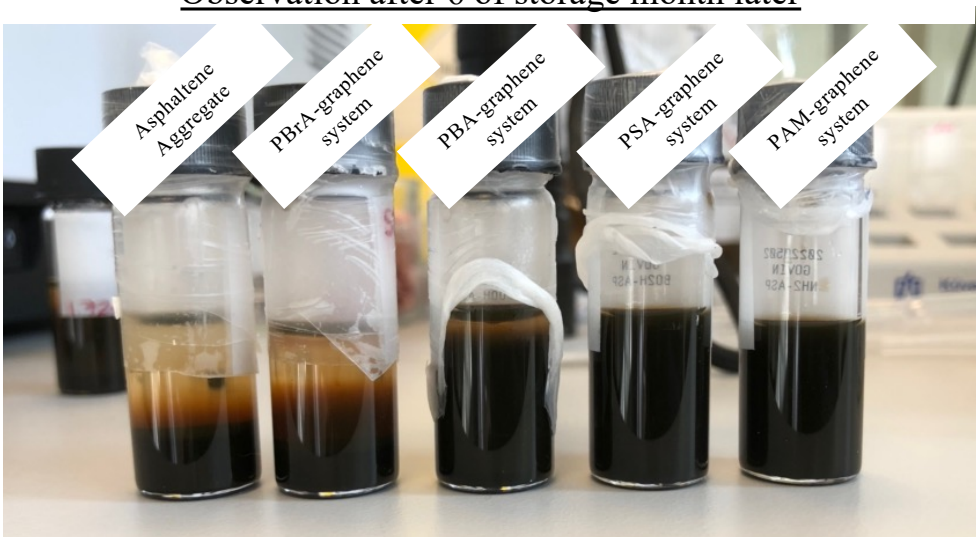

Figure 7.4: Visual observation of MW-graphene systems after 6 months of storage. The samples are in the order (left-right) of asphaltene aggregates, PBrA-graphene system, PBA-graphene system, PSA-graphene system, and PAM-graphene system.

the concentration of each aromatic molecule that was adsorbed onto graphene. The results indicated that all four functional groups were successfully functionalized, but the concentration varied. For example, PAM had the highest concentration of 1.5%, while PBrA and PBA had only 1% . PSA exhibited the least efficiency, i.e., only 0.5% of PSA-graphene's surface functionalized with PSA. We attribute this variation to several factors, including the nature of the heteroatomic groups present in the four molecules, such as differences in solubility, solvent-molecule interaction, pH, and the charge of the corresponding ions of the aromatic molecule in the solvent. Also, although the concentration of the adsorbed aromatic molecules onto graphene varied, all four MW-graphenes successfully formed their corresponding MW-graphene ensembles, as seen in figure 7.3.

Following this, we proceeded to investigate the stability of these ensembles as a function of time as well as temperature. Firstly, UV-Vis spectroscopy was employed to monitor the stability of all four systems over a period of one month. We observed that all four ensembles displayed similar signs of precipitation. However, we also examined the ensembles using microscopy (sample collected from the supernatant of the cuvettes), which showed that the PAM-graphene system and PSA-graphene system exhibited greater stability. In comparison, the PBrA-graphene system did not display any visible signs of ensembles. This difference was observed over a week. That said, after a month this difference was less prominent.

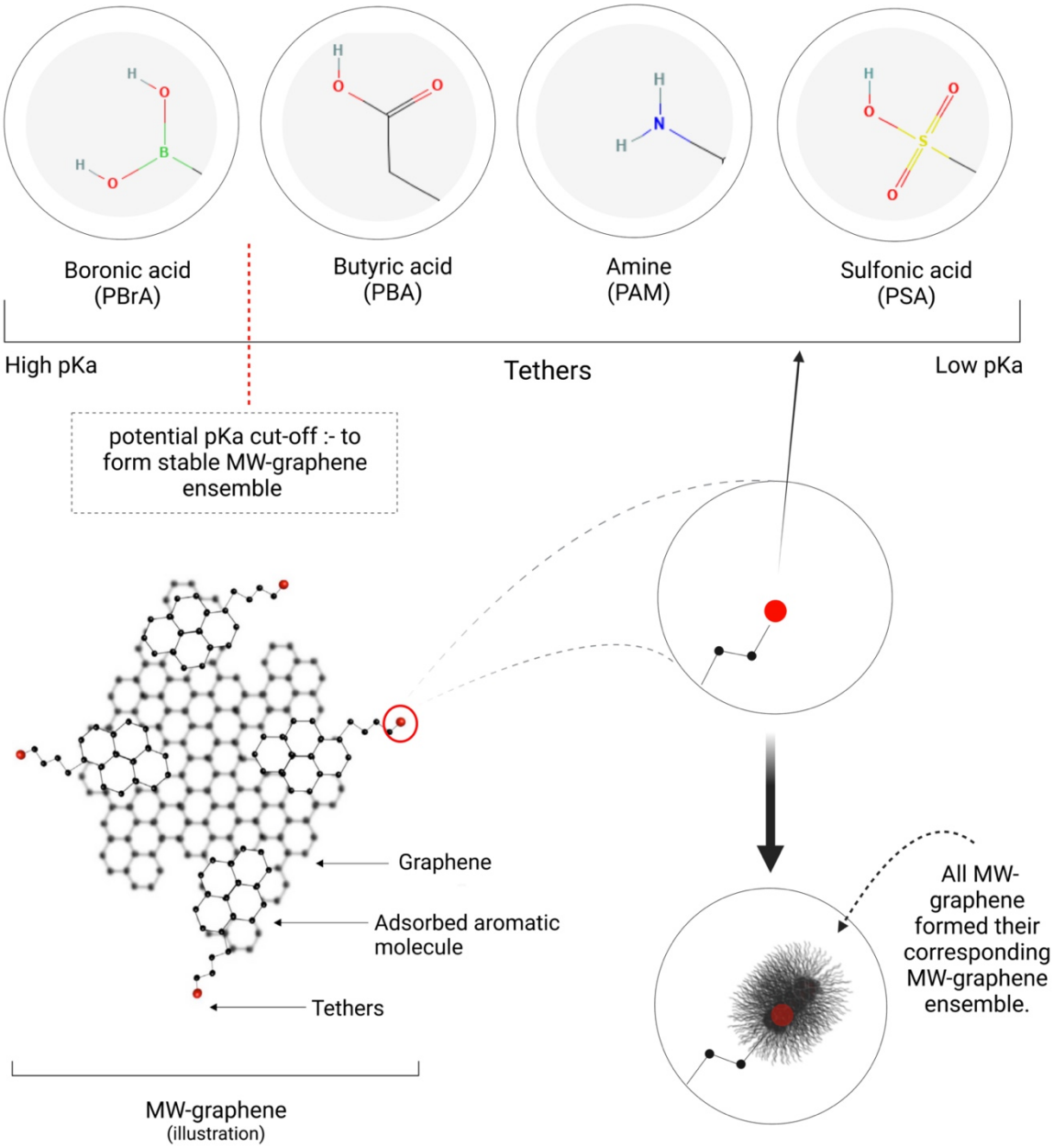

Figure 7.5: The results show that there might be a potential pKa cut-off value , below which MW-graphene can form stable ensembles with asphaltene aggregate.

Furthermore, the samples were stored for 6 months, and a visual inspection was performed, see figure 7.4. The inspection showed that the PSA-graphene and PAM-graphene systems exhibited the highest stability, while the PBrA-graphene system had almost completely precipitated. Further, the stability of the PSA-graphene and PAM-graphene systems was higher than that of the asphaltene aggregate system. Thus, implying that the mechanical stability of the model bitumen was improved due to the incorporation of MW-graphene.

Additionally, the PSA-graphene and PAM-graphene systems exhibited reduced melting behavior at 70°C, when compared to the PBA-graphene and PBrA-graphene systems.

Based on our findings, it can be concluded that the formation of stable MW-graphene ensembles with asphaltene aggregates might require a pKa ‘‘cut-off’’ or charge. Ensembles formed above this level could be metastable. Moreover, the tethers of the MW-graphene may influence their ability to interact with asphaltene aggregates. The size of the heteroatoms, their ability to bend, their charge, as well as the delocalization of the charge from the heteroatoms by the graphene surface might all affect the distribution of charge in MW-graphene.

Furthermore, the graphene surface also carries a charge, which can lead to the redistribution of asphaltene aggregates on the surface through weak interactions such as van der Waals forces. This effect could further distribute the asphaltene aggregates and contribute to the stability of the ensembles. This may explain why the PAM-graphene and PSA-graphene systems were more stable than the reference asphaltene aggregate system. These findings are consolidated in figure 7.5.

7.4. Paper 4: Functionalization strategy and design parameters involved in developing MW-graphene.

We conducted experimental investigations to develop our MW-graphene and the strategy to use asphaltene aggregates to form the MW-graphene ensemble. These investigations provided valuable insights into the real-time interactions between asphaltene aggregates and graphene derivatives in bitumen, helping us to gain a deep understanding of the possibilities, challenges, and limitations of using graphene derivatives in bitumen. For this, we developed model bitumen, modified graphene and characterized them. We transformed our findings into a single compiled work and presented the design criteria, testing method, and the findings in this work.

Throughout our study, we identified five critical design challenges, including the complex chemical structure of bitumen, the colloidal nature of bitumen, the interaction and stability of asphaltene aggregates and MW-graphene, and environmental factors. Despite these challenges, we found that MW-graphene is capable of overcoming the identified design challenges, which we present in the conclusion of our work. The design and development of a graphene-enhanced road is a complex and ongoing process. The purpose of this paper is to provide the reader with valuable information that can support in the further development of this technology.

8. Additional studies

In this section we discuss results that were not presented in the manuscripts but have relevance to the research.

8.1. SAXS measurements to investigate the stability of different MW-graphene systems in the presence of hexane.

The SAXS measurements were performed using a SAXSLAB Mat:Nordic, manufactured by SAXSLAB / Xenocs. All samples were diluted at a rate of 1:10 (in paraffin). Separate samples were prepared for measuring over time and at a n-hexane concentration. A n-hexane concentration of 0%, 1%, 5%, 10%, 25%, and 50% were used for the measurements. Following this, the samples were rested for 24 hrs and thereafter transferred to 1.5 mm diameter capillary tubes. Before the measurements, the instrument was aligned by using lanthanum hexaboride. Each sample was measured for 1200 seconds, and the measurements were performed with a sample-detector distance of ~1084 mm, which gives, a q-range of 0.0035 - 0.1 $Å^{-1}$, which corresponds to the range of 178 nm – 6 nm in real space. Further, a beam size of 0.3 mm was used. Finally, a sample of paraffin was measured. The scattering intensity of the paraffin was subtracted from all samples before comparing. For this, the scattering intensity of paraffin was first multiped with 0.99 (0.99 represents the total concentration of paraffin in both asphaltene aggregate system and MW-graphene system after dilution for the SAXS measurements), and following the multiplication, the scattering intensity at the corresponding q value was subtracted from the sample.

We conducted a series of experiments to investigate the stability of MW-graphene in various systems. We prepared 36 samples with varying concentrations of hexane (0%, 1%, 5%, 10%, 25%, and 50%) for saturates, PBrA-graphene system, PBA-graphene system, PSA-graphene system, PAM-graphene system, and asphaltene aggregates system. This allowed us to study the effect of increasing hexane concentration on the stability of the MW-graphenes. We also prepared 20 samples for each system to assess their stability over a period of a week (0, 1, 3, 5, and 7 days). However, during the course of analyzing the data, we discovered that a software update of the SAXS instrument might have caused errors in our measurements. The update led to a syntax error of the instrument, that might have affected the detector position. We are uncertain which samples were affected by this error, because of which, we have did not include the from the manuscript and placing it here under additional studies. We did observe that the scattering intensity of the systems may have been impacted, but the error

could have been local for each batch of measurement. *Due to this, we kindly recommend the reader to observe caution when interpreting the data as we cannot guarantee the correctness of the data. Additionally, when the instrument is functioning normally, we hope to repeat the measurements and provide an erratum to the reader.*

However, the SAXS data we obtained demonstrate similar trends for all four MW-graphenes. Although the magnitude of the change in scattering intensity varies depending on the MW-graphene, each system responds similarly to the introduction of hexane. In the concentration range of 0-1% hexane, the interactions between the structures in all systems appear to dominate. Specifically, introducing 1% hexane causes the larger structures to grow and flocculate, resulting in an immediate decrease in the scattering intensity, as shown in Figure 8.1. As the peak intensity decreases, the structures are predicted to move into a lower q range, which is outside the detection limit of the instrument. Thus, we can conclude that at 1% hexane, the dominating effect seems to be the formation of structural aggregates, with a size considerably larger than the probed size of approximately 125 nm.

Figure 8.1 shows that in the concentration range of 1-10% hexane, there is an increase in scattering intensity for all MW-graphene systems. This increase in scattering intensity is associated with smaller aggregates in the system clustering and flocculating to form larger structures of about the same size as the probed length scale of 125 nm. In **paper 2**, we discuss this in more detail about agglomeration and precipitation, which we predict to be a multistage process. The figure also reveals that the increased scattering intensity is not equal for all MW-graphene systems, possibly due to differences in their intrinsic stability. For example, our microscopy and DSC measurements suggest that the PBrA-graphene ensemble exhibits lower intrinsic stability, which could cause it to start agglomerating and begin precipitation even before the introduction of hexane. Therefore, with the addition of hexane, the PBrA ensemble experiences a cumulative effect of these two factors impacting its stability. In contrast, the other MW-graphene systems show lower variation in scattering intensity due to their higher intrinsic stability.

At concentrations above 10% n-hexane, the scattering intensity decreases for all MW-graphene systems due to the irreversible precipitation caused by the condensation of the tail of DBSA. Since the stabilization mechanism is the same for all four systems, it is possible that they all behave in a similar manner, and the choice of the aromatic molecule may not play a significant role in hexane. In **paper 2**, we observed a similar precipitation mechanism for the PBA-graphene system and asphaltene aggregates, confirming the significant role played by the tail of DBSA at high hexane concentrations. Therefore, if the choice of functional group affects the system's stability as the hexane concentration increases, further investigations are needed to verify this.

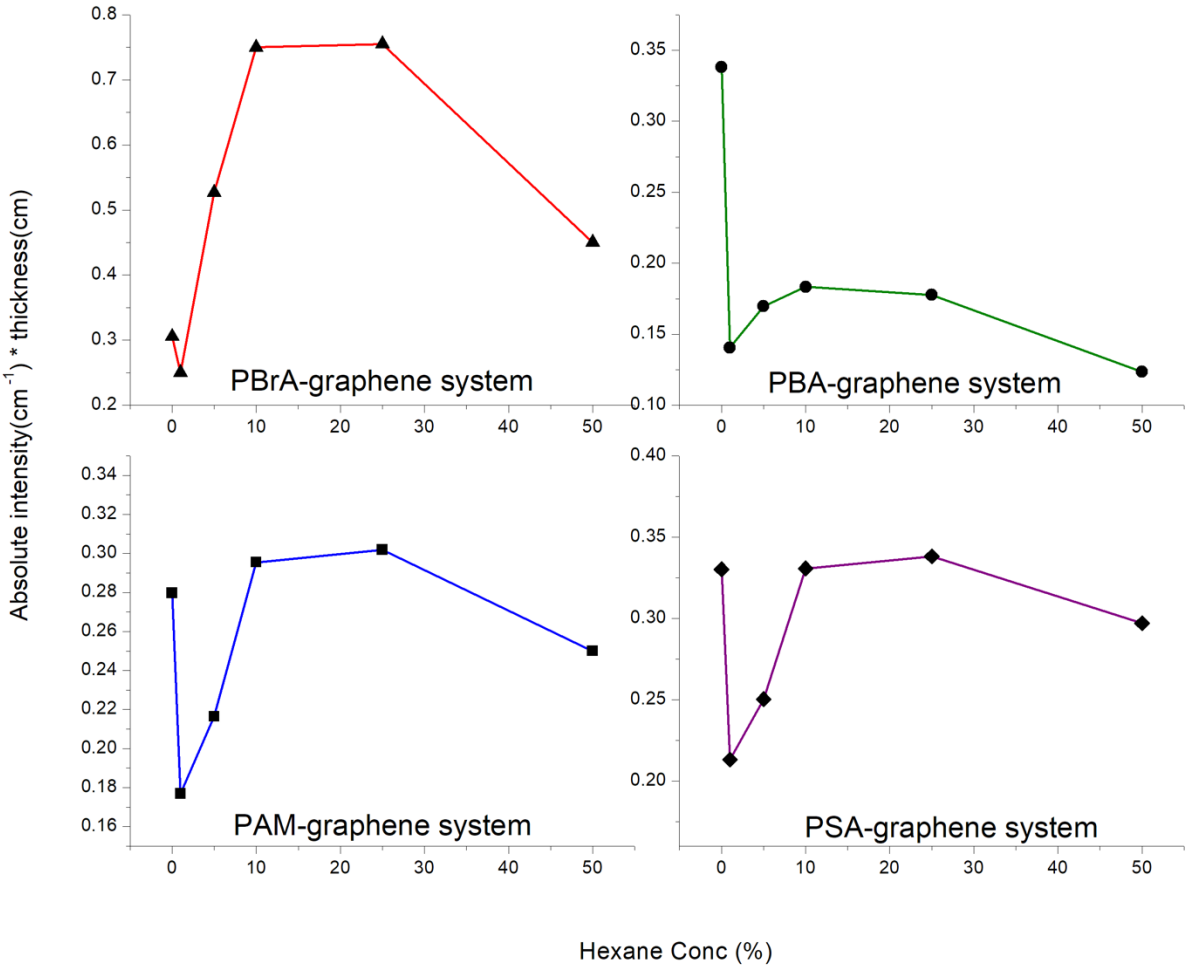

Figure 8.1: The scattering intensity of the 4 MW-graphene systems with increasing hexane concentration is presented in the graph. The scattering intensity is measured at q = 0.005 $Å^{-1}$ using SAXS. The data points shows the change in scattering intensity with increase in hexane concentration. The scattering intensity of saturates was subtracted from all the samples.

8.2. Molecularly wedged GO

In **paper 1** we showed that GO has a negative effect on asphaltene aggregates. The interaction that leads to the detrimental effect was assumed to be a cumulative effect of the functional groups and surface area of GO. To overcome this effect, we attempted to increase the amount of acidic functional groups on GO. The results of this study are presented here.

8.2.1. Preparation of MW-GO system

Graphene was first exfoliated using a shear-mixer. The shear-exfoliated graphite was converted into GO using the Modified Hummers method. 0.5 g graphene was mixed with 3 g potassium permanganate and 0.5 g sodium nitrate in the presence of 23 ml sulfuric acid and steered in an ice bath for 4 h. After which 46 ml of di-ionized water was introduced and the mixture was steered at 98 °C for 2 h. The mixture was thereafter allowed to cool, and 100 ml of sulfuric acid was then added. Thereafter, 50 ml of hydrogen peroxide was added. This mixture was filtered and 5% HCl was poured on the GO filter until the pH was neutral. Finally, the GO flakes were collected.

Later, GO was functionalized by the MW-method.100 mg of GO was dispersed in 50 ml methanol and sonicated for one hour to disperse the flakes. Following by that 16.5 mg PBA was added to the solution and the solution was further sonicated for an hour. After this, 200 ml of double-distilled de-ionized water was added, and the solution was sonicated for 24 hours at room temperature. Thereafter the solution was centrifuged. The precipitate was thereafter decanted and redispersed in de-ionized water. The redispersed solution was further sonicated for 45 minutes, filtered, and rinsed and thereafter the material was freeze-dried to ensure a totally water-free sample. The functionalised GO is called PBA-GO.

Then, to prepare the PBA-GO system, a volume fraction of 1 wt% MW-GO was introduced into the asphaltene aggregate system and sonicated for 10 minutes. A description of the involved steps and weight fractions of the different components are given in our previous work (**paper 2)**. A diagram of the preparation step is presented in figure 3 of **paper 3**. Further, the names of different stages of functionalized GO can be inferred from table 1 of **paper 3**.

8.2.2. Results and discussion

The experimental conditions used for the XPS study and microscopy of PBA-GO were consistent with those presented in **papers 2 and 3**. The -COO- peak, which is observed at 288 eV, was detected in both GO and PBA-GO, see figure 8.2 and 8.3. However, the XPS measurements revealed that the peak intensity of the -COO- and -C=O groups in PBA-GO was higher than that of the corresponding peaks in GO. This increase in peak intensity is attributed to the presence of additional functional groups. Further, Table 8.1 shows that the functionalization resulted in a reduction in the percentages of C-OH and C-O groups. The initial GO sample contained 8.5% C-OH groups and 7.5% C-O groups. Following the attachment of PBA molecules to GO, the percentage of C-OH groups decreased by 2%, while the percentage of C-O groups decreased by 3.5%. Additionally, the percentage of -COO- groups increased by 2%, from 3.5% to 5.5%, and the percentage of -C=O groups increased by 1% to 9.5%.

The decrease in the percentages of -C-OH and -CO (figure 8.2A)groups and the increase in the percentage of -COO- and -C=O (figure 8.2A and 8.2B) observed in PBA-GO could be attributed to three possible reasons. Firstly, it is possible that the acid group on PBA reacted with the hydroxyl and ester groups on GO, leading to esterification. This in turn could shift the percentage of functional groups. Additionally, the adsorption of PBA molecules on the GO surface could also lead to a shift in the percentage of the functional groups as observed in table 8.1. Finally, there is a minor possibility that the introduction of PBA molecules displaced water

Table 8.1: Fraction of the different oxygenated carbon groups on GO and PBA-GO.

Name	**C-OH**	**C-O**	**C=O**	**COO^-**	**CO_3^{2-}**
GO	8.5%	7.5%	8.5%	3.5%	1.0%
1-PBA-GO	6.0%	4.0%	9.5%	5.5%	1.0%

molecules from both -C-OH and -C-O groups. This could occur if PBA as a higher affinity for water compared to GO. Therefore, it can be concluded that the shift in the percentage of functional groups is likely due to a combination of these effects occurring simultaneously.

In **paper 1**, we experimentally demonstrated that the presence of functional groups such as hydroxyl and ketones groups cause an irreversible adsorption of asphaltene aggregates onto the surface of GO. Therefore, after the functionalization, the interaction between PBA-GO and asphaltene aggregates were observed. As seen in figure 8.4, PBA-GO does not show any signs of detrimental effect as what was seen in **paper 1**. Additionally, a stable dispersion is also visually observed for PBA-GO system, see figure 8.4. This is unlike what was observed in the case of graphene that can be seen to visually precipitate.

This finding helps us understand that multiple factors play a role in the adsorption of asphaltene aggregates on GO. These factors include, the nature and the concentration of the functional groups present on the surface of GO and asphaltene. Specifically, GO has a higher concentration of hydroxyl and ether groups, but a lower concentration of

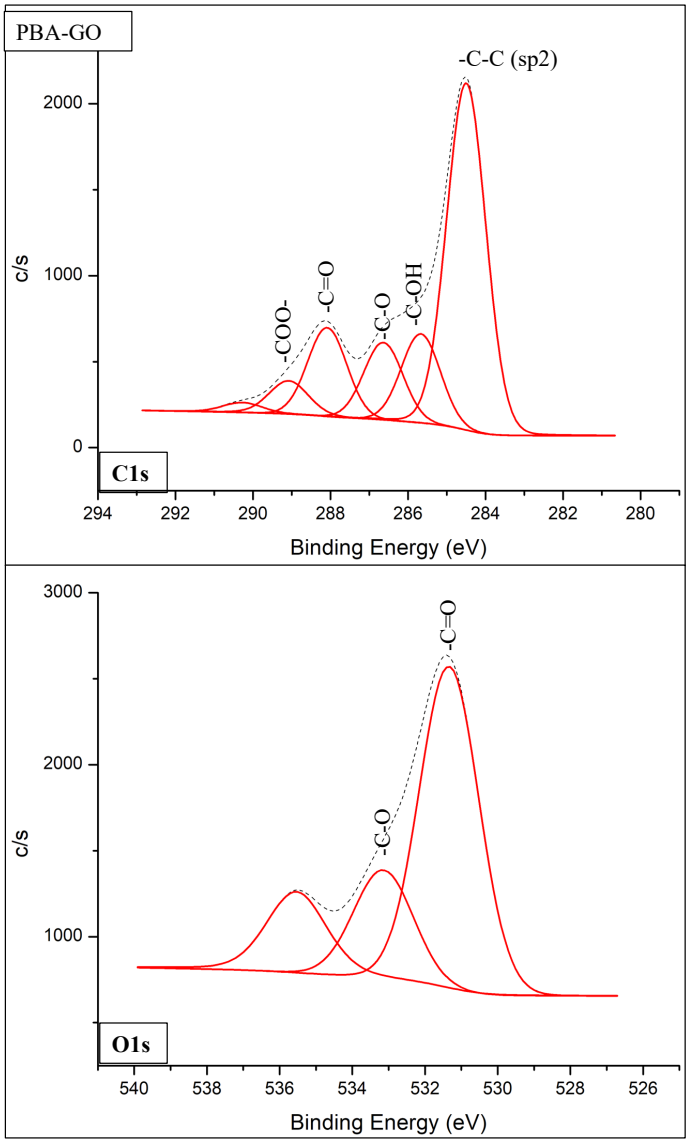

Figure 8.2: A XPS spectra of PBA-GO. The figure presents the C1s and O1s spectra of the functionalized graphene.

carboxyl groups (-COO-) compared to PBA-GO. In general, carboxyl groups are expected to be more negatively charged when compared to the other functional groups. Thus, the increase in the carboxyl groups could affect the interaction between PBA-GO and asphaltene. Moreover, as discussed in **paper 1**, the heteroatomic functional groups on asphaltene can

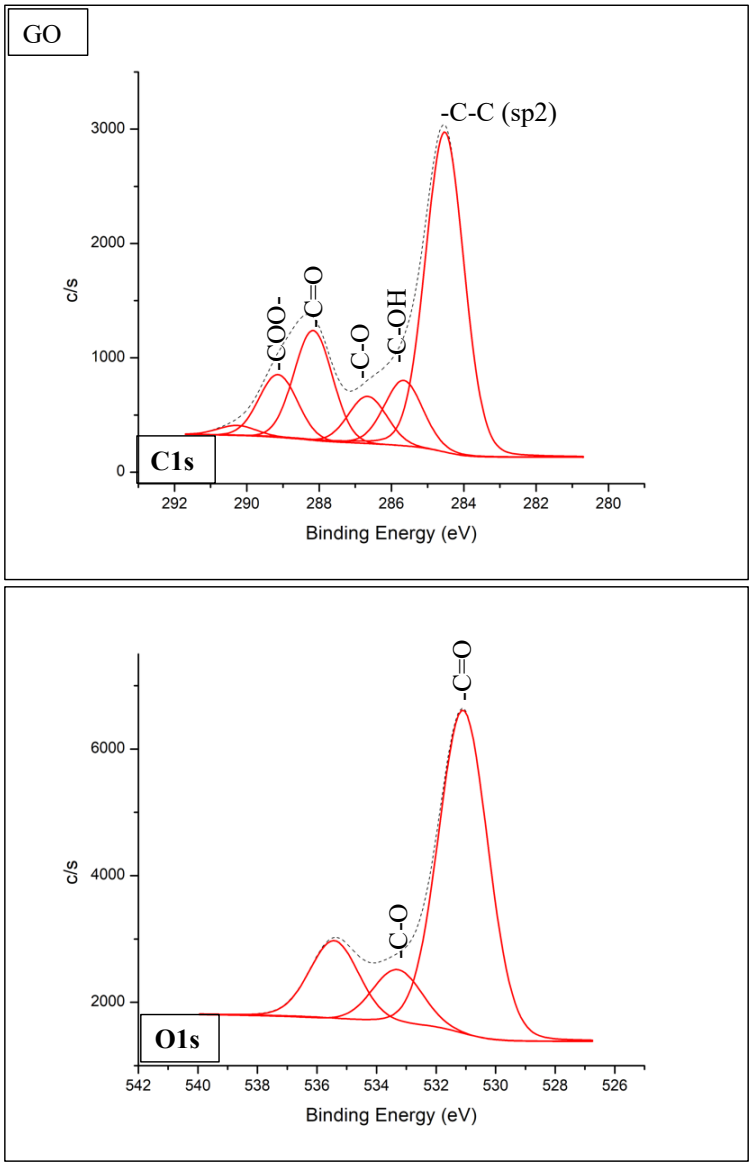

Figure 8.3: A XPS spectra of GO. The figure presents the C1s and O1s spectra of the functionalized graphene.

form hydrogen bonds and other electrostatic interactions with hydroxyl and ether groups on the GO surface. Hence, the higher concentration of hydroxyl and ether groups on GO may result in stronger adsorption of asphaltene molecules, whereas PBA-GO, with its lower percentage of hydroxyl and ether and higher percentage of carboxyl groups, may be less inclined to adsorb asphaltene on its surface. Nevertheless, it can be assumed that asphaltene aggregates could still be adsorbed onto the hydroxyl and ether groups, but at a lower rate.

While it could be assumed that for certain concentrations of functional groups, GO (or PBA-GO) might be able to form ensembles in bitumen, it must be remembered that asphaltene has a diverse surface chemistry. Thus, certain types of asphaltene might still be adsorbed onto the surface of PBA-GO while certain others could form ensembles in bitumen. Therefore, at an

industrial scale, it might be a colossal undertaking to determine the chemistry of asphaltene aggregate and GO, to determine if they can be used in that particular bitumen. Thus, from this study, it can be concluded that our findings from **paper 1** are still valid.

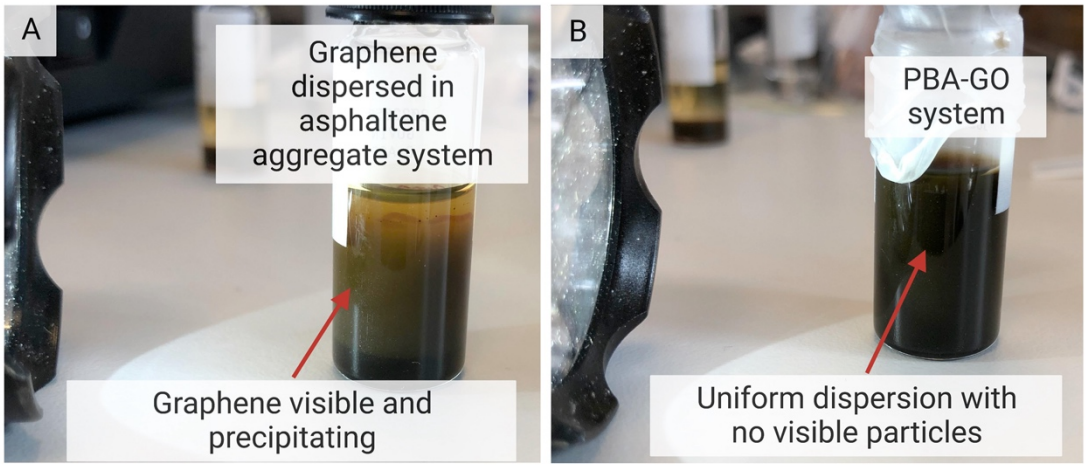

Figure 8.4: A). Graphene dispersed in asphaltene aggregate system is precipitating after an hour. While B) PBA-GO system is stable (after 1hour), PBA-GO ensemble is formed through interaction with asphaltene aggregates. This is unlike what was observed in **paper1.**

9. Conclusion

In this thesis, we conducted a comprehensive bottom-up study on functionalizing graphene derivatives and incorporating them into bitumen to improve its material properties. Initially, we created a model bitumen system consisting of asphaltene aggregates to investigate the interactions between graphene derivatives and bitumen. Through this model system, we identified graphene derivatives that could have a detrimental effect on bitumen's structure and function.

Subsequently, we developed a stable ensemble structure of non-covalently functionalized graphene and asphaltene aggregates, termed the MW-graphene ensemble, in an environment-friendly manner. The MW-graphene and its corresponding MW-graphene ensemble were found to be phase compatible. Furthermore, highly polar MW-graphene significantly improved the stability of our model bitumen.

Our aim in this thesis was to provide a solution using phase-compatible graphene that could help enhance the material properties of bitumen. This thesis demonstrates the feasibility of our recommended research direction. However, we recognized that improving material properties like thermal conductivity and viscoelasticity in bitumen requires further investigation. Therefore, we think this thesis answers a part of the bigger question,'' graphene incorporated bitumen,'' but there is a long journey ahead to answer the question truly.

10. Future outlook

The central issue addressed in this thesis is the use of graphene as a potential modifier for bitumen. There are various other nanoparticles available for this purpose, such as nanotubes, pristine graphene, CVD graphene, silica nanoparticles, metallic nanoparticles, and others, including fly ash. The choice of MW-graphene as the preferred modifier is based on its superior characteristics, which set it apart from other carbon allotropes. MW-graphene offers advantages in terms of flexibility, size, functionality, material properties, and the ability to interact with and modify asphaltene aggregates. MW-graphene can interact at the molecular level and modify the microstructure of bitumen, instead of merely serving as a bulk filler. *This is not to discredit the potential of other nanoparticles to achieve similar functionalities, but simply highlights that MW-graphene has a genuine role.* Further, it shows the potential MW-graphene can be a player in the realm of bitumen modification and its authentic applications. An interesting follow up to this would be to use dissimilar or alternative nanomaterials (in the same way) and investigate its potential in bitumen. For instance, there are other nanoparticles that are produced in the industries as a biproduct such as fly ash. Thus, it would be interesting to investigate the behavior of other nanoparticles with similar functionality. If we can successfully manipulate nanoparticles, we can trap them in a useful manner in roads and reduce their exposure.

In this study, we demonstrated that functionalized graphene can improve the stability of bitumen and modify asphaltene aggregate structure. While our preferred method of functionalizing and binding MW-graphene with asphaltene met our design constraints, it would be valuable to explore alternative methods and evaluate their advantages and disadvantages. Graphene also holds potential in areas such as thermal and electrical conductivity, smart sensing, and more. We did not explore these questions in this thesis.

Further, future research could examine the impact of manipulating asphaltene aggregate and the consequence of that on roads. Although our study successfully developed MW-graphene ensembles and demonstrated their interaction with asphaltene aggregates, further investigation is needed to gain a deeper understanding of this interaction. Incorporating graphene into bitumen presents unique challenges due to the chemical nature of bitumen. We discuss these challenges in detail in **chapters 1,3, and 5**. Thus, being able to overcome these challenges and investigate the potential of graphene in bitumen would be a major scientific contribution. Additionally, the impact of incorporating graphene on factors such as driving comfort and tire grip, must be investigated. This would also require producing and testing graphene incorporated asphalt. After all this, the true potential benefits of MW-graphene can be better understood. Lastly, performing cytotoxicity measurements will be a valuable future

direction, as bitumen is used globally and is often located in areas with diverse ecosystems. It is crucial to evaluate the potential positive and negative impacts of MW-graphene before implementing it in practice.

Most importantly, we demonstrated that asphaltene aggregates will interact with the tethers on MW-graphene. Still, we do not know the exact mechanism. More research is needed in understanding mechanism of whether it is asphaltene or DBSA that approaches the tether first, and how all 3 binds.

Finally, we can consider designing a scaled-up functionalization strategy for producing MW-graphene to be implemented in roads. One method we propose is to use a Taylor-Couette mixer with recirculating solvent and aromatic molecule. In such a system, graphene can be added to the solvent and subsequently, MW-graphene can be isolated and then removed. This system would require minimal maintenance and could be sustainable because it can reuse the solvent and unbound aromatic molecule. Additionally, exfoliating graphene requires a shear rate of 10^4 and the addition of an aromatic molecule or polymer. This can also be achieved using a rotar-stator mixer or sonication. Therefore, implementing such a system to upscale the processing of MW-graphene is a sensible future option.

Therefore, we think this thesis answers a part of the question ‘’graphene incorporated bitumen’’ but there is a long journey ahead to truly answer the question.

References

[1]. Petrauskas, D. And Ullah,S. 2015, Manufacture and storage of bitumen, Shell handbook, Sixth Edition, Shell bitumen. (book)

[2]. Yoo, B., Shin, H., Yoon, H. and Park, H., 2013. Graphene and graphene oxide and their uses in barrier polymers. Journal of Applied Polymer Science, 131(1),

[3]. Bualuang, T. et al. (2021) "Influence of asphalt emulsion inclusion on fly ash/hydrated lime alkali-activated material," Materials, 14(22), p. 7017. Available at: https://doi.org/10.3390/ma14227017.

[4]. Casado-Barrasa, R. et al. (2019) "Assessment of carbon black modified binder in a sustainable asphalt concrete mixture," Construction and Building Materials, 211, pp. 363–370. Available at: https://doi.org/10.1016/j.conbuildmat.2019.03.255.

[5]. Crucho, J. et al. (2019) "A review of nanomaterials' effect on mechanical performance and aging of asphalt mixtures," Applied Sciences, 9(18), p. 3657. Available at: https://doi.org/10.3390/app9183657.

[6]. Farooq, U. et al. (2021) "Review on application of nanotechnology for Asphaltene Adsorption, crude oil demulsification, and produced water treatment," Energy & Fuels, 35(23), pp. 19191–19210. Available at: https://doi.org/10.1021/acs.energyfuels.1c01990.

[7]. Moretti, L. et al. (2021) "Mechanical characteristics of graphene nanoplatelets-modified asphalt mixes: A comparison with polymer- and not-modified asphalt mixes," Materials, 14(9), p. 2434. Available at: https://doi.org/10.3390/ma14092434.

[8]. Porto, M. et al. (2019) "Bitumen and bitumen modification: A review on latest advances," Applied Sciences, 9(4), p. 742. Available at: https://doi.org/10.3390/app9040742.

[9]. Ramadhansyah, P.J. et al. (2020) "Nanoparticle in asphalt binder: A state-of-the-art review," IOP Conference Series: Materials Science and Engineering, 712(1), p. 012023. Available at: https://doi.org/10.1088/1757-899x/712/1/012023.

[10]. Wu, S. and Tahri, O. (2019) "State-of-art carbon and graphene family nanomaterials for asphalt modification," Road Materials and Pavement Design, 22(4), pp. 735–756. Available at: https://doi.org/10.1080/14680629.2019.1642946.

[11]. Yang, G.J. and Luo, X. (2012) "Study on the effect of fly ash to Modified Bitumen," Advanced Materials Research, 598, pp. 332–335. Available at:https://doi.org/10.4028/www.scientific.net/amr.598.332.

[12]. Vignisdottir, H.R. et al. (2019) "Life cycle assessment of winter road maintenance," The International Journal of Life Cycle Assessment, 25(3), pp. 646–661. Available at: https://doi.org/10.1007/s11367-019-01682-y.

[13]. Paredes, J.I. et al. (2008) "Graphene oxide dispersions in organic solvents," Langmuir, 24(19), pp. 10560–10564. Available at: https://doi.org/10.1021/la801744a.

[14]. Pavement interactive (no date) Pavement Interactive. Available at: https://pavementinteractive.org/reference-desk/maintenance-and-rehabilitation/maintenance/bituminous-surface-treatments/ (Accessed: March 2, 2023).

[15]. Moghtadernejad, S. et al. (2021) "Enhancement of asphalt performance by graphene-based bitumen nanocomposites." Available at: https://doi.org/10.31979/mti.2021.1918.

[16]. Kocjan, A., Logar, M. and Shen, Z. (2017) "The agglomeration, coalescence and sliding of nanoparticles, leading to the rapid sintering of Zirconia Nanoceramics," Scientific Reports, 7(1). Available at: https://doi.org/10.1038/s41598-017-02760-7.

[17]. Ruiz-Morales, Y. and Mullins, O. (2007). Polycyclic Aromatic Hydrocarbons of Asphaltenes Analyzed by Molecular Orbital Calculations with Optical Spectroscopy. Energy & Fuels, 21(1), pp.256-265.

[18]. Petrauskas, D. And Ullah,S. 2015, Manufacture and storage of bitumen, Shell handbook, Sixth Edition, Shell bitumen. (book)

[19]. Gruse, W.A. and Stevens, D.R. 1960. The Chemical Technology of Petroleum. McGraw-Hill. (book)

[20]. Çadýrcý, B., Abed, R., Abraham, W., Abraham, W., Adams, J., Aitken, C., Aitken, C., Al-Halbouni, D., Al-ramahi, Y., Alazard, D. and Albertin, K., 2011. Handbook of Hydrocarbon and Lipid Microbiology. Heidelberg, Germany: Springer-Verlag Berlin Heidelberg. (book)

[21]. Nalinakshan, S., Sivasubramanian, V., Ravi, V., Vasudevan, A., Sankar, M. and Arunachalam, K., 2019. Progressive crude oil distillation: An energy-efficient alternative to conventional distillation process. Fuel, 239, pp.1331-1337.

[22]. Severin, D., 1992. Characterization of high- and non-boiling crude oil fractions. Invited lecture. The Analyst, 117(3), p.305.

[23]. George A. Olah and Árpád Molnár. 2003. Hydrocarbon Chemistry, Second Edition. Wiley & Sons. (book)

[24]. Gary JH, Handwerk GE, Kaiser MJ. 2007. Petroleum Refining: Technology and Economics. CRCPress. (book)
[25]. James G. Speight. 2015. Handbook of Coal Analysis, First Edition. Wiley & Sons. (book)
[26]. Ruiz-Morales, Y. and Mullins, O. (2007). Polycyclic Aromatic Hydrocarbons of Asphaltenes Analyzed by Molecular Orbital Calculations with Optical Spectroscopy. Energy & Fuels, 21(1), pp.256-265.
[27]. Handle, F., Harir, M., Füssl, J., Koyun, A., Grossegger, D., Hertkorn, N., Eberhardsteiner, L., Hofko, B., Hospodka, M., Blab, R., Schmitt-Kopplin, P. and Grothe, H. (2017). Tracking Aging of Bitumen and Its Saturate, Aromatic, Resin, and Asphaltene Fractions Using High-Field Fourier Transform Ion Cyclotron Resonance Mass Spectrometry. Energy & Fuels, 31(5), pp.4771-4779.
[28]. Lesueur, D. (2009). The colloidal structure of bitumen: Consequences on the rheology and on the mechanisms of bitumen modification. Advances in Colloid and Interface Science, 145(1-2), pp.42-82.
[29]. Mullins, O. (2011). Asphaltenes, heavy oils, and petroleomics. New York: Springer. (book)
[30]. Bridot, J.-L., Langevin, D. and Mullins, O.C. (2022) "Role of asphaltene origin in its adsorption at oil–water interfaces," Energy & Fuels, 36(16), pp. 8749–8759. Available at: https://doi.org/10.1021/acs.energyfuels.2c00966.
[31]. Kostyukevich, Y. et al. (2016) "The investigation of the bitumen from ancient greek amphora using ft ICR ms, H/D Exchange and novel Spectrum Reduction Approach.," Journal of Mass Spectrometry, 51(6), pp. 430–436. Available at: https://doi.org/10.1002/jms.3769.
[32]. Subramanian, S., Simon, S. and Sjöblom, J. (2015). Asphaltene Precipitation Models: A Review. Journal of Dispersion Science and Technology, 37(7), pp.1027-1049.
[33]. Mullins, O.C. (2010) "The modified Yen Model," Energy & Fuels, 24(4), pp. 2179–2207. Available at: https://doi.org/10.1021/ef900975e.
[34]. Nguyen, L. and Truong, T. (2018). Quantitative Structure-Property Relationships for the Electronic Properties of Polycyclic Aromatic Hydrocarbons. ACS Omega, 3(8), pp.8913-8922.
[35]. Andreatta, G., Bostrom, N. and Mullins, O., 2005. High-QUltrasonic Determination of the Critical Nanoaggregate Concentration of Asphaltenes and the Critical Micelle Concentration of Standard Surfactants. Langmuir, 21(7), pp.2728-2736.
[36]. Abdel-Raouf, M. (2012). Crude Oil Emulsions- Composition Stability and Characterization. 1st ed. InTech. (Book)
[37]. Andersen, S. and Christensen, S. (2000). The Critical Micelle Concentration of Asphaltenes As Measured by Calorimetry. Energy & Fuels, 14(1), pp.38-42.
[38]. Ashoori, S., Sharifi, M., Masoumi, M. and Mohammad Salehi, M. (2017). The relationship between SARA fractions and crude oil stability. Egyptian Journal of Petroleum, 26(1), pp.209-213.
[39]. Geim, A. and Novoselov, K., 2007. The rise of graphene. Nature Materials, 6(3), pp.183-191.
[40]. Li, X., Li, B., Fan, X., Wei, L., Li, L., Tao, R., Zhang, X., Zhang, H., Zhang, Q., Zhu, H., Zhang, S., Zhang, Z. and Zeng, C., 2018. Atomically flat and thermally stable graphene on Si (111) with preserved intrinsic electronic properties. Nanoscale, 10(18), pp.8377-8384.
[41]. Gudarzi, M. (2016). Colloidal Stability of Graphene Oxide: Aggregation in Two Dimensions. Langmuir, 32(20), pp.5058-5068.
[42]. Castro Neto, A., Guinea, F., Peres, N., Novoselov, K. and Geim, A. (2009). The electronic properties of graphene. Reviews of Modern Physics, 81(1), pp.109-162.
[43]. Gioia, L., Z√ºlicke, U., Governale, M. and Winkler, R., 2018. Dirac electrons in quantum rings. Physical Review B, 97(20).
[44]. Novoselov, K., Geim, A., Morozov, S., Jiang, D., Katsnelson, M., Grigorieva, I., Dubonos, S. and Firsov, A., 2005. Two-dimensional gas of massless Dirac fermions in graphene. Nature, 438(7065), pp.197-200.
[45]. Jiang, Z., Zhang, Y., Tan, Y., Stormer, H. and Kim, P., 2007. Quantum Hall effect in graphene. Solid State Communications, 143(1-2), pp.14-19.
[46]. Morozov, S., Novoselov, K., Katsnelson, M., Schedin, F., Ponomarenko, L., Jiang, D. and Geim, A., 2006. Strong Suppression of Weak Localization in Graphene. Physical Review Letters, 97(1).
[47]. Baringhaus, J., Ruan, M., Edler, F., Tejeda, A., Sicot, M., Taleb-Ibrahimi, A., Li, A., Jiang, Z., Conrad, E., Berger, C., Tegenkamp, C. and de Heer, W., 2014. Exceptional ballistic transport in epitaxial graphene nanoribbons. Nature, 506(7488), pp.349-354.
[48]. Partoens, B. and Peeters, F., 2006. From graphene to graphite: Electronic structure around the K point. Physical Review B, 74(7).
[49]. De Leo, F., Magistrato, A. and Bonifazi, D., 2015. Interfacing proteins with graphitic nanomaterials: from spontaneous attraction to tailored assemblies. Chemical Society Reviews, 44(19), pp.6916-6953.
[50]. Randviir, E., Brownson, D. and Banks, C., 2014. A decade of graphene research: production, applications and outlook. Materials Today, 17(9), pp.426-432.
[51]. Zhu, S., Yuan, S. and Janssen, G. (2014). Optical transmittance of multilayer graphene. EPL (Europhysics Letters), 108(1), p.17007.

[52]. Skoda, M., Dudek, I., Jarosz, A. and Szukiewicz, D., 2014. Graphene: One Material, Many Possibilities-Application Difficulties in Biological Systems. Journal of Nanomaterials, 2014, pp.1-11.
[53]. Inagaki, M. and Kang, F., 2014. Graphene derivatives: graphane, fluorographene, graphene oxide, graphyne and graphdiyne. J. Mater. Chem. A, 2(33), pp.13193-13206.
[54]. Inc., C., 2020. Understanding Graphene Nanoplatelets. [online] AZoNano.com. Available at: <https://www.azonano.com/article.aspx?ArticleID=4846> (Accessed: March 2, 2023).
[55]. Dreyer, D., Park, S., Bielawski, C. and Ruoff, R., 2010. The chemistry of graphene oxide. Chem. Soc. Rev., 39(1), pp.228-240.
[56]. Szab√≥, T., Berkesi, O., Forg√≥, P., Josepovits, K., Sanakis, Y., Petridis, D. and D√©k√°ny, I., 2006. Evolution of Surface Functional Groups in a Series of Progressively Oxidized Graphite Oxides. Chemistry of Materials, 18(11), pp.2740-2749.
[57]. Oye, M. (2013). Graphene Synthesis and Applications (Choi, W. and Lee, J.-W., Eds.) [Book Review]. IEEE Nanotechnology Magazine, 7(1), pp.39-40.
[58]. Liu, J., Tang, J. and Gooding, J., (2012). Strategies for chemical modification of graphene and applications of chemically modified graphene. Journal of Materials Chemistry, 22(25), p.12435.
[59]. Georgakilas, V., Otyepka, M., Bourlinos, A., Chandra, V., Kim, N., Kemp, K., Hobza, P., Zboril, R. and Kim, K. (2012). Functionalization of Graphene: Covalent and Non-Covalent Approaches, Derivatives and Applications. Chemical Reviews, 112(11), pp.6156-6214
[60]. S. Tiwari, A. Purabgola, B. Kandasubramanian, (2020). Functionalised graphene as flexible electrodes for polymer photovoltaics, Journal of Alloys and Compounds. 825 153954. doi:10.1016/j.jallcom.2020.153954.
[61]. R. Goyat, Y. Saharan, J. Singh, A. Umar, S. Akbar, (2022). Synthesis of graphene-based nanocomposites for environmental remediation applications: A Review, Molecules. 27 6433. doi:10.3390/molecules27196433.
[62]. An, X., Simmons, T., Shah, R., Wolfe, C., Lewis, K., Washington, M., Nayak, S., Talapatra, S. and Kar, S., (2010). Stable Aqueous Dispersions of Noncovalently Functionalized Graphene from Graphite and their Multifunctional High-Performance Applications. Nano Letters, 10(11), pp.4295-4301.
[63]. X. An, T. (2011). Simmons, Stable aqueous dispersions of non-covalently functionalized graphene from graphite and their multifunctional high-performance AP, SciVee.. doi:10.4016/27226.01.
[64]. Hinnemo, M., Zhao, J., Ahlberg, P., H.gglund, C., Djurberg, V., Scheicher, R., Zhang, S. and Zhang, Z., (2017). On Monolayer Formation of Pyrenebutyric Acid on Graphene. Langmuir, 33(15), pp.3588-3593.
[65]. Cai, X., Wang, J., Chi, R., Song, Y., Li, J., Sun, Q. and Jia, Y., (2016). Direct Exfoliation of. Graphite into Graphene by Pyrene-Based Molecules as Molecular-Level Wedges: A Tribological View. Tribology Letters, 62(2).37
[66]. Mahalingam, D., Wang, S. and Nunes, S. (2018). Graphene Oxide Liquid Crystal Membranes in Protic Ionic Liquid for Nanofiltration. ACS Applied Nano Materials, 1(9), pp.4661-4670.
[67]. Hernandez, Y., Lotya, M., Rickard, D., Bergin, S. and Coleman, J. (2010). Measurement of Multicomponent Solubility Parameters for Graphene Facilitates Solvent Discovery. Langmuir, 26(5), pp.3208-3213.
[68]. Draude, A. and Dierking, I. (2019). Lyotropic Liquid Crystals from Colloidal Suspensions of Graphene Oxide. Crystals, 9(9), p.455.
[69]. Li, P., Wong, M., Zhang, X., Yao, H., Ishige, R., Takahara, A., Miyamoto, M., Nishimura, R. and Sue, H. (2014). Tunable Lyotropic Photonic Liquid Crystal Based on Graphene Oxide. ACS Photonics, 1(1), pp.79-86.
[70]. Habte, A. and Ayele, D. (2019). Synthesis and Characterization of Reduced Graphene Oxide (rGO) Started from Graphene Oxide (GO) Using the Tour Method with Different Parameters. Advances in Materials Science and Engineering, 2019, pp.1-9.
[71]. Schultz, B., Dennis, R., Lee, V. and Banerjee, S., (2014). An electronic structure perspective of graphene interfaces. Nanoscale, 6(7), p.3444.
[72]. Pérez, E. and Martín, N., (2015). π–π interactions in carbon nanostructures. Chemical Society Reviews, 44(18), pp.6425-6433.
[73]. Wang, J., Chen, Z. and Chen, B., (2014). Adsorption of Polycyclic Aromatic Hydrocarbons by Graphene and Graphene Oxide Nanosheets. Environmental Science & Technology, 48(9), pp.4817-4825.
[74]. Cimino, R., Rasmussen, C., Brun, Y. and Neimark, A., (2016). Mechanisms of chain adsorption on porous substrates and critical conditions of polymer chromatography. Journal of Colloid and Interface Science, 481, pp.181-193.
[75]. Yang, W. et al. (2013) "Noncovalent functionalization of graphene in suspension," ISRN Organic Chemistry, 2013, pp. 1–7. Available at: https://doi.org/10.1155/2013/656185.
[76]. Christian Kemp, K. et al. (2014) "Noncovalent functionalization of graphene," Functionalization of Graphene, pp. 199–218. Available at: https://doi.org/10.1002/9783527672790.ch7.

[77]. Luján, S. and Román, V. (2019) “Environmental impact of the production of graphene oxide and reduced graphene oxide,” SN Applied Sciences , 179(1). Available at: https://doi.org/10.1021/acsami.7b16736.s001.
[78]. Texter, J. (2014) “Graphene dispersions,” Current Opinion in Colloid & Interface Science, 19(2), pp. 163–174. Available at: https://doi.org/10.1016/j.cocis.2014.04.004.
[79]. Dimiev, A. and Eigler, S., n.d. Graphene Oxide: Fundamentals and Applications. 1st ed. Wiley Online Library, pp.85-164. (book)
[80]. D4124-09. 2018. Standard Test Method for Separation of Asphalt into Four Fractions. ASTM international
[81]. Priyanto, S., Mansoori, G. and Suwono, A. (2001). Measurement of property relationships of nano-structure micelles and coacervates of asphaltene in a pure solvent. Chemical Engineering Science, 56(24), pp.6933-6939.
[82]. Buenrostro-Gonzalez, E., Lira-Galeana, C., Gil-Villegas, A. and Wu, J. (2004). Asphaltene precipitation in crude oils: Theory and experiments. AIChE Journal, 50(10), pp.2552-2570.
[83]. Natarajan, A., Xie, J., Wang, S., Masliyah, J., Zeng, H. and Xu, Z. (2011). Understanding Molecular Interactions of Asphaltenes in Organic Solvents Using a Surface Force Apparatus. The Journal of Physical Chemistry C, 115(32), pp.16043-16051.
[84]. Us'yarov, O., 2020. Critical Micellization Concentration of Ionic Surfactants: Comparison of Theoretical and Experimental Results.
[85]. Chang, C. and Fogler, H. (1994). Stabilization of Asphaltenes in Aliphatic Solvents Using Alkylbenzene-Derived Amphiphiles. 1. Effect of the Chemical Structure of Amphiphiles on Asphaltene Stabilization. Langmuir, 10(6), pp.1749-1757.
[86]. Painter, P., Veytsman, B. and Youtcheff, J., 2015. Guide to Asphaltene Solubility. Energy & Fuels, 29(5), pp.2951-2961.
[87]. Larichev, Y., Nartova, A. and Martyanov, O. (2016). The influence of different organic solvents on the size and shape of asphaltene aggregates studied via small-angle X-ray scattering and scanning tunneling microscopy. Adsorption Science & Technology, 34(2-3), pp.244-257.
[88]. Sato, T., Araki, S., Morimoto, M., Tanaka, R. and Yamamoto, H. (2014). Comparison of Hansen Solubility Parameter of Asphaltenes Extracted from Bitumen Produced in Different Geographical Regions. Energy & Fuels, 28(2), pp.891-897.
[89]. Goual, L. and Sedghi, M., 2015. Role of ion-pair interactions on asphaltene stabilization by alkylbenzenesulfonic acids. Journal of Colloid and Interface Science, 440, pp.23-31.
[90]. Alhreez, M. and Wen, D. (2019) “M2olecular structure characterization of asphaltene in the presence of inhibitors with nanoemulsions,” RSC Advances, 9(34), pp. 19560–19570. Available at: https://doi.org/10.1039/c9ra02664a.
[91]. Chang, C.-L. and Fogler, H.S. (1993) “Asphaltene Stabilization in alkyl solvents using oil-soluble amphiphiles,” All Days [Preprint]. Available at: https://doi.org/10.2118/25185-ms.
[92]. Chang, C.-L. and Fogler, H.S. (1994) “Stabilization of asphaltenes in aliphatic solvents using alkylbenzene-derived amphiphiles. 1. effect of the Chemical Structure of Amphiphiles on Asphaltene Stabilization,” Langmuir, 10(6), pp. 1749–1757. Available at: https://doi.org/10.1021/la00018a022.
[93]. Chang, C.-L. and Fogler, H.S. (1994) “Stabilization of asphaltenes in aliphatic solvents using alkylbenzene-derived amphiphiles. 2. study of the asphaltene-amphiphile interactions and structures using Fourier transform infrared spectroscopy and small-angle X-ray scattering techniques,” Langmuir, 10(6), pp. 1758–1766. Available at: https://doi.org/10.1021/la00018a023.
[94]. González, G. and Middea, A. (1991) “Peptization of asphaltene by various Oil Soluble Amphiphiles,” Colloids and Surfaces, 52, pp. 207–217. Available at: https://doi.org/10.1016/0166-6622(91)80015-g.
[95]. Goual, L. and Firoozabadi, A. (2004) “Effect of resins and DBSA on Asphaltene Precipitation from Petroleum Fluids,” AIChE Journal, 50(2), pp. 470–479. Available at: https://doi.org/10.1002/aic.10041.
[96]. Hashmi, S.M., Zhong, K.X. and Firoozabadi, A. (2012) “Acid–base chemistry enables reversible colloid-to-solution transition of asphaltenes in non-polar systems,” Soft Matter, 8(33), p. 8778. Available at: https://doi.org/10.1039/c2sm26003d.
[97]. “Impact of HBonds and Porphyrins on Asphaltene Aggregation as revealed by Molecular Dynamics Simulations” (no date). Available at: https://doi.org/10.1021/acs.energyfuels.8b01901.s001.
[98]. “Molecular mechanisms of suppressing asphaltene aggregation and Flocculation by Dodecylbenzenesulfonic acid probed by molecular dynamics simulations” (no date). Available at: https://doi.org/10.1021/acs.energyfuels.9b00821.s001.
[99]. Pan, H. and Firoozabadi, A. (2000) “Thermodynamic micellization model for asphaltene precipitation inhibition,” AIChE Journal, 46(2), pp. 416–426. Available at: https://doi.org/10.1002/aic.690460219.

[100]. Skartlien, R., Simon, S. and Sjöblom, J. (2016) "A DPD study of Asphaltene Aggregation: The role of inhibitor and asphaltene structure in Diffusion-limited aggregation," Journal of Dispersion Science and Technology, 38(3), pp. 440–450. Available at: https://doi.org/10.1080/01932691.2016.1172972.
[101]. Konios, D., Stylianakis, M., Stratakis, E. and Kymakis, E., 2014. Dispersion behaviour of graphene oxide and reduced graphene oxide. Journal of Colloid and Interface Science, 430, pp.108-112.
[102]. Murphy, D. and Davidson, M., 2013. Fundamentals of Light Microscopy and Electronic Imaging. Hoboken, N.J.: Wiley-Blackwell. (book)
[103]. Reimer, L., 2013. Transmission Electron Microscopy. Berlin, Heidelberg: Springer Berlin / Heidelberg. (book)
[104]. Choudhary, O. and ka, P., 2017. Scanning Electron Microscope: Advantages and Disadvantages in Imaging Components. International Journal of Current Microbiology and Applied Sciences, 6(5), pp.1877-1882.
[105]. Pascual, E. and Sivera, F. (2019) "Crystal analysis in synovial fluid," Gout, pp. 47–58. Available at: https://doi.org/10.1016/b978-0-323-54823-6.00005-1.
[106]. Stuart, B., 2009. Infrared Spectroscopy: Fundamentals and Applications. 1st ed. J. Wiley & Sons.
[107]. Hernandez, V., Ramirez, F., Zotti, G. and L√≥pez Navarrete, J., 1992. Resonance Raman and FTIR spectra of pristine and doped polyconjugated polyfuran. Chemical Physics Letters, 191(5), pp.419-422.
[108]. Polavarapu, P., 1998. Vibrational Spectra: Principles and Applications with Emphasis on Optical Activity, Volume 85. 1st ed. Elsevier.
[109]. Levine, S., Li-Shi, Y., Strang, C. and Hong-Kui, X., 1989. Advantages and Disadvantages in the Use of Fourier Transform Infrared (FTIR) and Filter Infrared (FIR) Spectrometers for Monitoring Airborne Gases and Vapors of Industrial Hygiene Concern. Applied Industrial Hygiene, 4(7), pp.180-187.
[110]. Watts, J.F. and Wolstenholme, J. (2020) An introduction to surface analysis by XPS and AES. Hoboken, NJ: Wiley. (book)
[111]. Paul, V.der H. (2012) X-ray photoelectron spectroscopy: An introduction to principles and practices. Hoboken, NJ: Wiley. (book)
[112]. Crist, B.V. (1999) Handbooks of monochromatic XPS spectra. Mountain View, CA: XPS International. (book)
[113]. Workman, J. (2001) *Handbook of Organic Compounds*. San Diego: Academic Press.
[114]. Waseda, Y., Matsubara, E. and Shinoda, K., 2014. X-Ray Diffraction Crystallography. Berlin: Springer Berlin. (book)
[115]. Hammond, C., 2015. The Basics of Crystallography and Diffraction. 4th ed. Oxford: Oxford University Press. (book)
[116]. Feshbach, H., 1951. Elastic Scattering of Electrons. Physical Review, 84(6), pp.1206-1210.
[117]. Pecharsky, V. and Zavalij, P., 2009. Fundamentals of Powder Diffraction and Structural Characterization of Materials. New York: Springer. (book)
[118]. R., K.C.S.S. (2016) X-ray and neutron techniques for nanomaterials characterization. Berlin: Springer. (book)
[119]. Svergun, D.I., Feĭgin, L.A. and Taylor, G.W. (2016) *Structure analysis by small-angle X-ray and neutron scattering*. New York: Springer Science+Business Media, LLC.
[120]. Barnes, H., Hutton, J. and Walters, K., 1989. An Introduction to Rheology. Amsterdam: Elsevier. (book)
[121]. Macosko, C., 1994. Rheology: Principles, Measurements, and Applications. New York, N.Y. etc.: Wiley-VCH. (book)
[122]. Barnes, H., 2000. A Handbook of Elementary Rheology. Aberystwyth: Institute of non-newtonian fluid mechanics, University of Wales. (book)
[123]. *Handbook of Differential Scanning Calorimetry Volume 1* (2022). S.l.: butterworth-heinemann inc. (book)